Reconstructing glacier evolution using a flowline model

Development of an initialization method

Julia Eis

November 26, 2020

University of Bremen

Institute of Geography

PhD Thesis

Reconstructing glacier evolution using a flowline model

Development of an initialization method

Julia Eis

November 26, 2020

1st Reviewer Prof. Dr. Ben Marzeion
Institute of Geography
University of Bremen

2nd Reviewer Prof. Dr. Daniel Farinotti
Laboratory of Hydraulics, Hydrology and Glaciology
Swiss Federal Institute of Technology (ETH) Zürich

Supervisors Prof. Dr. Ben Marzeion
Prof. Dr. Fabien Maussion

Julia Eis

Reconstructing glacier evolution using a flowline model
Development of an initialization method

PhD Thesis
Date of doctoral colloquium: November 26, 2020
Reviewers: Prof. Dr. Ben Marzeion and Prof. Dr. Daniel Farinotti
Supervisors: Prof. Dr. Ben Marzeion and Prof. Dr. Fabien Maussion

University of Bremen
Institute of Geography

Abstract

Glacier mass change is one of the main causes of past sea-level rise and glaciers will continue to be a major contributor in the 21st century. Despite their importance, knowledge about past glacier mass changes is strongly limited. Whereas detailed observations exist for a very small number of glaciers, empirical evidence on a regional or global scale is largely incomplete, both spatially and temporally. The reconstruction of past glacier states by automatic numerical methods could fill this lack of information. Such reconstructions play a major role to fully understand the sea-level budget. They are crucial in terms of model validation, can be used to detect and improve model uncertainties, and they increase the confidence in projections. A framework, which provides all requirements to obtain these reconstructions is the Open Global Glacier Model (OGGM). It is an open source numerical glacier model, that is globally applicable by modeling each glacier individually, and developed for the simulation of glacier changes. OGGM comprises data downloading tools (e.g. for glacier outlines, topography), a preprocessing module, a mass-balance model, a distributed ice-thickness estimation model, and an ice flow model. However, providing realistic glacier changes with OGGM during the course of the entire 20th century requires an adequate initial state for every of the $\sim$200.000 glaciers worldwide. To find these initial states, this thesis presents an approach using the only given information for every individual glacier: past climate information and present-day geometry. Synthetic experiments showed that even under perfectly known but incomplete boundary conditions, this is an ill-posed inverse problem, leading to non-unique solutions. Therefore, an ensemble approach is used to narrow the range of possible initial glacier states. The method is composed of three parts: (i) a large set of physically plausible glacier candidates for a given year in the past (e.g.1850) is generated, (ii) a selection of them is then modeled forward to the date of the observed glacier outline and (iii) evaluated by comparing the results of the forward run to the present-day states. The synthetic environment enables the determination of the accuracy of the method, but on the other hand comparisons with real world observations are not possible. In order to facilitate such comparisons, a glacier-specific calibration of the mass balance model is introduced. This procedure finally allows for a validation.

Zusammenfassung

Massenänderungen von Gletschern sind eine der Hauptursachen für den bisherigen Meeresspiegelanstieg und sie werden auch im 21. Jahrhundert einen wesentlichen Beitrag dazu leisten. Trotz ihrer großen Bedeutung, ist das Wissen über vergangenge Gletscheränderungen sehr begrenzt. Zwar existieren detailierte Beobachtungen für einige wenige Gletscher, aber empirische Nachweise auf regionaler bzw. globaler Skala sind lückenhaft, sowohl räumlich als auch zeitlich. Rekonstruktionen vergangener Gletscherzustände mit Hilfe automatisierter, numerischer Methoden könnten diese Wissenslücke füllen. Diese Rekonstuktionen spielen eine wichtige Rolle, um die Veränderungen des Meerespiegels vollständig zu verstehen. Außerdem sind sie unerlässlich für die Modell-Validierung, sie werden benutzt um Modellfehler zu erkennen und zu beheben und sie steigern die Verlässlichkeit für Zukunftsvorhersagen. Ein Modell, welches alle notwendigen Vorraussetzungen mitbringt um Rekonstruktionen zu erzeugen, ist das Open Global Glacier Model (OGGM). Es ist quelloffen, global anwendbar, indem es jeden Gletscher individuell modelliert und wurde speziell für die Simulation von vergangenen und zukünftigen Gletscheränderungen entwickelt. OGGM umfasst Werkzeuge zum Herunterlanden von Daten (z.B. Gletscherumrisse, Topographie), Module zur Vorverarbeitung, ein Massenbilanz-Modell, ein Modell zur Schätzung der Eisdicke und ein Eisstrom-Modell. Um jedoch realistische Gletscheränderungen aus dem 20. Jahrundert mit OGGM zu berechnen, wird ein entsprechender Anfangszustand für jeden einzelnen der $\sim$200.000 Gletscher weltweit benötigt. Um diese Anfangszustände zu finden, stellt diese Arbeit ein Konzept vor, das ausschließlich auf Informationen basiert, die für jeden Gletscher vorhanden sind: Daten über das vergangene Klima und den heutigen Zustand des Gletschers. Dank synthetischer Experimente wurde herausgefunden, dass dieses inverse Problem selbst unter idealen Vorraussetzungen, aber mit unvollständigen Randbedingungen, schlecht konditioniert ist und somit zu nicht eindeutigen Lösungen führt. Daher wurde ein Ensemble-Ansatz genutzt, um die Spanne möglicher Anfangszustände einzugrenzen. Die Methode setzt sich aus drei Teilen zusammen: Zunächst wird eine große Menge physikalisch plausibler Gletscher-Kandidaten für ein gegebenes Jahr in der Vergangenheit (z.B. 1850) generiert. Eine Auswahl davon wird dann bis zum Zeitpunkt der Beobachtung des Gletscher-Umrisses vorwärts modelliert. Abschließend werden diese durch Vergleich mit den heutigen Gletscher-Zuständen evaluiert. Die synthetische Umgebung ermöglicht zwar die Bestimmung der Genauigkeit der Methode, andererseits sind Vergleiche mit realen Beobachtungen damit nicht möglich. Deshalb werden die synthetischen Experimente weiter entwickelt und um eine Gletscher spezifische Kalibrierung des Masse-Bilanz-Models erweitert. Dieses Verfahren ermöglicht schließlich die Validierung.

Contents

List of Abbreviations

Abbreviation	Description
ASTER	Advanced Spaceborn Thermal Emission and Reflection Radiometer
CMIP	Coupled Model Intercomparison Project
CPU	Central Processing Unit
CRU	Climatic Research Unit
DEM	Digital Elevation Model
ELA	Equilibrium Line Altitude
FoG	Fluctuations of Glaciers
GDEM V2	Global Digital Elevation Model Version 2
GIMP	Greenland Mapping Project
GLIMS	Global Land Ice Measurements from Space
GMSLR	Global Mean Sea-Level Rise
HISTALP	Historical Instrumental Climatological Surface Time Series Of The Greater Alpine Region
IPCC	Intergovernmental Panel on Climate Change
MAE	Mean Absolute Error
MBE	Mean Bias Error
OGGM	Open Global Glacier Model
RAMP	Radarsat Antarctic Mapping Project
RCP	Representative Concentration Pathways
RGI	Randolph Glacier Inventory
RMSE	Root Mean Square Error
SIA	Shallow Ice Approximation
SLE	Sea Level Equivalent
SLR	Sea Level Rise
SRTM	Shuttle Radar Topography Mission
WGI	World Glacier Inventory
WGMS	World Glacier Monitoring Service
WRF	Weather Research Forecasting Model

1 Introduction

1.1 Distribution of Glaciers in the World

Glaciers exists where climate conditions and topographic characteristics allow snow to accumulate over several years and finally transform to ice (Vaughan et al., 2013). The first complete global inventory of glacier outlines[1], the Randolph Glacier Inventory (RGI), was released in 2012 and further developed in the last years (RGI Consortium, 2017). The current version 6 of the RGI counts 216 502 glaciers, covering a total area of 705 739 km^2 worldwide. The majority of the glacierized area is located in the Antarctic and Subantarctic (region 19, 132 867 km^2), followed by Arctic Canada North (region 3, 105 111 km^2). On the contrary, the smallest amount of ice can be found in the Caucasus and Middle East (region 12, 1 307 km^2), as well as New Zealand (region 18, 1 162 km^2). However, Figure 1.1 illustrates that glaciers

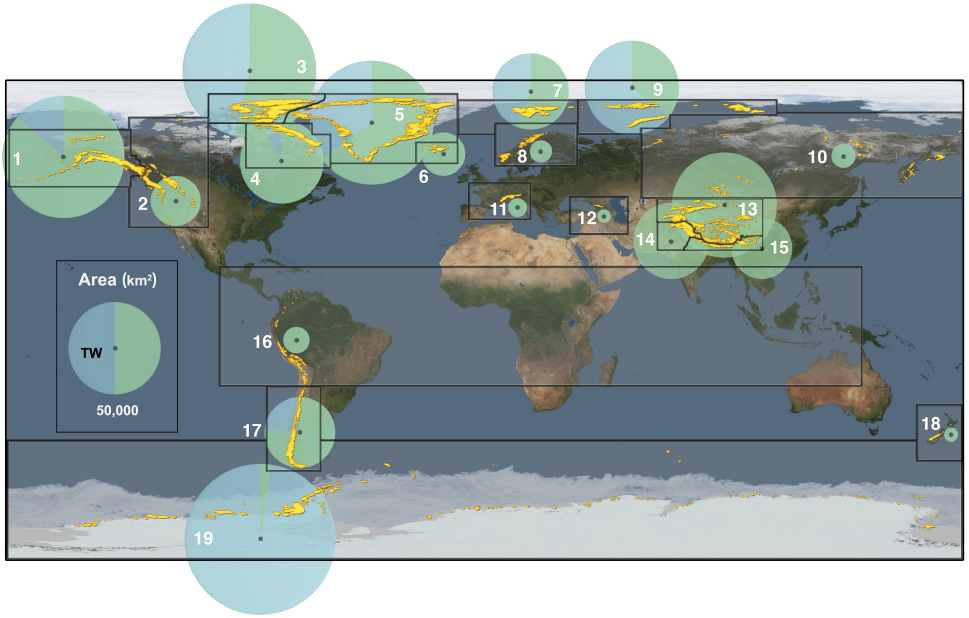

Fig. 1.1: Global distribution of glaciers (in yellow) and area (diameter of circles) per region. Adapted from Vaughan et al. (2013), using RGI version 3

are located in all latitudes and continents of the world. They can be found even in the tropics , e.g. Central Asia, but also Africa and Indonesia.

[1] excluding the Greenland and Antarctic ice sheets

It has to be noted that the RGI does not contain glacierets and other very small glaciers, as all outlines with a size smaller than 0.01 km^2 are not accounted for (recommended minimum-area threshold from the World Glacier Inventory (WGI)). Assuming an inverse power-law scaling, the underestimation of the global total glacierized area due to missing small glaciers/glacieretes is between zero and an upper bound of 1.1–1.4% (Pfeffer et al., 2014). This small error of the present day inventory can result in proportional large errors while e.g. reconstructing these glaciers. Parkes and Marzeion (2018) showed that the disappeared ice mass of missing glaciers accounts for a sea-level equivalent (SLE) of approximately 16.7 to 48.0 millimetres from 1901-2015.

1.2 Glaciers in the Climate System

To understand the behavior of glaciers, it is useful to see them as systems consisting of inputs, stores, transfers and outputs. All processes that add mass to the glacier system present the input and can be summarized under the term accumulation. Usually the most important source is snowfall, but also freezing rain, solid precipitation, windblown snow or avalanches can lead to mass gain. The amounts of the individual contributors vary strongly from location to location and differs throughout the year. Each year new snow layers are build up and compress the previous ones. Under its own weight, the snow first transform to firn and later to ice. Driven by gravity, the glacier flow transfers ice to areas where ice is lost. All processes that reduce the mass of a glacier present the output of the system and are referred as ablation. Surface melting is the most dominant ablation process (for most land-terminating glaciers), but also evaporation, sublimation, scourcing by wind, frontal ablation and avalanching can play important roles (Benn and Evans, 2010).
With this, glaciers can be divided into two parts: the accumulation area, where annual accumulation exceeds mass loss and the ablation area, where annual ablation exceeds mass gain. The two areas are separated by the equilibrium line, where mass gain is equal to mass loss. Its position is called equilibrium line altitude (ELA) and is closely linked to climate conditions. The ELA rises in response to decreasing winter precipitation and/or increasing summer air temperatures, and vice versa (Benn and Evans, 2010). As air temperature decreases with increasing altitude, the topography also plays an important role. Under constant climate conditions a glacier shows a constant ELA, which implies that the amounts of mass gain in the accumulation area and of mass loss in the ablation area are in balance and the glacier has thus established a constant geometry.
However, the climate is not constant in reality and thus, the ELA fluctuates and the glacier responds to climate change with glacier advance or retreat (Leclercq, 2012). Compared to pre-industrial times, the global mean near surface temperatures

increased by approximately $0.87°$C for the decade 2005-2016, but in most land regions (where glaciers are located) a stronger warming has been evident (Allen et al., 2018). Shrinking of glaciers all over the world increases the visibility of climate change for everyone. As glaciers react to climate change, making them so called *climate indicators*. The past decades have been characterized by changing landscapes. The significant change at the Muir Glacier (Alaska) (see Fig. 1.2) is only one example out of thousands. The Glacier Photograph Collection from the National Snow and Ice Data Center contains over 24 000 photographs (as of June 2019), some of them date back to the mid-19th century and therefore provide historical evidence for past glacier change.

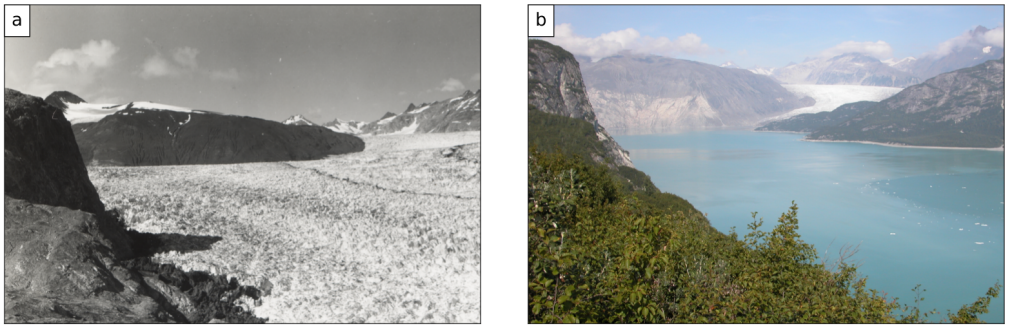

Fig. 1.2: Muir Glacier (Alaska), photographed **a:** by William O. Field in 1941, and **b:** by Bruce F. Molnia on 31.August 2004. source: National Snow and Ice Data Center (comp.) (2002, updated 2019)

Since 1950, most of the world's mountain glaciers are retreating because of global warming, but their response is delayed (Jóhannesson et al., 1989a). Depending on the size of the glacier it can take several decades until the adjustment to a specific change in climate is completed. Consequently, most glaciers are currently larger than they would be if they were in balance with current climate. This will cause continuing glacier mass loss even in the absence of future temperature rise (Church et al., 2013).

Consequences from continuous glacier melt are diverse and cover local, regional and global scales. The local retreat of glaciers can lead to increasing geohazards. For example, glacier lake outburst results from increased water storage behind unstable dams at high altitude and can involve the loss of many lives and cause damages in important infrastructure. An overview of possible glacial hazards is presented in Kääb et al. (2005). However, glaciers are also important regulators of water availability in many regions of the world. Especially in regions with seasonal rainfall, melt water from glaciers is one of the most important water resources during dry seasons. In Southern and Southeastern Asia alone more than 1.4 billion humans depend on the large rivers which are fed by glacier melt water of the Himalayan (Immerzeel et al., 2010). However, beside these wide-ranging local and regional

implications glacier melt is one of the main contributors to the global mean sea-level rise (GMSLR).

1.3 Sea Level Change

Sea-level change is one of the best-known consequences of climate change. Different components of the climate system, like land, ocean, atmosphere and also cryosphere impact the sea-level (Slangen et al., 2017b). Relative to the year 2000 the global mean sea-level is projected to rise 9-18 cm by 2030, 15-38 cm by 2050 and 30-130 cm by 2100 (Sweet et al., 2017). These partly large intervals illustrate that future emission pathways affect the projections for the second half of the century significantly. Hoegh-Guldberg et al. (2019) noted that the global mean sea-level rise (GMSLR) will also continue beyond 2100, but the amount depends strongly on future emissions. The contribution from thermal expansion will increase with global warming 0.20 to 0.63 m $^{\circ}C^{-1}$ (Hoegh-Guldberg et al., 2019). Rises of several meters could result from long-term mass losses by ice-sheets (Church et al., 2013) and this contribution is possibly not reversible independent on the (plausible) future scenario (Hoegh-Guldberg et al., 2019). In contrast, the contribution of glaciers will decrease over time in conjunction with their smaller total mass starting with a value of about 0.21 m $^{\circ}C^{-1}$. The total future contribution from glaciers is calculated to meet a vaule of 0.6 m. But sea level change can be observed already today and even in the past. Using long tide gauge records and satellite altimetry data (available since 1993), the GMSLR is estimated at a value of approximately 20 cm since 1900 (Rhein et al., 2013). From that, roughly 7 cm are occurred in the short interval from 1993 onward (Sweet et al., 2017). Walsh et al. (2014) noted that this recent rise was much faster than at any time over the last 2000 years. Although the contribution of the Greenland and Antarctic ice sheets increased since the early 1990's, ocean thermal expansion and ice mass loss from glaciers all over the World (excluding Antarctic glaciers and the ones on Greenlands periphery) are the dominant contributors to GMSLR of the 20th century (Church et al., 2013).

1.4 Glacier Response Time

A change in mass balance, which means in climate conditions, takes time to translate into a change in glacier geometry (Cuffey and Paterson, 2010). The response is therefore delayed and it can take from decades to thousands of years until a glacier adjusts its geometry. The timescale over which a glacier responds to past climate changes is referred as response time of a glacier. Its determination was the topic of multiple studies in the past (e.g. Nye and Frank, 1960; Jóhannesson et al., 1989a;

Oerlemans, 1997b; Bahr et al., 1998; Raper and Braithwaite, 2009; Harrison, 2013; Zekollari and Huybrechts, 2015). However, the utilization of this term in several different ways in the literature caused confusion (Benn and Evans, 2010). Bahr et al. (1998) defined the response time as "the time required to move from one steady state [...] to another steady state following a change in the mass balance environment". Whereas others (e.g. Oerlemans, 1997b; Jóhannesson et al., 1989a; Cogley et al., 2011; Harrison, 2013) define the response time as the time the glacier takes to complete *most* of its adjustment. But the term 'response time' is also used as a synonym of the 'reaction time', the time lag between the climatic change and the first sign of change in glacier length (Benn and Evans, 2010).

The first analytic attempt to determine the response time T_M was based on linear kinematic wave theory (Nye and Frank, 1960; Nye, 1963; Nye, 1965), in which the response time is determined as the ratio between the glacier length l and the velocity at the terminus $u(l)$:

$$T_M \sim \frac{l}{u(l)} \tag{1.1}$$

Results derived from kinematic wave theory estimate the response time of even small glaciers to be in order of 10^2 to 10^3 years, but Wal and Oerlemans (1995) showed that the kinematic approach usually leads to a strong overestimation. As a consequence Jóhannesson et al. (1989a) and Schwitter and Raymond (1993) suggested a multiplication of Eq. (1.1) with the shape factor (ratio of mean thickness change to local thickness change at the terminus). A problem is that Eq. (1.1) as well as the variation using the shape factor are sensitive on details at the terminus. Thus, Jóhannesson et al. (1989a, 1989b) provided the following estimate of T_M:

$$T_M \sim \frac{h}{-b(l)} \tag{1.2}$$

where h is the ice thickness scale of the glacier and $b(l)$ the ablation rate at the terminus. Jóhannesson et al. (1989b) showed that Eq. (1.2) leads to estimates in order of 10^1 to 10^2 for typical glaciers ($h \sim 100 - 500$ m, $-b(l) \sim 1 - 10$ ma^{-1}). But h is not clearly defined (Zekollari et al., 2014): Pelto and Hedlund (2001) e.g. used the maximum ice thickness over the glacier, to obtain an upper bound of T_M, whereas e.g. Harrison et al. (2001) suggested to define h as the ratio of volume change to area change.

Oerlemans (1997b) presented a different approach and defined the response time as the e-folding time. This is the time taken to achieve a proportion ($\frac{1}{e}$) of the total net change. The volume response time T_V is defined as the time it takes to go from one steady state (with volume V_1) to another steady state (with volume V_2) under a given climate change:

$$T_V = t\left(V = V_2 - \frac{V_2 - V_1}{e}\right) \tag{1.3}$$

This assumption rely on the idea that the glacier approaches the new equilibrium state following an exponential curve, implied by an rapid initial change. Accordingly, the response time for glacier length can be written as:

$$T_L = t\left(L = L_2 - \frac{L_2 - L1}{e}\right) \tag{1.4}$$

Ice volume is more directly affected by changes in specific mass balance and consequently T_V is usually smaller than T_L (Oerlemans, 1997b).

Apart from the fact that determining the response time of a glacier is not straightforward, all theories are based on steady glacier states and constant changes in climate and do not take into account that a change in climate condition is continuous. Thus a steady state can never be achieved, due to the non-steady climate (Schwitter and Raymond, 1993; Pelto and Hedlund, 2001). Nevertheless, all of these theoretical studies show that many factors influence the future development of a glacier, i.e. its size, slope, elevation range, distribution of area with elevation, and its surface characteristics (Vaughan et al., 2013). All these factors can vary from region to region, but also between neighbouring glaciers.
The delayed glacier response also illustrates that past climate conditions still influence the present state of the cryosphere. Currently, glaciers are larger than they would be, if they were in balance with the current climate and even if temperatures stabilize, glacier mass loss will continue over the next decades (Hoegh-Guldberg et al., 2019). Marzeion et al. (2018) showed that $36 \pm 8\%$ of mass loss is already committed in response to past greenhouse gas emissions and consequently future emissions will have only very limited influence on glacier mass change in the twenty-first century.

1.5 Glacier Observations

Various observation techniques have been developed in the past to measure glacier changes. The broad range of methods includes complex climate-related measurements at a few single glaciers, mass balance measurements at about a hundred glaciers, glacier length variations for a few hundred glaciers, and geodetic area and volume changes at regional scales based on remote sensing techniques (Vaughan et al., 2013). The worldwide collection of information about glacier changes was initiated in 1894 (Zemp et al., 2014). Today, the World Glacier Monitoring Service (WGMS) collects standardized observations on changes in mass, volume, area and length of glaciers with time. However, especially in situ measurements (e.g. length variations and direct mass balance observations) are biased towards accessible

glaciers in the world. On the other hand, these observations go further back in time than non biased satellite observations starting with the beginning of the Landsat missions in 1972.

1.5.1 Glacier Length Variations

Glacier length variations are usually obtained through annual measurements of the terminus position, but they can also be reconstructed from geomorphologic landforms (e.g. moraines), biological (e.g. overridden trees, lichens) (e.g. Bushueva et al., 2016) or historical evidence such as paintings, photos and early maps (e.g. Nussbaumer and Zumbühl, 2012). The first direct measurement of glacier length dates back to the 19th century (Zemp et al., 2015). Over the past decades, satellite imaging and aerial photography allowed to detect the terminus positions also in regions that are difficult to access and the number of measurements increased strongly.

The current version of the Fluctuations of Glaciers (FoG) Database from WGMS (2018) includes 45.214 length observations for 2500 glaciers and covers the time period from 1600-2017. The spatial distribution of the length observations covers all regions. Central Europe, Scandinavia, Iceland, Western North America, New Zealand and the Southern Andes are the best covered regions (half or more of the glacierized area is covered), whereas only limited information for glaciers around the Greenland and Antarctic ice sheets, Arctic Canada, Asia and the Low Latitudes are available.

Zemp et al. (2015) showed that glacier retreat has been dominant in the last 100-150 years. Cumulative values for large, land-terminating glaciers typically reach a few kilometers. Periods of re-advancement can be found e.g. in the Alps (around 1920 and 1970) and in the 1990s in Scandinavia, but the advances are small (a few 100 m only) compared to the observed retreat (Marzeion et al., 2016). The identification of the advancement periods is impeded by the different response times. Individual glaciers readvance in different years and some glaciers did not show a readvance at all (Zemp et al., 2015).

Leclercq et al. (2014) presented a worldwide dataset of long-term length fluctuations for 471 glaciers, which is meanwhile included in the WGMS database. Only records starting before 1950 and covering several decades are included in Leclercq's dataset. The length of the records vary largely, the shortest record covers 40 years and the longest 450 years. Most of the observations start in the 19th century, only 30 records date back to 1700 and the first observation stems from 1535. The records are spatially well distributed over all continents and almost all latitudes. However, for some regions with large glacier coverage (e.g. Alaska, Antarctic periphery) the number of records is sparse, whereas for other regions (e.g. Scandinavia, Pyrenees,

Alps, Caucasus) more information are available. Equally to Zemp et al. (2015), Leclercq et al. (2014) discovered a global trend of glacier retreat since the middle of the 19th century. The median retreat rate is with a value of 12.5 m yr^{-1} larger in the period from 1921-1960 than in the second half of the 20th century (7.4 m yr^{-1} in 1961-2000). The global mean length change in the 20th century is -1.56$\pm$ 0.03 km, but records from this time period vary widely on an individual and also regional scale.

Length change observations were used in several studies to determine the glacier contribution to sea-level change. For example, Oerlemans et al. (2007) scaled global relative length changes to global relative volume changes. These are then translated to global glacier mass loss by using a calibration against the global glacier mass loss estimates over the period 1961-2000 from Dyurgerov and Meier (2005). The same method was used in Leclercq et al. (2011), but with a more extended data set (more glacier length fluctuations and more geodetic mass balance observations from Cogley (2009)). An update of Leclercq et al. (2011), containing again additional data for length observations and geodetic mass balance, finally resulted in an estimate of of 80.4 $\pm$ 21.1 mm SLE for the glacier contribution during the 20th century (Marzeion et al., 2015).

1.5.2 Glacier Mass Balance

A net change in mass of a glacier over a specific time period is defined as mass balance. Often annual changes are measured, but the definition of one "year" can vary between different studies. Common time systems used are the balance year (also known as stratigraphic system), the fixed-date system and the floating-date system (Cogley et al., 2011). The balance year covers the period between the two successive annual minima in mass of the glacier. In the fixed-date system a year always starts at the same calender date, e.g. in the mid and high latitudes of the northern hemisphere this often corresponds to the time between 1 October and 30 September. In the floating-date system a year is defined by the calendar dates of the two successive surveys, which may vary from year to year, because the visit of field sites is not always possible at a pre-defined date. The different types of glacier mass balance measurements range from direct (also known as glaciological methods) over hydrological, geodetic and gravimetric methods.
The oldest method to derive glacier mass balances is the direct method, which is based on field measurements of the total accumulation and ablation. The accumulation can be measured by the snowpack depth, which can be obtained from ice cores, snowpits or crevasses. Annual increase can be identified from changes in density, from crystal size or by a dirt layer (Benn and Evans, 2010). The net annual accumulation consequently can be calculated from the thickness of the layer and

the average density of the layer. The ablation is measured with the help of stakes, drilled into the ice. They are used to measure the drop of ice surface over the year. As all direct measurements are only point measures on parts of the glacier surface, interpolation and extrapolation methods are used to calculate the total net balance of the whole glacier area. The annual mass balance (b_n) can be described as the sum of the mass change during the accumulation period (winter balance) and the mass change during the ablation period (summer balance). Often, the term mean specific mass balance is used. This refers to the total change in mass divided by the the area of the glacier (e.g. as in WGMS, 2018). Mass balance changes are typically given in water equivalent (w.e.) which allows a better comparison between different glaciers and years. The World Glacier Monitoring Service (WGMS) collects and publishes information about glacier mass balance changes. The latest release of the Fluctuations of Glaciers (FoG) database contains 6986 annual mass balances from 459 glaciers, but only 30 of them (so called reference glaciers) have a continuous series going back to 1976. (Zemp et al., 2019).
The WGMS additionally collects mass balance measurements obtained through geodetic methods. They rely on aerial photographs or on satellite data to determine volume changes, which then can be converted to mass changes by using estimates of the average density for the different parts of the glacier (Benn and Evans, 2010). Geodetic mass balance observations have a better spatial coverage than the direct methods and are not biased to accessible glaciers only in contrast to the direct measurements. The current version of the Fluctuations of Glaciers (FoG) database contains geodetic mass balance measurements for 19 130 glaciers and thus cover 9% of the total number of glaciers, compared to the 1% coverage from the direct methods Zemp et al. (2019). A significant disadvantage is the lack in temporal resolution. Airborne and spaceborne surveys usually only cover multiyear or even only decadal periods Zemp et al. (2019). Furthermore, they do not date back as long as the direct measurements.

1.6 Numerical Glacier Models

In the past, many different types of numerical glacier models were developed. The existing models can be divided into two classes: diagnostic and prognostic models. Diagnostic simulations are used to study parts of the glacier or a specific physical process in great detail, whereas prognostic models simulate the glacier evolution to predict e.g. the change in geometry or ice thickness in time. Consequently, they usually combine two fundamental processes. First, they have to model the change in mass (accumulation and ablation) at the surface of the glacier. To this end, different mass balance models were developed. Secondly, they have to model the resulting change of the glacier (e.g. through a change in ice flux). Depending on the purpose

of the study different levels of complexity are necessary. With increasing complexity also computational costs increase and often more input data and with this a better knowledge of the glacier system is required. Thus, less complex models are used to study e.g. all glaciers in the world or large regions to compute their contribution to sea level change, whereas higher complexity is necessary to get detailed insights in very narrow areas and for a better understanding of physical principals.
Basically two types of mass balance models exists. Energy-balance models evaluate detailed surface energy fluxes, whereas the more simple temperature-index approaches (also called degree-day models) basically use the air temperature to compute glacier melt and snow accumulation can be derived from precipitation using an air temperature threshold. Most models additionally apply some kind of bias correction and derive model parameters (e.g. degree-day factor, precipitation correction factor, temperature and/or precipitation lapse rates, temperature bias and a rain-snow temperature threshold) through a model calibration with available glacier mass balance observations. In global approaches, temperature-index models are usually used because of their simplicity (e.g. Marzeion et al., 2012b; Radić et al., 2014; Hirabayashi et al., 2013; Huss and Hock, 2015), but simple energy-balance models also allow an application on a global scale (e.g. Giesen and Oerlemans, 2013).
Beside the different complexities of the mass balance models, glacier models can also differ in their dimension: simplest models only have one dimension (e.g. depth-integrated flowline models), while more complex models include a spatial distribution in two or three dimensions. Another type of complexity is the approximation of ice dynamics from the Shallow Ice Approximation (SIA) over Higher-Order models to Full Stokes. The Full Stokes equations are based on the equations of mass balance and momentum balance adapted for the incompressible material ice. The very high computational effort needed to solve them can be reduced by using e.g. the Higher Order approximation derived by Blatter (1995) and Pattyn (2003). They assume the horizontal gradient of the vertical velocity are negligible compared to the vertical gradient of horizontal velocities and they ignore bridging effects. SIA goes one step further and keeps only the vertical gradients of the vertical shear stresses and pressure gradients from the original Full Stokes equations.

There even exists models without any ice dynamics, e.g. Volume-Area scaling approaches (Chen and Ohmura, 1990; Bahr et al., 1997). For this approach the glacier volume V, which is hard to measure, is estimated from the often known area A using the following power law:

$$V = cA^y \tag{1.5}$$

The parameter y is usually a constant and the recommended value for glaciers is $y = 1.35$ (e.g. Bahr et al., 1997; Dyurgerov et al., 2009), whereas c should not

be treated as a constant value. Even though Eq. (1.5) does not explicitly show a dependence in time, the terms V, A and c can vary in time (Bahr et al., 1998). A similar method is the Volume-Length scaling, for which in Eq. (1.5) the glacier area A is replaced by its length L (e.g. Hirabayashi et al., 2013; Radić et al., 2014).
In order to provide volume changes over time (e.g. for hindcast simulations or projections) the scaling approach can be combined with a surface mass balance model. Since 1988, the volume-area scaling approach was applied in more than 60 studies (Bahr et al., 2015) and is often used to calculate glacier contributions to sea level change. Its simplicity allows the application on a global scale. For this purpose each glacier can be modelled individually (as in Marzeion et al., 2012b; Hirabayashi et al., 2013; Radić et al., 2014) or a subset can be explicitly modelled and the remaining glaciers are then upscaled (like in Giesen and Oerlemans, 2013) or the scaling method can be applied for different glacier size classes as in Slangen et al. (2012).
Although all scaling approaches produce consistent results on the global scale, greater uncertainties on regional and local scales originate from e.g. the missing representation of the glacier geometry, ice dynamics or the accounting for frontal ablation. For this reasons, Huss and Hock (2015) presented the first global glacier evolution model, which includes mass loss due to frontal ablation and accounts for glacier advance/retreat and surface elevation changes. The model is based on the Δh-parameterization from Huss et al. (2010) and was applied on a global scale.
Another way to include simple ice dynamics is realized by flowline models. These approaches simulate the ice flow along a single line, the flowline of the glacier. Flowlines can be obtained by intensive manual digitization (e.g Oerlemans, 1997a; Sugiyama et al., 2007), but also through automated algorithms, which are for instance based on hydrology tools (Schiefer et al., 2008) or centerlines[2] can automatically be calculated by a least-cost route on a cost grid (Kienholz et al., 2014). The latter approach has the main advantage that multiple centerlines per glacier can be derived and the main branch as well as major tributaries are well represented.
Flowline models solve the model equations along this line, and then spatially interpolate the result over the complete area of the glacier. To derive estimates of ice thickness, methods rely on the parameterization of basal shear-stress (e.g. Linsbauer et al., 2009; Linsbauer et al., 2012), on observed surface velocities (e.g. Gantayat et al., 2014) or on mass conservation (e.g. Farinotti et al., 2009; Clarke et al., 2013; Maussion et al., 2019). A detailed review of the different methods can be found in Farinotti et al. (2017). The first ice thickness model applied on a global scale is presented in Huss and Farinotti (2012). Their approach is a further development of Farinotti et al. (2009). To avoid the manual digitization of flowlines, the method is applied on elevation bands, instead of flowlines. Using an ensemble of up to five

[2]Centerlines can differ slightly from flowlines, mostly in areas with converging branches. Instead of running side by side to the glacier terminus (as in Farinotti et al., 2009), centerlines will converge (Kienholz et al., 2014).

models, Farinotti et al. (2019) presents a consensus with distributed ice thickness estimates of all glaciers in the world.

Oerlemans (1997a) developed the first prognostic flowline model which assumes a trapezoidal bed shape and includes simple shearing flow and sliding. The change of ice thickness over time is defined by a non-linear diffusion equation. A similar approach was adopted by Maussion et al. (2019) and Zekollari et al. (2019). However, none of the recent studies presented past or future glacier changes on the global scale.

1.7 Thesis Objectives

In order to reconstruct glacier mass changes over the course of the entire 20th century, global glacier models are absolutely essential. However, this requires automatic initialization methods. To this aim, the main objective of this thesis is:

1. The development of an initialization method that allows the reconstruction of past glacier states by using only information about the past climate and the present day states.

The method is based on synthetic experiments and thus a further development becomes necessary in order to succeed with the second objective:

2. The application to real-world cases.

Finally, the performance of the initialization method should be analyzed. To this aim, the third objective is:

3. The identification of uncertainties of the initialization method itself and its validation by comparing the modeled glacier changes with glacier observations.

1.8 Thesis Outline

This thesis presents a new method for the initialization of the Open Global Glacier Model (OGGM) that allows the reconstruction of past glacier states. An overview of relevant facts related to glaciers and glacier modeling was given in this Chapter 1. First, a data set containing a global inventory of glaciers was presented to give an overview about the distribution of glaciers over the world. Next, fundamental principles of glacier mass balance were explained and the influence of a changing

climate on the world's glaciers was discussed, followed by information about sea-level changes in the past and future. As the response of glaciers to changes in climate is delayed, the next part presented fundamental aspects of the glacier response time theory. Afterwards an overview about the state-of-the-art of numerical glacier models and various glacier observation techniques that provide information about the temporal evolution of glacier changes in the past were presented.

The Open Global Glacier Model (OGGM), the model for which the initialization method is developed, is presented in Chapter 2. This section shows profound principles of the model, as well as the general workflow and a detailed explanation of important modules.

Chapter 3 introduces the new initialization method which was developed in order to initialize OGGM in the past by only using information about the past climate ant the present day state. In the first instance, the method is applied for synthetic experiments only. The motivation and the design of the synthetic experiments are described first. Afterwards, the workflow of the method and the results from the application to 2660 Alpine glaciers is presented. Finally, the uncertainty of the method is identified and glacier characteristics that influence the reconstructability are determined.

Chapter 4 address the problem of real-world applications. To this end, a glacier-specific calibration of the mass balance offset is introduced. This improvement enables the presented validation of the method trough glacier observations. For this purpose observations of glacier length fluctuations and mass balance changes are taken into account. The good agreement between the modeled and observed glacier changes open the door to a future global application. Chapter 5 summarizes all results and gives perspective ideas.

2

The Open Global Glacier Model (OGGM) v1.1

Published 2019 in *Geoscientific Model Development*, **12**, pages 909–931

Authors and Affiliations

Fabien Maussion [1], Anton Butenko [2], Nicolas Champollion [2], Matthias Dusch [1], Julia Eis [2], Kévin Fourteau [1,3], Philipp Gregor [1], Alexander H. Jarosch [1], Johannes Landmann [1,4,5], Felix Oesterle [1,6], Beatriz Recinos [2,7], Timo Rothenspieler [2], Anouk Vlug [7,8], Christian T. Wild [1,9] and Ben Marzeion [2,7]

1 Department of Atmospheric and Cryospheric Sciences, Universität Innsbruck, Innsbruck, Austria
2 Institute of Geography, University of Bremen, Bremen, Germany
3 Université Grenoble Alpes, CNRS, IRD, Grenoble INP, IGE, 38000 Grenoble, France
4 Laboratory of Hydraulics, Hydrology and Glaciology (VAW), Swiss Federal Institute of Technology (ETH), Zürich, Switzerland
5 Swiss Federal Institute for Forest, Snow and Landscape Research (WSL), Birmensdorf, Switzerland
6 Institute of Mountain Risk Engineering, University of Natural Resources and Life Sciences, Vienna, Austria
7 MARUM - Center for Marine Environmental Sciences, Bremen, Germany
8 Faculty of Geosciences, University of Bremen, Bremen, Germany
9 Gateway Antarctica, Centre for Antarctic Studies and Research, University of Canterbury, Christchurch, New Zealand

Context

To provide estimates about the contribution of glacier mass change to global sea-level rise, global glacier models are the most relevant tools. They can be used to estimate the present day state of glaciers (e.g. Farinotti et al., 2019), to provide glacier mass change projections (e.g. Hock et al., 2019), and they are useful to reconstruct

past changes. These reconstructions play a major role to fully understand the sea-level budget e.g. to close the budget of the observed SLR. Additionally, they are crucial for the model validation and can be used to detect and improve model uncertainties. Consequently, the confidence in projections of future glacier mass change will increase, if we manage to reproduce past glacier mass change (Marzeion et al., 2015). Despite their importance, so far only one global model (Marzeion et al., 2012b) was able to provide estimates over the course of the entire 20th century. In fact, global estimates exclusively based on mass and length change observations exist (e.g. Leclercq et al., 2011), but a large uncertainty originate from the large under-sampling of the world's glaciers. Long-term observations of glacier changes are only available for a few hundreds of glaciers (see Sect. 1.5) and remote sensing derived observations have a good spatial coverage, but they do not date back far enough. Thus, the global representation of the available sample is questionable and can be verified only for periods where global observations exists (Marzeion et al., 2015). It is therefore a pressing task to develop more approaches that enable the global reconstruction of past glacier mass change based on glacier modeling e.g. like the study from Marzeion et al. (2012b). To this end, this Chapter presents the Open Global Glacier Model (OGGM; `www.oggm.org`), which combines the mass balance model from Marzeion et al. (2012b) with an ice-flow model and thus more complexity (e.g. in ice dynamics) is added. The model is developed to provide a modular and open source numerical model framework for simulating glacier change in the past and future on a global scale. The paper provides detailed information about the model including the presentation of the model workflow, a detailed description of the model structure and the individual modules (including specific model parameters and their default values). With global simulations under idealized climate forcing, we were able to show that the model behavior is realistic and the results are close to expectations. The studies presented in the following chapters, rely on this model and thus the detailed model description in this chapter is so important and form the basis of this thesis.

Personal Contribution

J. Eis developed the glacier partitioning tool (see Sect. 2.3.6.3). This includes the implementation and testing of this external OGGM module and its documentation including the supply of examples. J.Eis was involved in the development of the manuscript by critically discussing the presented results and early drafts of the manuscript. Moreover, J. Eis contributed to the general development of OGGM. For example, with code developments, issue and bug reports and their correction, as well as further additions to the documentation. All authors continuously discussed the model development including e.g. changes on the code base, potential further

developments, parameter choices and their default settings. A more detailed description about the individual contribution of all authors can be found in the author contribution section on page 52.

Abstract

Despite their importance for sea-level rise, seasonal water availability, and being a source of geohazards, mountain glaciers are one of the few remaining sub-systems of the global climate system for which no globally applicable, open source, community-driven model exists. Here we present the Open Global Glacier Model (OGGM, `www.oggm.org`), developed to provide a modular and open source numerical model framework for simulating past and future change of any glacier in the world. The modelling chain comprises data downloading tools (glacier outlines, topography, climate, validation data), a preprocessing module, a mass-balance model, a distributed ice thickness estimation model, and an ice flow model. The monthly mass-balance is obtained from gridded climate data and a temperature index melt model. To our knowledge, OGGM is the first global model explicitly simulating glacier dynamics: the model relies on the shallow ice approximation to compute the depth-integrated flux of ice along multiple connected flowlines. In this paper, we describe and illustrate each processing step by applying the model to a selection of glaciers before running global simulations under idealized climate forcings. Even without an in-depth calibration, the model shows very realistic behaviour. We are able to reproduce earlier estimates of global glacier volume by varying the ice dynamical parameters within a range of plausible values. At the same time, the increased complexity of OGGM compared to other prevalent global glacier models comes at a reasonable computational cost: several dozen glaciers can be simulated on a personal computer, while global simulations realized in a supercomputing environment take up to a few hours per century. Thanks to the modular framework, modules of various complexity can be added to the codebase, which allows new kinds of model intercomparisons studies in a controlled environment. Future developments will add new physical processes to the model as well as automated calibration tools. Extensions or alternative parameterizations can be easily added by the community thanks to a comprehensive documentation. OGGM spans a wide range of applications, from ice-climate interaction studies at millenial time scales to estimates of the contribution of glaciers to past and future sea-level change. It has the potential to become a self-sustained community-driven model for global and regional glacier evolution.

2.1 Introduction

Glaciers constitute natural low-pass filters of atmospheric variability. They allow people to directly perceive slow changes of the climate system, that would otherwise be masked by short-term noise in human perception. Since glaciers form prominent features of many landscapes, shrinking glaciers have become an icon of climate change.

However, impacts of glacier change – whether growth or shrinkage – go far beyond this sentimental aspect: glaciers are important regulators of water availability in many regions of the world (Kaser et al., 2010; Huss, 2011; Immerzeel et al., 2012), and retreating glaciers can lead to increased geohazards (see Richardson and Reynolds, 2000, for an overview). Even though the ice mass stored in glaciers is small compared to the Greenland and Antarctic ice sheets ($< 1\%$), glacier melt has contributed significantly to past sea-level rise (SLR; e.g. Cogley, 2009; Leclercq et al., 2011; Marzeion et al., 2012b; Gardner et al., 2013). They probably have been the biggest single source of observed SLR since 1900 and they will continue to be a major source of SLR in the 21st century (e.g. Church et al., 2013; Gregory et al., 2013).

It is therefore a pressing task to improve the knowledge of how glaciers change when subjected to climate change, both natural and anthropogenic (Marzeion et al., 2014a). The main obstacle to achieve progress is a severe undersampling problem: direct glaciological measurements of mass balances have been performed on $\sim$300 glaciers world wide ($\approx 0.1\%$ of all glaciers on Earth). The number of glaciers on which these types of measurements have been carried out for time periods longer than 30 years, i.e. over periods that potentially allow for the detection of a climate change signal, is one order of magnitude smaller (Zemp et al., 2009). Length variations of glaciers have been observed for substantially longer periods of time (Oerlemans, 1994; Oerlemans, 2005). These variations are, however, much more difficult to understand, as large glacier length fluctuations may arise from intrinsic climate variability (Roe and O'Neal, 2009; Roe, 2011). Data obtained by remote sensing allow for gravimetric assessments of ice mass change or volume change estimates obtained by differencing digital elevation models. Unfortunately, they are only available for the past decade (e.g. Gardner et al., 2013).

During the past few years, great progress has been made in methods to model glaciers globally (Radić and Hock, 2011; Radić and Hock, 2014; Giesen and Oerlemans, 2012; Giesen and Oerlemans, 2013; Marzeion et al., 2012a; Marzeion et al., 2012b; Marzeion et al., 2014a; Marzeion et al., 2014b; Huss and Hock, 2015). While these approaches yield consistent results at the global scale, all of them suffer from

greater uncertainties at the regional and local scales. These stem from the great level of abstraction of the key processes (Marzeion et al., 2012b; Marzeion et al., 2014b), from the need to spatially interpolate model parameters (Radić and Hock, 2011; Radić and Hock, 2014; Giesen and Oerlemans, 2012; Giesen and Oerlemans, 2013), and from uncertainties of the boundary and initial conditions. All models lack ice dynamics, most lack frontal ablation (with the exception of Huss and Hock, 2015), and all lack modulation of the surface mass balance by debris cover and snow redistribution (wind and avalanches). Only one model (Marzeion et al., 2012b) was able to provide estimates of past glacier volume changes for the 20th century. None of these models is open-source.

Mountain glaciers are one of the few remaining subsystems of the global climate system for which no globally applicable, open source, community-driven model exists. The ice sheet modelling community shows a better example, with models such as the *Parallel Ice Sheet Model* (Winkelmann et al., 2011), *Elmer/Ice* [1], Glimmer-CISM [2], or ISSM [3]. These models have been applied to mountain glaciers as well, but cannot be applied globally out-of-the-box. While the atmospheric modelling community has a long tradition of sharing models (e.g. the *Weather Research and Forecasting model*, or WRF) or comparing them (e.g. the *Coupled Model Intercomparison Project* or CMIP), recent initiatives originating from the glaciological community show a new willingness to better coordinate global research efforts following the CMIP example (e.g. the *Glacier Model Intercomparison Project*[4] or the *Glacier Ice Thickness Estimation Working Group*[5]).

In the recent past, great advances have been made in the global availability of data and methods relevant for glacier modelling, spanning glacier outlines (Pfeffer et al., 2014), automatized glacier centerline identification (e.g., Kienholz et al., 2014), bedrock inversion methods (e.g. Huss and Farinotti, 2012), and global topographic data sets (e.g. Farr et al., 2007). Taken together, these advances now allow the ice dynamics of glaciers to be simulated at the global scale, provided that adequate modelling platforms are available. In this paper, we present the **Open Global Glacier Model (OGGM)**, developed to provide a modular and open source numerical model framework for consistently simulating past and future global scale glacier change.

Global not only in the sense of leading to meaningful results for all glaciers combined, but also for any small ensemble of glaciers, e.g. at the headwater catchment scale. *Modular* to allow different approaches to the representation of ice flow and surface mass balance to be combined and compared against each other. *Open source* so that

[1] `http://elmerice.elmerfem.org/`
[2] `https://csdms.colorado.edu/wiki/Model:Glimmer-CISM`
[3] `https://issm.jpl.nasa.gov/`
[4] `http://www.climate-cryosphere.org/activities/targeted/glaciermip`
[5] `http://www.cryosphericsciences.org/wg_glacierIceThickEst.html`

the code can be read and used by anyone and so that new modules can be added and discussed by the community, following the principles of open governance. *Consistent* between past and future in order to provide uncertainty measures at all realisable scales.

This paper describes the basic structure and primordial assumptions of the model (as of version 1.1). We present the results of a series of single glacier and global simulations demonstrating the model's usage and potential. This will be followed by a description of the software requirements and the testing framework. Finally, we will discuss the potential for future developments that could be conducted by any interested research team.

2.2 Fundamental Principles

The starting point of OGGM is the Randolph Glacier Inventory (RGI; RGI Consortium, 2017; Pfeffer et al., 2014): our goal is to simulate the past and future evolution of all of the 216,502 inventoried glaciers worldwide (as of RGI V6). This "glacier centric" approach is the one followed by most global and regional models to date; its advantages and disadvantages will be discussed in Sect. 2.3.6.4. Provided with the glacier outlines, topographical and climate data at reasonable resolution and accuracy, the model should be able to (i) provide a local map of the glacier including topography and hypsometry, (ii) estimate the glacier's total ice volume and compute a map of the bedrock topography, (iii) compute the surface climatic mass balance and (if applicable) at its front via frontal ablation, (iv) simulate the glacier's dynamical evolution under various climate forcings, and (v) provide an estimate of the uncertainties associated with the modelling chain.

For each of these steps, several choices are possible regarding the input data to be used, the numerical solver or the parameterisations to be applied. Any given choice is driven by subjective considerations about data availability, the estimated accuracy of boundary conditions (such as topography), and by technical considerations such as the available computational resources. In this paper we present one way to realize these steps using OGGM, which to date is in our opinion the best compromise between model complexity, data availability and computational effort. The OGGM software, however, is built in such a way that future improvements and new approaches can be implemented, tested, and applied at minimal cost by ourselves or a larger community.

2.2.1 Example Workflow

We illustrate with an example how the OGGM workflow is applied to Tasman glacier, New Zealand (Fig. 2.1). Here we describe shortly the purpose of each processing step, and more details will be provided in Sect. 2.3:

Preprocessing The glacier outlines extracted from the RGI are projected onto a local gridded map of the glacier (Fig. 2.1a). Depending on the glacier's location, a suitable source for the topographical data is downloaded automatically (here SRTM) and interpolated to the local grid. The map's spatial resolution depends on the size of the glacier (here, 150 m).

Flowlines The glacier centerlines are computed using a geometrical routing algorithm (adapted from Kienholz et al., 2014, Fig. 2.1b), filtered and slightly modified to become glacier flowlines with a fixed grid spacing.

Catchment areas and widths The geometrical widths along the flowlines are obtained by intersecting the normals at each grid point with the glacier outlines and the tributaries' catchment areas (Fig. 2.1c). Each tributary and the main flowline has a catchment area, which is then used to correct the geometrical widths so that the flowline representation of the glacier is in close accordance with the actual altitude-area distribution of the glacier (Fig. 2.1d, note that the normals are now corrected and centred).

Climate data and mass balance Gridded climate data (monthly temperature and precipitation) are interpolated to the glacier location and temperature is corrected for altitude using a linear gradient. These climate time series are used to compute the glacier mass balance at each flowline's grid point for any month in the past.

Ice thickness inversion Using the mass balance data computed above and relying on mass-conservation considerations, an estimate of the ice flux along each glacier cross-section can be computed. By making assumptions about the shape of the cross-section (parabolic or rectangular) and using the physics of ice flow, the model computes the thickness of the glacier along the flowlines and the total volume of the glacier (Fig. 2.1e).

Glacier evolution A dynamical flowline model is used to simulate the advance and retreat of the glacier as a response of the surface mass-balance forcing. Here (Fig. 2.1f), a 100-yr long random climate sequence leads to a glacier advance.

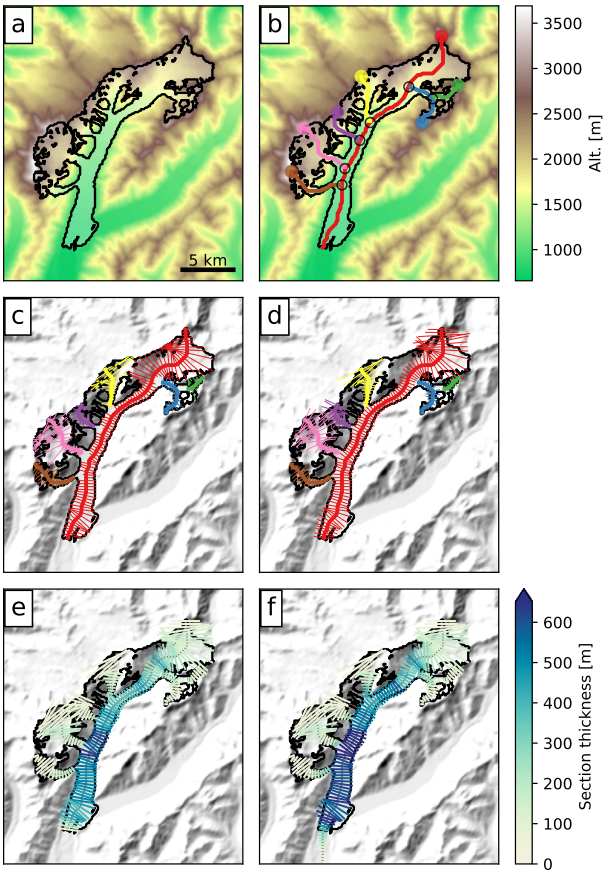

Fig. 2.1: Example of the OGGM workflow applied to Tasman glacier, New Zealand; **a**: topographical data preprocessing; **b**: computation of the flowlines; **c**: geometrical glacier widths determination (the colors indicate the different flowlines); **d**: width correction according to catchment areas and altitude-area distribution (see Fig. 2.2 and main text for details); **e**: ice thickness inversion; **f**: random 100-yr long glacier evolution run leading to a glacier advance. See Sect. 2.2.1 for details.

2.2.2 Model Structure

The OGGM model is built around the notion of tasks, which have to be applied sequentially to single or a set of glaciers. There are two types of tasks:

Entity tasks are tasks which are applied on single glaciers individually and do not require information from other glaciers (this encompasses the majority of OGGM's tasks). Most often they need to be applied sequentially (for example, it is not possible to compute the centerlines without having read the topographical data first).

Global tasks are tasks which are run on a set of glaciers. This encompasses the calibration and validation routines, which need to gather data across a number of reference glaciers.

This model structure has several advantages: the same entity task can be run in parallel on several glaciers at the same time, and they allow a modular workflow. Indeed, a task can seamlessly be replaced by another similar one, as long as the required input and output formats are agreed upon beforehand. The output of each task is made persistent by storage on disk, allowing a later use by a subsequent task, even in a separate run or on another machine. For example, the preprocessing tasks store the topography data in a netCDF file, which is then read by the centerlines task, which itself writes it's output in a vector file format.

In this paper we will refrain from naming the tasks by their function name in the code, as these are likely to change in the future and are sometimes organised in a non-trivial way as a result of implementation details. The next section therefore is called "Modules", where each module can be seen as a collection of tasks developed towards a certain goal.

2.3 Modules

The modules are described in the order in which they are applied for a model run. When we provide a specific value for a model parameter in the text, we refer to the model's default parameter value: it can be changed by the user at runtime.

2.3.1 Preprocessing

The objective of the preprocessing module is to set up the geographical input data for each glacier (the glacier outlines and the local topography). First, a Cartesian local map projection is defined: we use a local Transverse Mercator projection centred on the glacier. Then, a suitable topographical data source is chosen automatically, depending on the glacier's location. Currently we use:

- the Shuttle Radar Topography Mission (SRTM) 90m Digital Elevation Database v4.1 (Jarvis et al., 2008) for all locations in the [60°S; 60°N] range (data acquisition: 2000)

- the Greenland Mapping Project (GIMP) Digital Elevation Model (Howat et al., 2014) for mountain glaciers in Greenland (data acquisition: 2003 to 2009)

- the Radarsat Antarctic Mapping Project (RAMP) Digital Elevation Model, Version 2 (Liu et al., 2015) for mountain glaciers in Antarctica with the exception of some peripheral islands (data acquisition: 1940 to 1999)

- the Viewfinder Panoramas DEM3 product (`http://viewfinderpanoramas.org/dem3.html`) elsewhere (most notably: North America, Russia, Iceland, Svalbard)

All datasets have a comparable spatial resolution (from 30 to 90 m, or 3 arcseconds). Using different data sources is problematic but unavoidable since there is no consistent, gap-free and globally available Digital Elevation Model (DEM) to date. The Advanced Spaceborne Thermal Emission and Reflection Radiometer (ASTER) Global Digital Elevation Model Version 2 (GDEM V2) is available globally but was quickly eliminated because of large data voids and artefacts, in particular in the Arctic. These artefacts are often tagged as valid data and cannot be detected automatically in an easy way. The Viewfinder Panoramas products rely on the same sources but have been corrected manually (mostly with topographic maps; J. de Ferranti, Pers. Comm.) and thus ensure a more realistic void filling. Although having a nearly global coverage, the DEM3 products are not used in place of established and citable digital elevation models such as SRTM, GIMP or RAMP, because it is not easy to retrieve the original data sources used to generate them (the information is scattered around the website, although ASTER and SRTM are the main data sources in most cases). It must be noted that a number of glaciers will still suffer from poor topographic information, and/or a date of data acquisition which doesn't match that of the RGI outlines. Either the errors are large or obvious (in which case the model

won't run), or they are left unnoticed. The importance of reliable topographic data for global glacier modelling will be the topic of a follow-up study[6].

The spatial resolution of the target local grid depends on the size of the glacier: the default is to use a square relation to the glacier size ($dx = aS^{\frac{1}{2}}$ with $a = 14$ and S the area of the glacier in km^2) clipped to a predefined minimum (10 m) and maximum (200 m) value. After the interpolation to the target grid, the topography is smoothed with a Gaussian filter of 250 m radius (this value does not change with the local glacier map resolution because it is meant to be applied to the original DEM, not the interpolated one). This smoothing is driven by practical considerations, since the model becomes unstable if the boundary conditions are too noisy (see also Bahr et al., 2014, for a discussion about the unavoidable trade-off between resolution and accuracy).

2.3.2 Flowlines and Catchments

The glacier centerlines are computed following an algorithm developed by Kienholz et al., 2014 and adapted for our purposes. This algorithm was chosen because it allows one to compute multiple centerlines and to define a main branch fed by any number of tributaries. In general we found the method to be very robust, although some glaciers obviously won't have the optimal number of centerlines, with either too many (frequent in the case of large cirque glaciers) or not enough (some tributary branches have no centerlines). These errors however are assumed to play a relatively minor role compared to other uncertainties in the model chain.

In the model semantics, the original "centerlines" are then converted to "flowlines": the points defining the line geometries are interpolated to be equidistant from each other (the default spacing along the line is twice that of the local glacier map, i.e. varying between 20 m and 400 m depending on glacier size), and the tail of the tributaries are cut before reaching their descendant (see the differences between Figs. 2.1b and c, or between Figs. 2.2a and b). Each grid point's elevation is obtained from the underlying topography. By construction, upslope trajectories or sinks along the flowline are rare: this can still occur when the glacier outlines are poorly defined or because of errors in the gridded topography. In these cases, we interpolate the heights (in the case of a deepening) or cut the first grid points of the line (in case of an upslope starting from the flowline's head) until only positive slopes larger than 1.5° remain. This is necessary because sinks along a flowline are incompatible with the forward dynamical model, which will fill them with ice and create undesirable spin-up issues.

[6] See also `https://rgitools.readthedocs.io/en/latest/dems.html` for an ongoing evaluation of further DEM products.

The flowlines are then sorted according to their Strahler number (a measure of branching complexity defined by Strahler, 1952, and commonly used in hydrological applications), from the lowest (line without tributaries but with possible descendants) to the highest (the main – and longest – centerline). This ordering is important for the mass flow routing: indeed, each flowline contains a reference to its descendant, and this reference is used by the inversion and dynamical models to transfer mass from the tributaries towards the main flowline.

The width of each grid point along the flowline is computed in four steps. First, the catchment area of each flowline is computed using a routing algorithm similar to that used to compute the centerlines (Fig. 2.2a). Then the geometrical widths are computed by intersecting the flowline's normal to the boundaries of either the individual catchments or the glacier itself (Fig. 2.2b). These geometrical widths are then corrected by a factor specific for each altitudinal bin (Fig. 2.2c), so that the true altitude area distribution of the glacier is approximately preserved (Fig. 2.2d). Finally, these widths are multiplied by a single factor ensuring that the total area of the glacier is the exact same as the one provided by the RGI, ensuring consistency with future model intercomparisons.

At this stage, it is important to note that the map representation of the flowline glacier presented in Fig. 2.2c is purely artificial. The fact that the glacier cross-sections are overlapping is irrelevant: the role of the flowlines is to represent the actual flow of ice as accurately as possible while conserving the fundamental aspects of the real glacier: slope, altitude, area, geometry. The flowline approximation is going to work better for valley glaciers (like Tasman glacier shown above) than for cirque glaciers (like the Upper Grindelwald). For ice-caps, the flowline representation is likely to work poorly, as discussed in Sect. 2.3.6.2. From Fig. 2.2c one can see that future improvements of the mass balance model based on e.g. topographical shading or snow redistribution are made possible by the knowledge about the flowlines' location.

2.3.3 Climate Data and Mass Balance

The mass balance model implemented in OGGM is an extended version of the temperature index melt model presented by Marzeion et al., 2012b. The monthly mass balance m_i at an elevation z is computed as:

$$m_i(z) = p_f \, P_i^{Solid}(z) - \mu^* \; max\left(T_i(z) - T_{Melt}, 0\right) + \varepsilon \tag{2.1}$$

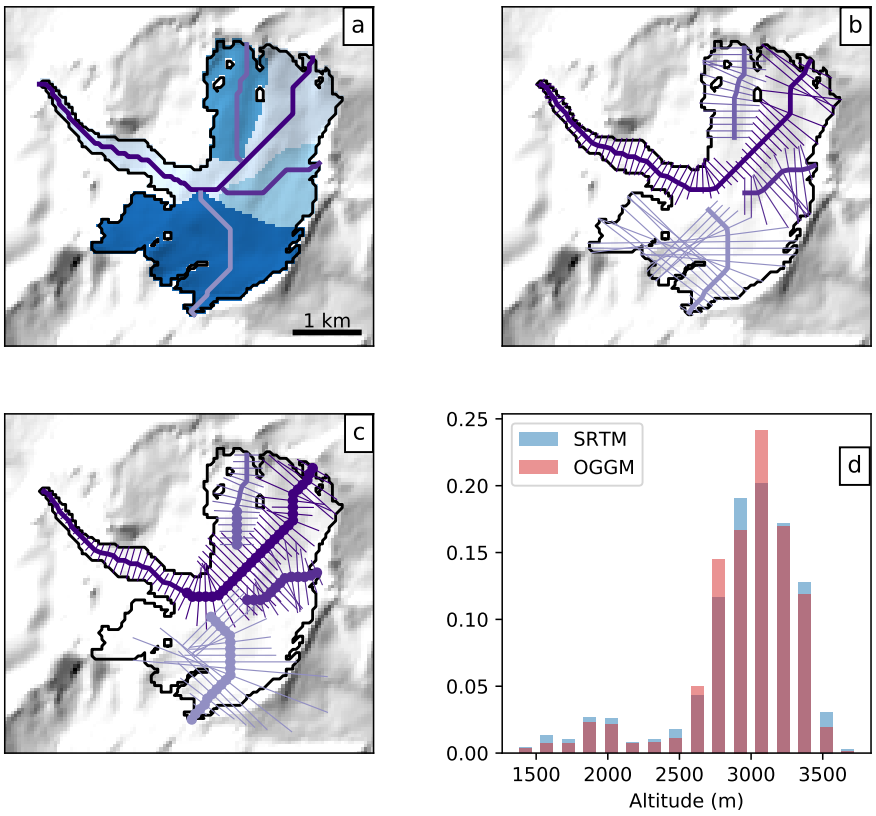

Fig. 2.2: Example of the flowlines' width determination algorithm applied to the Upper Grindelwald glacier, Switzerland; **a**: determination of each flowline's catchment area; **b**: geometrical widths; **c**: widths corrected for the altitude-area distribution, the bold lines representing the grid points where the cross-section touches a neighbouring catchment; **d**: frequency distribution of the glacier area per altitude bin, as represented by OGGM and by the SRTM topography.

where P_i^{Solid} is the monthly solid precipitation, p_f a global precipitation correction factor (defaults to 2.5, see Appendix 2.7.1), μ^* the glacier's temperature sensitivity, T_i the monthly air temperature, T_{Melt} the monthly air temperature above which ice melt is assumed to occur (default: -1°C, chosen because melting days can occur even if the monthly average temperature is below 0°C), and ε a residual (or bias correction) term. Solid precipitation is computed as a fraction of the total precipitation: 100% solid if $T_i <= T_{Solid}$ (default: 0°C), 0% if $T_i >= T_{Liquid}$ (default: 2°C), and linearly interpolated in between. The parameter μ^* indicates the temperature sensitivity of the glacier and needs to be calibrated. For this paper, the temperature and precipitation time series (1901–2016) are obtained from gridded observations (CRU TS4.01; Harris et al., 2014, see Appendix 2.7.1). The temperature lapse-rate is set to a constant value (default: 6.5 K km^{-1}) or it can be time-dependant and computed from a linear fit of the 9 surrounding grid-points.

For the calibration of the temperature sensitivity parameter μ^* we use the method described by Marzeion et al., 2012b and successfully applied many times since then (e.g. Marzeion et al., 2014a; Marzeion et al., 2015; Marzeion et al., 2018). Although the general procedure didn't change, its peculiarity justifies describing it here. We will start by noting that μ^* depends on many factors, most of them being glacier-specific (e.g. avalanches, topographical shading, cloudiness), and others being related to systematic biases in the input data (e.g. climate, topography). As a result, μ^* can vary greatly between neighbouring glaciers without obvious physical reasons. The calibration procedure implemented in OGGM makes use of these apparent handicaps by turning them into assets.

The procedure begins with glaciers for which we have direct observations of specific mass balance ($N = 254$, see Appendix 2.7.2). For each of these glaciers, annual sensitivities $\mu(t)$ are computed from Eq. 2.1 by requiring that the glacier specific mass balance $\overline{m}(t)$ is equal to zero[7]. $\overline{m}(t)$ is the glacier integrated mass balance computed for a 31-yr period centred around the year t and *for a constant glacier geometry fixed at the RGI outline's date* (e.g. 2003 in the Alps). The process is illustrated in Fig. 2.3c (blue line): around 1920 the climate was cold and wet (Figs. 2.3a and b), and as a consequence the hypothetical temperature sensitivity required to maintain the 2003 glacier geometry needs to be high. Inversely, the more recent climate is warmer and the temperature sensitivity needs to become smaller for the glacier to remain stable.

These hypothetical, time-dependent $\mu(t)$ are called "candidates": it is likely (but not certain) that at least one of them is the correct μ^*. To determine which of the

[7]Note that this is not valid for water-terminating glaciers where mass loss happens at the glacier front and the equilibrium surface mass-balance budget doesn't have to be closed. See Sect. 2.3.6.1 for more details.

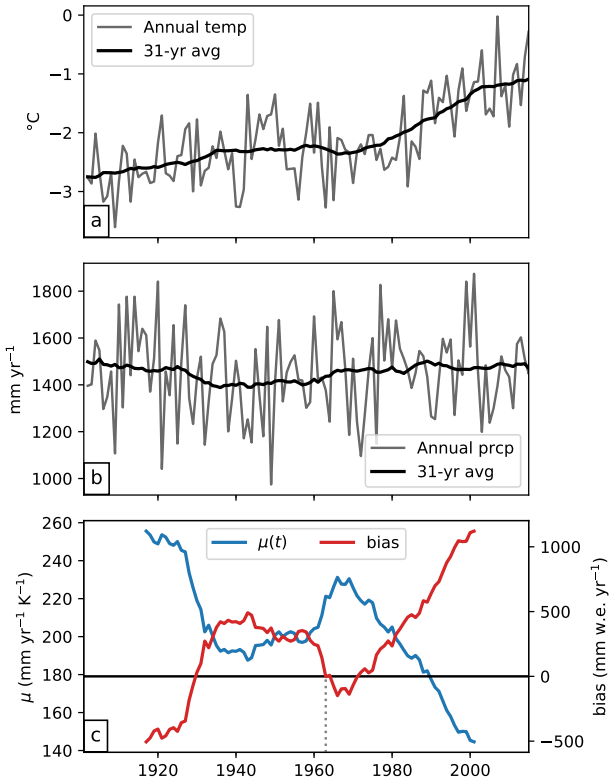

Fig. 2.3: Calibration procedure for μ^* applied to the Hintereisferner glacier, Austria. **a** and **b**: annual and 31-yr average of temperature and precipitation obtained from the nearest CRU grid point (altitude 2700 m a.s.l.). **c**: time series of the μ candidates (mm yr^{-1} K^{-1}) and their associated mass balance bias (mm w.e. yr^{-1}, right-axis) in comparison to observations. The vertical dashed line marks the time where the bias is closest to zero (t^*).

candidates is suitable, we then compute the mass balance time series for each of the $\mu(t)$ and compute their bias ε with respect to observations (red line in Fig. 2.3c). Note that the period over which the observations are taken is not relevant for the bias computation: each μ candidate can produce a mass balance for any year, as per Eq. 2.1. In comparison to observations, $\mu(t = 2000)$ is too low and produces mass balances with a positive bias. Inversely, $\mu(t = 1920)$ is too high and leads to a negative bias. For three years, the bias is close to or crossing the zero line and $\mu(t)$ is therefore very close to the ideal μ^*. These dates represent the center of a 31-yr long climate period where *today's* glacier would be in equilibrium and maintain its *current* geometry. From these three candidates, we pick the date with the smallest bias and call it t^*. This t^* is an actual date but is mostly an abstract concept: we are going to make use of it for the next step.

For the vast majority of the glaciers, μ^* and t^* are unknown. For these we could interpolate the μ^* (probably the most obvious solution), or we could interpolate t^*: indeed, the procedure above can be reversed and t^* can be used to retrieve μ^*, again by requiring that $\overline{m}(t^*)$ is equal to zero (Eq. 2.1). We interpolate t^* to all glaciers without observations using inverse distance interpolation from the 10 closest locations (which can be quite far away, see Appendix 2.7.2 and 2.7.3). The residual bias ε for glaciers with observations can be close to zero (the case for Hintereisferner in Fig. 2.3, where the bias curve crosses the zero line) but can also be higher (indicating that no 31-yr period in the last century would sustain the current glacier geometry). When no perfect t^* is found, the date with the smallest absolute bias is chosen. This residual ε is also interpolated between locations and added to the modelled mass balance. This residual may be significant at certain locations (up to 1.5 m yr^{-1}, median of 6 cm yr^{-1}) and would benefit from further calibration e.g. with regional geodetic mass-balance estimates. The benefit of this approach is best shown by cross-validation (Fig. 2.4), where one can see that the error increases considerably when using μ^* interpolation instead of the proposed method. This is due to several factors:

- the equilibrium constraint applied on $\mu(t)$ implies that the sensitivity cannot vary much during the last century. In fact, $\mu(t)$ at one glacier often varies less in one century than between neighbouring glaciers, because of the local driving factors mentioned earlier. In particular, it will vary comparatively little around a given year t: errors in t^* (even large) will result in relatively small errors in μ^*.

- the equilibrium constraint will also imply that systematic biases in temperature and precipitation (no matter how large) will automatically be compensated by all $\mu(t)$, and therefore also by μ^*. In that sense, the calibration procedure can be seen as an empirically driven downscaling strategy: if a glacier is located

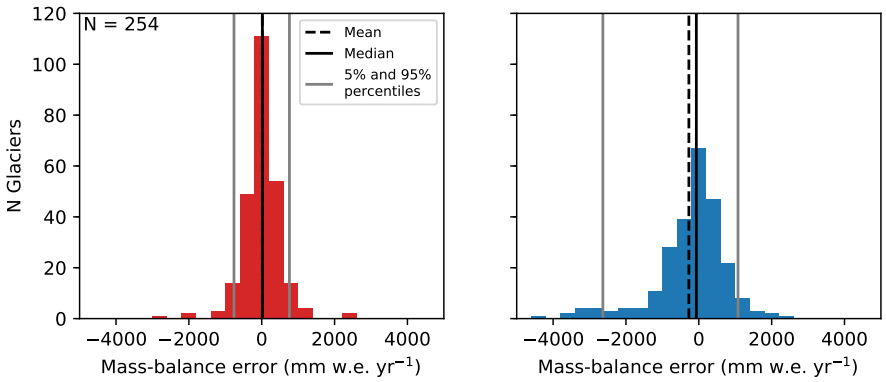

Fig. 2.4: Benefit of spatially interpolating t^* instead of μ^* as shown by leave-one-out cross-validation ($N = 254$). **Left**: error distribution of the computed mass balance if determined by the interpolated t^*. **Right**: error distribution of the mass balance if determined by interpolation of μ^*. The vertical lines indicate the mean, median, 5% and 95% percentiles. See `https://cluster.klima.uni-bremen.de/~github/crossval` for an online visualisation of model performance for each glacier.

there, then the local climate (or the glacier temperature sensitivity) *must* allow a glacier to be there. For example, the effect of avalanches or a negative bias in precipitation input will have the same impact on calibration: the value of μ^* should be lowered to take these effects into account, even though they are not resolved by the mass balance model.

The most important drawback of this calibration method is that it assumes that two neighbouring glaciers should have a similar t^*. This is not necessarily the case, as other factors than climate (such as the glacier size) will influence t^* too. Our results (and the arguments listed above) show however that this is an approximation we can cope with.

In a final note, it is important to mention that μ^* and t^* should not be over-interpreted in terms of real temperature sensitivity or response time of the glacier. This procedure is primarily a calibration method, and as such it can be statistically scrutinized (for example with cross-validation). It can also be noted that the mass balance observations play a relatively minor role in the calibration: they could be entirely avoided by fixing a t^* for all glaciers in a region (or even worldwide), without much performance loss. The observations, however, play a major role for the assessment of model uncertainty (Fig. 2.4). For more information about the climate data and the calibration procedure, refer to Appendix 2.7.1.

2.3.4 Ice Thickness

Measuring ice thickness is a labour-intensive and complex task, therefore only a fraction of the world's glaciers is monitored and direct measurements are sparse. A physical or statistical approach is necessary for modelling glacier evolution at the global scale. For a recent review of available techniques for ice thickness modelling, see Farinotti et al., 2017. OGGM implements a new ice thickness inversion procedure, physically consistent with the flowline representation of glaciers and taking advantage of the mass balance calibration procedure presented in the previous section. It is a mass-conservation approach largely inspired by Farinotti et al. (2009), but with distinct characteristics.

The principle is quite simple. The flux of ice q [m^3 s^{-1}] through a glacier flux-gate (cross-section) of area S [m^2] reads:

$$q = uS \tag{2.2}$$

with u the average velocity [m s^{-1}]. Using an estimate for u and q obtained from the physics of ice flow and the mass balance field, S and the local ice thickness h [m] can be computed relying on some assumptions about the bed geometry. We compute the depth-integrated ice velocity using the well known shallow-ice approximation (Hutter, 1981; Hutter, 1983):

$$u = \frac{2A}{n+2} h \tau^n \tag{2.3}$$

with A the ice creep parameter [s^{-1} Pa^{-3}], n the exponent of Glen's flow law (n=3), and τ the basal shear stress, computed as:

$$\tau = \rho g h \alpha \tag{2.4}$$

with ρ the ice density (900 kg m^{-3}), g the gravitational acceleration (9.81 m s^{-2}) and α the surface slope computed numerically along the flowline. Optionally, a sliding velocity u_s can be added to the deformation velocity to account for basal sliding. We use the same parameterisation as Oerlemans, 1997a, who relied on Budd et al., 1979:

$$u_s = \frac{f_s \tau^n}{h} \tag{2.5}$$

with f_s a sliding parameter (default: 5.7 $\times$ 10^{-20} s^{-1} Pa^{-3}). If we consider a point on the flowline and the catchment area Ω upstream of this point, mass conservation implies:

$$q = \int_\Omega (\dot{m} - \rho \frac{\partial h}{\partial t})\, dA = \int_\Omega \widetilde{m}\, dA \tag{2.6}$$

with $\dot{m}$ the mass balance [kg m^{-2} s^{-1}], and $\widetilde{m} = \dot{m} - \rho \partial h / \partial t$ the "apparent mass balance" after Farinotti et al. (2009). If the glacier is in steady state, the apparent mass balance is equivalent to the actual (and observable) mass balance. In the non-steady state case, $\partial h / \partial t$ is unknown, and neither is the time integrated (and delayed) mass balance $\int_\Omega \dot{m}$ responsible for the flux of ice through a section of the glacier at a certain time. Farinotti et al. (2009) and Huss and Farinotti (2012) deal with the issue by prescribing an apparent mass balance profile as a parameterized linear gradient which is, arguably, more a semantic than a physical way to deal with the transience of the problem.

Like Huss and Farinotti (2012), OGGM cannot deal with the transient problem yet: we deliberately assume steady state and therefore set $\widetilde{m} = \dot{m}$. This has the strong advantage that we can make direct use of the equilibrium mass balance $\overline{m}(t^*)$ computed earlier, which satisfies $\int \overline{m} = 0$ by construction. q is then obtained by integrating the equilibrium mass balance $\overline{m}$ along the flowline(s). The tributaries will have a positive flux at their last grid point: this mass surplus is then transferred to the downstream line, normally distributed around the 9 grid points centred at the flowlines' junction. By construction, q starts at zero and increases along the major flowline, reaches its maximum at the equilibrium line altitude (ELA) and decreases towards zero at the tongue (for glaciers without frontal ablation).

Equation 2.2 turns out to be a polynomial of degree 5 in h with only one root in $\mathbb{R}_+$, easily computable for each grid point. Singularities due to flat areas are avoided since the constructed flowlines are not allowed to have a local slope α below a certain threshold (default: 1.5°, see Sect. 2.3.2). The equation varies by a factor of 2/3 if one assumes a parabolic ($S = \frac{2}{3} h w$, with w the glacier width) or rectangular ($S = h w$) bed shape. The default in OGGM is to use a parabolic bed shape, unless the section touches a neighbouring catchment (see Fig. 2.2c), neighbouring glacier (ice divides, computed from the RGI), or at the terminus of a calving glacier. In these cases the bed shape is rectangular. Optionally, OGGM can also compute the effect of lateral bed stresses (Cuffey and Paterson, 2010) following a parameterization and tabular correction factors developed by Adhikari and Marshall (2012b).

Figure 2.5 displays some examples taken from the OGGM test suite, where the automated inversion procedure is applied on idealized glaciers generated with OGGM's flowline model (see Sect. 2.3.5). In the equilibrium cases (Fig. 2.5a to c), the inverted topography is nearly perfect. Differences arise at strong surface gradients, mostly because of numerical differences (the inversion method uses a second order central difference which tends to smooth the slope). The transient case (Fig. 2.5d) illustrates the consequences of the steady-state assumption: although the glacier is retreating, the constraint $\int \widetilde{m} = 0$ leads to a lowered ELA and, even with a perfectly known mass balance gradient, leads to an overestimated ice thickness

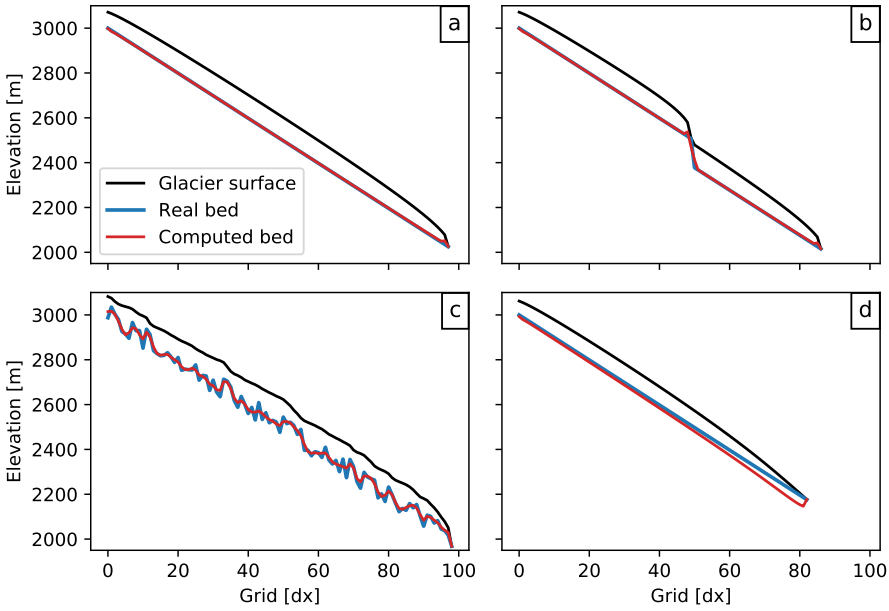

Fig. 2.5: Idealized inversion experiments: we compute the bed topography out of the surface elevation obtained from a flowline model applied to a predefined bed topography. (**a**), (**b**) and (**c**): glacier grown to equilibrium with different bed topographies (flat, cliff, random). (**d**): transient experiment with a shrinking glacier. The same mass balance profile is used for all experiments (linear gradient of 3 mm w.e. m^{-1}, ELA altitude of 2600 m a.s.l.). For (d), the glacier is first grown to equilibrium then shrunk for 60 years after an ELA shift of +200 m.

(in this case, 25%). This effect is visible everywhere, but is strongest at the tongue. The importance of the steady state assumption on ice thickness estimates has been studied with numerical experiments (e.g. Adhikari and Marshall, 2012a) and is often compensated by calibration in real world applications.

The sensitivity of the inversion procedure to various parameters is illustrated with the example of the Hintereisferner glacier (Fig. 2.6). The total volume (and the local thickness) is very sensitive to the choice of the creep parameter A, varied from a factor 1/10 to 10 times the default value of 2.4×10^{-24} s^{-1} Pa^{-3} (Cuffey and Paterson, 2010). With a smaller A, the ice is stiffer and the glacier gets thicker (A is expected to get smaller by one or more orders of magnitude with colder ice temperatures). Inversely, softer ice leads to a thinner glacier. The shape of the curve is proportional to the fifth root of the fraction $1/A$, explaining why the volume gets very sensitive to small values of A. Adding sliding reduces the original thickness significantly for the same reasons as an increasing A, since both sliding and ice rheology (A) have a strong influence on the computed ice flux q. Inversely, adding lateral bed stresses reduces ice velocity and increases the computed ice volume. Changing from a rectangular to a parabolic bed shape yields a volume loss of exactly 1/3: this is expected from geometrical considerations. The mixed

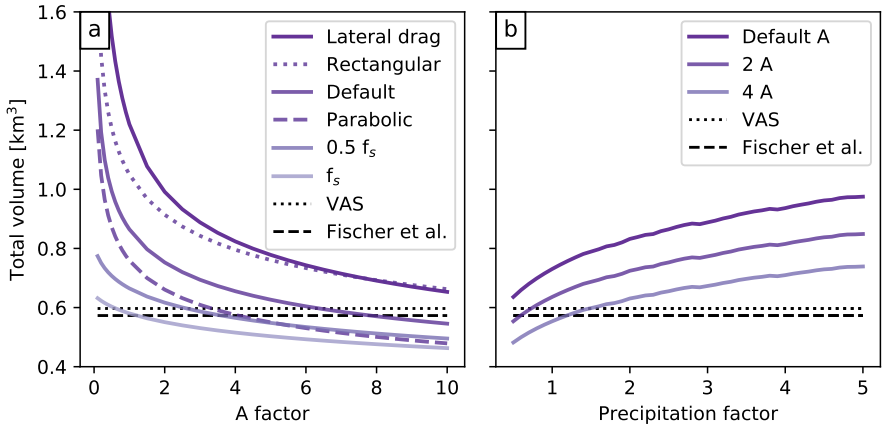

Fig. 2.6: Total volume of the Hintereisferner glacier computed with (**a**) varying factors for the default creep parameter A, and (**b**) varying precipitation factors. The dotted and dashed black lines display the total volume estimated with volume-area scaling (VAS, Bahr et al., 1997; Bahr et al., 2015) and based on point observations (Fischer and Kuhn, 2013). For (**a**), additional sensitivities are computed with an additional sliding velocity (Oerlemans, 1997a) and his sliding parameter f_s. For (**b**), additional sensitivities are computed with a varying creep parameter A.

parabolic/rectangular bed shape model implemented by default therefore lies in between.

The total precipitation amount, by acting on the mass balance gradient and therefore on the ice flux q will also play a non-negligible role for the ice thickness (Fig. 2.6b). The effect is small in comparison to the influence of A, but it is noticeable: glaciers located in maritime climates (with high values of accumulation) will be thicker on average than similar glaciers in drier conditions.

This example shows that one can always find an optimum (and non-unique) set of parameters leading to the correct total volume. In practice, however, calibrating the model for accurate global glacier volume estimates is a major challenge for global glaciological models and will be the topic of a separate study. The IACS Working Group on Glacier Ice Thickness Estimation[8] is working towards this goal: OGGM participated in the first Ice Thickness Models Intercomparison eXperiment (ITMIX, Farinotti et al., 2017), ranking amongst the best models with limited data requirements.

[8] `http://www.cryosphericsciences.org/wg_glacierIceThickEst.html`

2.3.5 Ice Dynamics

At this stage of the processing workflow, the ice-dynamics module is straightforward to implement. Provided with the mass balance, slope, width w and bed topography along the flowline, we solve the equation:

$$\frac{\partial S}{\partial t} = w\,\dot{m} - \nabla \cdot uS \tag{2.7}$$

numerically with a forward finite difference approximation scheme on a staggered grid. Numerical stability is ensured by the use of an adaptive time stepping scheme following the Courant-Friedrichs-Lewy (CFL) condition $\Delta t = \gamma \frac{\Delta x}{max(u)}$ with γ as the dimensionless Courant number chosen between zero and one. Unlike many solvers of the shallow-ice equation, we do not transform Eq. 2.7 to become a diffusivity equation in h, but solve it as it is formulated here. This has the advantage that the numerical solver is the same regardless of the shape of the bed (parabolic, trapezoidal or rectangular). The new section S at time $t + \Delta t$ allows to compute $h(t + \Delta t)$ according to the local bed geometry. Therefore, it is possible to have changing bed geometries along a single flowline using the same numerical solver. The drawback of our approach is that we cannot take advantage of the diffusivity equation solvers already available elsewhere. We tested our solution against the robust and and mass-conservative solver presented by Jarosch et al., 2013: our model yields accurate (and faster) results in most cases, but fails to ensure mass-conservation for very steep slopes like most other solvers to date. While a flowline version of the solver presented by Jarosch et al., 2013 is available in OGGM, it is not used operationally since it cannot yet handle varying bed shapes and multiple flowlines – it will become the default solver when these elements are implemented.

At a junction between a tributary and its downstream line, an artificial grid point is added to the tributary line. This grid point has the same section area S and thickness h as the previous one, but the surface slope is computed from the difference in elevation between tributary and descendant flowline. This is necessary to ensure a dynamical connection between the two lines: when the main flowline is at a higher elevation than its tributary, no mass exchange occurs and the tributary will build up mass until enough ice is available. At a junction point, Eq. 2.7 therefore contains an additional mass flux term from the tributary.

Before the actual run, a final task merges the output of all preprocessing steps and initialises the flowline glacier for the model. For the glaciers to be allowed to grow, a downstream flowline is computed using a least cost routing algorithm leading the glacier towards the domain boundaries (this algorithm is similar to the algorithm

used to compute the glacier centerlines). The bed geometries along the downstream line are computed by fitting a parabola to the actual topography profile. In case of bad fit, the values are interpolated or a default parabola is used. Along the glacier, where the bed geometries are unknown before the inversion, the bed geometries are either rectangular (ice divides and junctions) or parabolic. Very flat parabolic shapes can happen occasionally, for wide sections with a shallow ice thickness. These geometries are unrealistically sensitive to changes in h. They create a strong positive feedback (the thickening of ice leading to a highly widening glacier) and are therefore prevented: when the parabola parameter falls below a certain threshold, the geometry is assumed to be trapezoidal instead.

The coupling between the mass-balance and ice dynamics modules is a user choice. The spatially distributed mass-balance used by the dynamical model can be updated: (i) at each time-step of the dynamical model's computation, (ii) each month, (iii) each mass-balance year (the default), or (iv) only once (for testing and feedback sensitivity investigations). In practice, this does not make much difference for the yearly averages of glacier change (except for option iv), and the choice of a yearly update is mostly driven by performance considerations. Note that the mass-balance model can compute the mass-balance at shorter time intervals if required by the physical parameterizations: the interface between the model elements simply requires the mass-balance model to integrate the mass-balance over a year before giving it to the dynamical model.

The results of two idealized simulations with an advancing and a shrinking scenario are shown in Fig. 2.7. When put under the cold and wet climate of the beginning of the 20th century, Hintereisferner would grow about 2/3 larger than it is today. Inversely, the glacier is in strong disequilibrium with today's climate: it would lose about 2/3 of it's volume if the climate remained as it was during the past 31 years. The response time of the glacier is approximately twice as fast in the shrinking case, and the natural random variations of the glacier are much smaller than for a large glacier with more inertia and a longer response time.

The previous results were obtained with the default set-up of OGGM. In Fig. 2.8 we assess the sensitivity of the dynamical model to changes in the creep parameters A and to the addition of lateral drag and basal sliding velocity. As expected, these dynamical parameters affect the equilibrium volume and the response time of the glacier (faster ice leading to a thinner glacier, and inversely). Because of the mass-balance elevation feedback, the stiffer and therefore thicker glacier is also larger and longer, but its response to climate variability is smaller in amplitude than that of the fast moving sliding glacier.

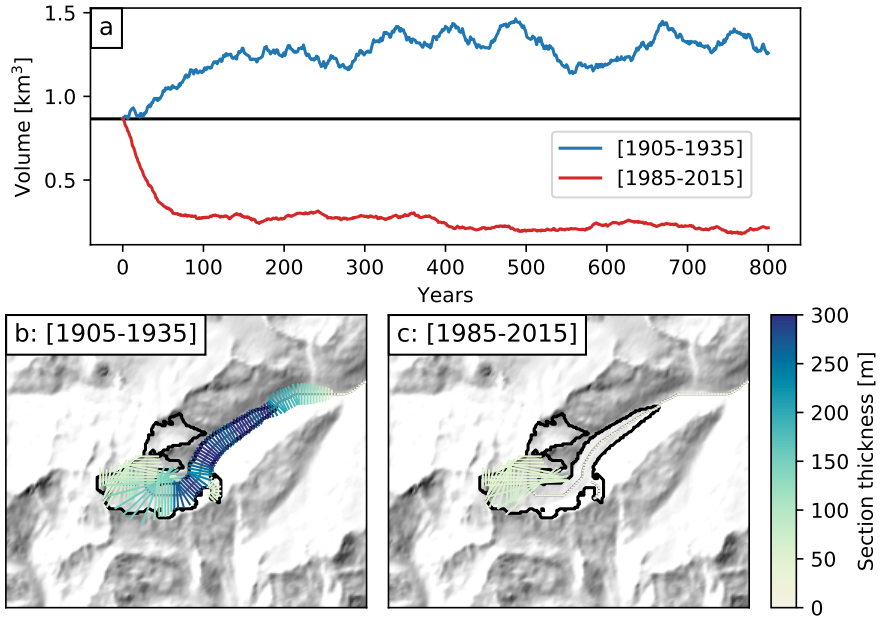

Fig. 2.7: Evolution of the Hintereisferner under two random forcing scenarios and for the default parameter set. For each scenario, the "climate years" during a 31-yr period are shuffled randomly, therefore creating a realistic climate representative for a given period. (**a**): the glacier volume evolution for each scenario (the black line marks the initial computed glacier volume). (**b**) and (**c**): the glacier shape at the end of the 800 yrs simulation for each case.

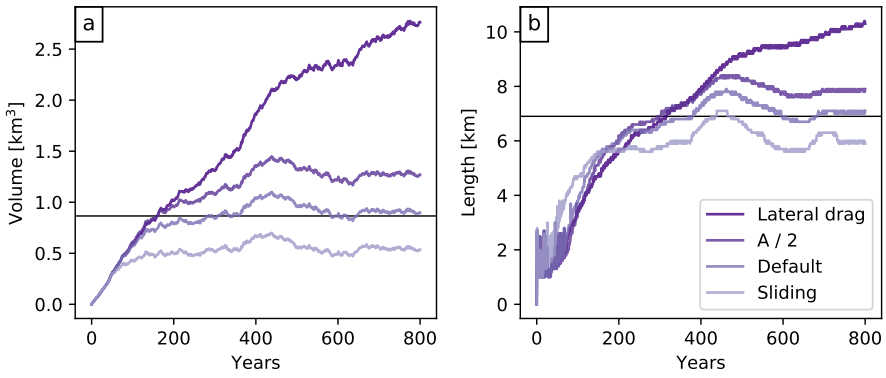

Fig. 2.8: Evolution of volume (a) and length (b) of the Hintereisferner glacier under a random climate forcing generated by shuffling the "climate years" representative for the 31-yr period centred on t*. The glacier is reset to zero for each simulation, and the bed topography is obtained with the default parameters. The sensitivity to the addition of a sliding velocity or to a halving of the creep parameter A are also shown. The noisy patterns of the length time series are due to the fact that the length of a glacier on a discrete grid is sensitive to small interannual variations.

A and f_s depend on many factors such as ice temperature or basal characteristics and they cannot be assumed to be globally constant. They are considered as calibration parameters in OGGM, and will be tuned towards observations of ice thickness or glacier length changes. In this study we only calibrate the mass-balance model while the ice dynamics parameters are set to their default values (A = 2.4 $\times$ 10^{-24} s^{-1} Pa^{-3}, f_s = 0, no lateral drag). Nevertheless, we discuss the model sensitivity to these dynamical parameters for individual glaciers (Fig. 2.8) or global runs (Fig. 2.10).

2.3.6 Special Cases and Model Limitations

The previous experiments demonstrate that the OGGM model is capable of simulating the dynamics of glaciers in a fully automated manner. In this section we describe the implications of the flowline approximation in the special cases of water-terminating glaciers and ice caps, and discuss some examples of glaciers with a less trivial geometry.

2.3.6.1 Water-Terminating Glaciers

Glaciers are defined as "water-terminating" in OGGM when their RGI terminus attribute is either flagged as marine-terminating or lake-terminating. The major difference between a water-terminating glacier and a valley glacier is the additional mass-loss that occurs at the glacier front (frontal ablation). This has implications for the bed thickness inversion which currently assumes that the mass-flux at the front is zero (by setting $\int \widetilde{m} = 0$, see Sect. 2.3.4) and for the dynamics of the glacier. The current treatment of water-terminating glaciers in OGGM is very simple but explicit: we do not take frontal ablation into account for the bed inversion (i.e. the original glacier front has a thickness of zero), but we do have a basic parametrisation in the ice dynamics module. We add a grid point behind the glacier front which is reset to zero ice thickness at each time step: the ice mass suppressed this way is the frontal ablation flux, that we store. This parametrisation has the advantage of preventing water-terminating glaciers from advancing while still allowing them to retreat (in which case they stop calving). We are working on a more advanced frontal ablation parametrisation for both the ice dynamics and the ice thickness inversion (Recinos et al., 2019).

2.3.6.2 Ice Caps and Ice Fields

Ice caps and ice fields in the RGI are divided in single dynamical entities separated by their ice divide (Fig. 2.9). However, the entities that belong to an ice cap are classified as such in the RGI: currently, the only special treatment for these entities

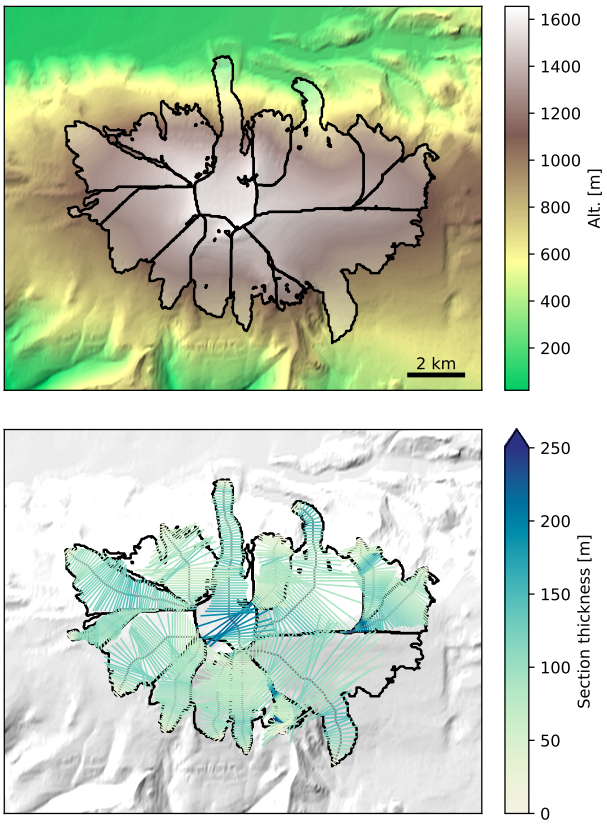

Fig. 2.9: OGGM inversion workflow applied to the RGI entities of the Eyjafjallajökull ice cap, Iceland. **Upper panel**: outlines and topography. **Lower panel**: glacier thickness.

in OGGM is that only one major flowline is computed (without tributaries). Indeed, the geometry of ice caps is often non trivial and it is not clear whether tributaries would really improve the model results. An example of an ice cap is shown in Fig. 2.9: while the general behaviour of the ice cap is reasonably simulated by the flowline model (e.g. at the outlet glaciers), other features appear to be unrealistic (e.g. close to the ice-divides). Moreover, the mass-conservation inversion method is probably underestimating the real ice-thickness at the location of the ice-divide, where other processes related to the past history of the ice cap are at play. A possible way forward would be to run a distributed shallow-ice model instead of the flowline representation, and it is part of our long-terms plans to do so.

2.3.6.3 Glacier Complexes

Single glaciers can be defined as the smallest dynamically independent entity, i.e. the boundaries between two glaciers should approximately follow the ice divides or hydrological basin boundaries. The flowline assumption strongly relies on this condition being true, and indeed most of the RGI glaciers are properly outlined. Unfortunately there are notable exceptions, for three main reasons:

- human decision: some well known glaciers have historical boundaries that the inventory provider wanted to keep, although the glacier is now disintegrated in smaller entities. A good example is the Hintereisferner glacier (Fig. 2.7), which should have three outlines instead of one.

- uncertainties in the topography: the inventories are often generated using both automated processes and manual editing. There is no guarantee that we use the same DEM as the original inventory, and therefore OGGM and RGI might disagree on the ideal position of an ice divide.

- unavailable data: some remote glaciers and ice caps are outlined in the RGI, but not divided at all. These are the most problematic cases, and should be a matter of concern for all RGI users. For example, the largest glacier in RGI (an ice cap in north-eastern Greenland with id RGI60-05.10315 and area 7537 km^2) is wrongly outlined and should be separated in at least a dozen of smaller entities.

Most of the small errors are filtered out by OGGM with algorithms based on surface slope thresholds (see Sect. 2.3.2), but the latter group of glaciers should be handled upstream. We have developed an open source tool to automatically compute glacier divides (`https://github.com/OGGM/partitioning`, based on Kienholz et al., 2013), but do not use it here. This issue is a large source of uncertainty for ice thickness estimates and dynamical modelling of glaciers in general, and could be the subject of a dedicated study.

2.3.6.4 Glacier Centric Modelling

Like most global glacier models, OGGM simulates each glacier individually. This has evident practical advantages, and is also a strong asset for our mass balance model calibration algorithm. However, this has two major drawbacks: (i) neighbouring glaciers won't merge although they grow together, and (ii) we can only simulate glaciers which are already inventoried, while uncharted glaciers are simply ignored. Both errors are a source of uncertainty for long or past simulations but less for short term projections in a warming world. The most obvious way to deal with this issue is to use distributed models (e.g. Clarke et al., 2015), with their own drawbacks (mostly: computational costs and the need for distributed mass balance fields). Another way would be to allow the dynamical merging of neighbour flowline glaciers at run time. While both are viable options for the OGGM workflow, they represent a considerable increase in complexity and are not available yet. Like other fundamental issues described in this paper (such as missing topographical data or wrongly outlined glaciers), this problem will affect other glacier models as well. We

hope that some of the tools we introduce here will help to solve some of these issues upstream, and that the community will soon be able to put pressure on commercial data providers for better data availability.

2.4 Global Simulations

Thanks to its automated workflow, OGGM is able to apply all processes described in the previous section to all glaciers of the globe with the exception of Antarctica, where no CRU data is available (see Appendix 2.7.3 for an overview of the RGI regions). No special model setup is needed, we use all model default settings without any calibration (this is not strictly true for the μ^* calibration, which is an automated process and cannot be tuned or turned off). In the following analyses the focus is put on the model behaviour and not on the quantitative results. However, as we are going to see our results are close to expectations even without calibration, indicating a realistic model behaviour.

2.4.1 Hardware Requirements and Performance

Thanks to the computational efficiency of the flowline model, OGGM runs quickly enough to be used on a personal computer for up to a hundred glaciers. At the global scale a high performance computing environment is required. For these global simulations we used a small-sized cluster comprising two nodes with 16 quad-core processors each, resulting in 128 parallel threads. With this configuration, the model preprocessing chain (including the ice thickness inversion) takes about 7 hours to complete (without data download). The total size of the (compressed) preprocessed output is 122G, an amount which can be reduced by deleting intermediate computing steps. The amount of required storage increases with each dynamical run; here again it is possible to reduce the data amounts by storing only diagnostic variables such as volume, area, length, ELA instead of the full model output. The dynamical runs are the most expensive computations: running five 300-yr long global runs takes about 24 hours on our small cluster, a very satisfying performance. It is interesting to note that because of the adaptive time-step, glacier shrinkage scenarios run faster than growing ones.

Tab. 2.1: Statistics of the model errors for each RGI region. The column names indicate which processing step produces an error, the value is the number of invalid glaciers and (in parentheses) the percentage of regional area they represent.

	N	Area (km2)	Climate	Dynamics	Others	All
01: Alaska	27108	86725	166 (0.1%)	1 (0.0%)	19 (0.1%)	186 (0.3%)
02: Western Canada and US	18855	14524	4 (0.0%)	7 (0.0%)	50 (0.5%)	61 (0.6%)
03: Arctic Canada North	4556	105111	155 (2.1%)		16 (0.1%)	171 (2.2%)
04: Arctic Canada South	7415	40888	58 (0.0%)	8 (0.0%)	11 (0.2%)	77 (0.2%)
05: Greenland	20261	130071	4422 (8.4%)	531 (0.7%)	33 (0.2%)	4986 (9.3%)
06: Iceland	568	11060				
07: Svalbard	1615	33959			6 (0.1%)	6 (0.1%)
08: Scandinavia	3417	2949		3 (0.0%)	4 (0.1%)	7 (0.1%)
09: Russian Arctic	1069	51592		2 (0.0%)	4 (0.2%)	6 (0.2%)
10: North Asia	5151	2410	55 (1.3%)	1 (0.0%)	15 (2.6%)	71 (3.9%)
11: Central Europe	3927	2092	30 (0.1%)		7 (0.0%)	37 (0.1%)
12: Caucasus and Middle East	1888	1307			2 (0.0%)	2 (0.0%)
13: Central Asia	54429	49303	59 (0.1%)	121 (0.6%)	23 (0.6%)	203 (1.3%)
14: South Asia West	27988	33568	110 (0.1%)	34 (0.1%)	31 (0.9%)	175 (1.1%)
15: South Asia East	13119	14734	178 (0.6%)	37 (0.1%)	10 (0.3%)	225 (1.0%)
16: Low Latitudes	2939	2341	383 (8.4%)	5 (0.2%)	10 (0.5%)	398 (9.1%)
17: Southern Andes	15908	29429	375 (8.4%)	21 (0.1%)	60 (0.4%)	456 (8.9%)
18: New Zealand	3537	1162	5 (0.0%)	1 (0.1%)	11 (0.1%)	17 (0.2%)
TOTAL	213750	613226	6000 (2.6%)	772 (0.2%)	312 (0.3%)	7084 (3.1%)

2.4.2 Invalid Glaciers

Due to uncertainties in the input data (topography, outlines, climate), a certain number of glaciers fail to be modelled by OGGM. The statistics of these invalid glaciers are summarized in Table 2.1. The largest amount of errors (2.6% of the total area) is due to invalid climate series. Errors occur mostly when the climate is too cold for melt to happen or, inversely, too warm or too dry for accumulation to happen. While some of these errors are directly due to incorrect climate data, some can also be attributed to missing processes in the OGGM mass balance model: sublimation and frontal ablation, both leading to mass-loss even at cold temperatures. The least problematic source of error (0.2% of the total area) is due to failures during the actual dynamical run. The large majority of dynamical failures (751 out of 772) happen because the glacier exceeded the domain boundaries at run time. Some of these errors could be mitigated by increasing the domain size (at the cost of computational efficiency). Only 21 glaciers fail due to numerical instabilities. Finally, there is a number of other errors (0.3% of the total area) happening at other stages of the model chain. Examples include errors in processing the geometries or failures in computing certain topographical properties due to invalid DEMs. Altogether, 7084 glaciers (3.1% of the total area) cannot be modelled by OGGM. There are strong regional differences, remote low and high latitude regions accounting for most of the errors.

2.4.3 Volume Inversion

A summary of the volume inversion results is presented in Fig. 2.10. As expected from theory (Bahr et al., 1997; Bahr et al., 2015), our glacier volume estimates approximately follow a power law relationship with the glacier area ($V = c\,S^{\gamma}$). The coefficients obtained by a linear fit in log space are close, but not equal to the coefficients computed by Bahr et al., 1997. In particular, the OGGM fit is slightly flatter than the theoretical value (Fig. 2.10, upper panel), in accordance with empirical coefficients (e.g. Bahr et al., 2015; Grinsted, 2013). This is an encouraging result, especially because it was reached with the OGGM default settings and without calibration.

The global volume estimates are particularly sensitive to the choice of the ice dynamics parameters, as shown in Fig. 2.10 (lower panel). As for individual glaciers, the total volume follows an inverse polynomial curve as expected from the equations of ice flow. Changing from a rectangular to a parabolic bed shape yields a volume loss of exactly 1/3 (see Sect. 2.3.4). Adding lateral drag yields a volume very close to the rectangular case: although this is fortuitous (individual glaciers can show different results, see Fig. 2.6), it matches nicely the original purpose of the parametrization,

which is to compute a more realistic ice flow for parabolic bed shapes. The three independent estimates plotted as straight dotted lines (VAS; Huss and Farinotti, 2012; Grinsted, 2013) illustrate that A is a relatively straightforward parameter to act upon in order to fit the model to observations. The effect of A, however, is going to be the same on all glaciers and therefore will be a poor measure of performance (see also Bahr et al., 2015, Sect. 8.11). In fact, the added value of OGGM is more likely to be found in the *deviations* from the scaling law (Fig. 2.10, lower panel). The deviations are the result of a range of possible factors such as slope, total accumulation, or altitude area distribution. With accurate boundary conditions, OGGM should be able to provide more accurate estimates, within the limits of the assumptions and simplifications behind the model equations. The calibration and validation of the OGGM inversion model will be the topic of a subsequent study.

2.4.4 Dynamical Runs

We test the model behaviour by running several 300-yr long global simulations under various climate "scenarios". In the first simulations (Fig. 2.11), we run the model under the climate of the past 31 years. In order to keep the forcing realistic, we create a pseudo-random climate by shuffling the years infinitely. We also run two additional simulations with a 0.5°C positive and negative bias. The unbiased simulation illustrates the committed glacier mass-loss, i.e. the ice mass which is not sustainable under the current climate. Figure 2.11 shows that all regions will continue to lose ice even if the climate remains constant. The regions with the largest committed mass loss relative to the initial volume are Western Canada and US (02), Svalbard (07), and the three High Mountain Asia regions (13, 14, 15). Inversely, the regions Arctic Canada South (04), Greenland (05) and Iceland (06) are least affected. The reasons for these regional differences are complex: they are due to the climate itself of course, but also to glacier properties such as size, slope, and continentality. The regions that are far from equilibrium also tend to be less sensitive to the temperature bias experiments, although this should not be over-interpreted (indeed, the range of the y-axes can hide differences which appear small in comparison to the large regional glacier loss).

In general, the model behaviour looks reasonable and the regional differences are in qualitative agreement with other global studies (e.g. Huss and Hock, 2015, where the regions with a stronger response to 21st century climate change are the same as the ones listed above). Also our global estimate of the committed mass loss (approx. 33% at the end of the 300-yr simulation, probably more at equilibrium) is in agreement with other studies (27±5%, 38±16%, and 36±8% for Bahr et al., 2009; Mernild et al., 2013; Marzeion et al., 2018, respectively).

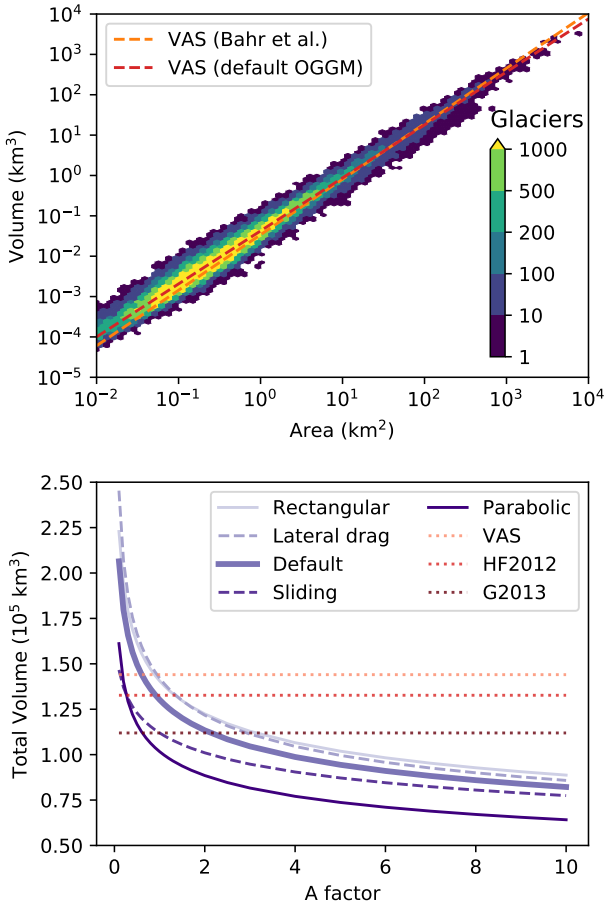

Fig. 2.10: Global glacier volume modelling. **Upper panel**: binned scatter plot of volume versus area for all valid glaciers (N=207,438) with the default OGGM setup. Color shading indicates the number of glaciers in each bin. Note the logarithmic scale of the axes and the irregular color scale levels. The dashed lines indicates the volume area scaling relationship with either the theoretical parameters from Bahr et al., 1997 ($V = 0.034\,S^{1.375}$) or fitted on our own data ($V = 0.042\,S^{1.313}$). **Lower panel**: global volume estimates as a function of the multiplication factor applied to the ice creep parameter A, with five different set-ups: defaults, with sliding velocity, with lateral drag, and with rectangular and parabolic bed shapes only (instead of the default mixed parabolic/rectangular). In addition, we plotted the estimates from standard volume area scaling (VAS, $V = 0.034\,S^{1.375}$), Huss and Farinotti, 2012 (HF2012) and Grinsted, 2013 (G2013). The two latter estimates are provided for indication only since they are based on a different glacier inventory.

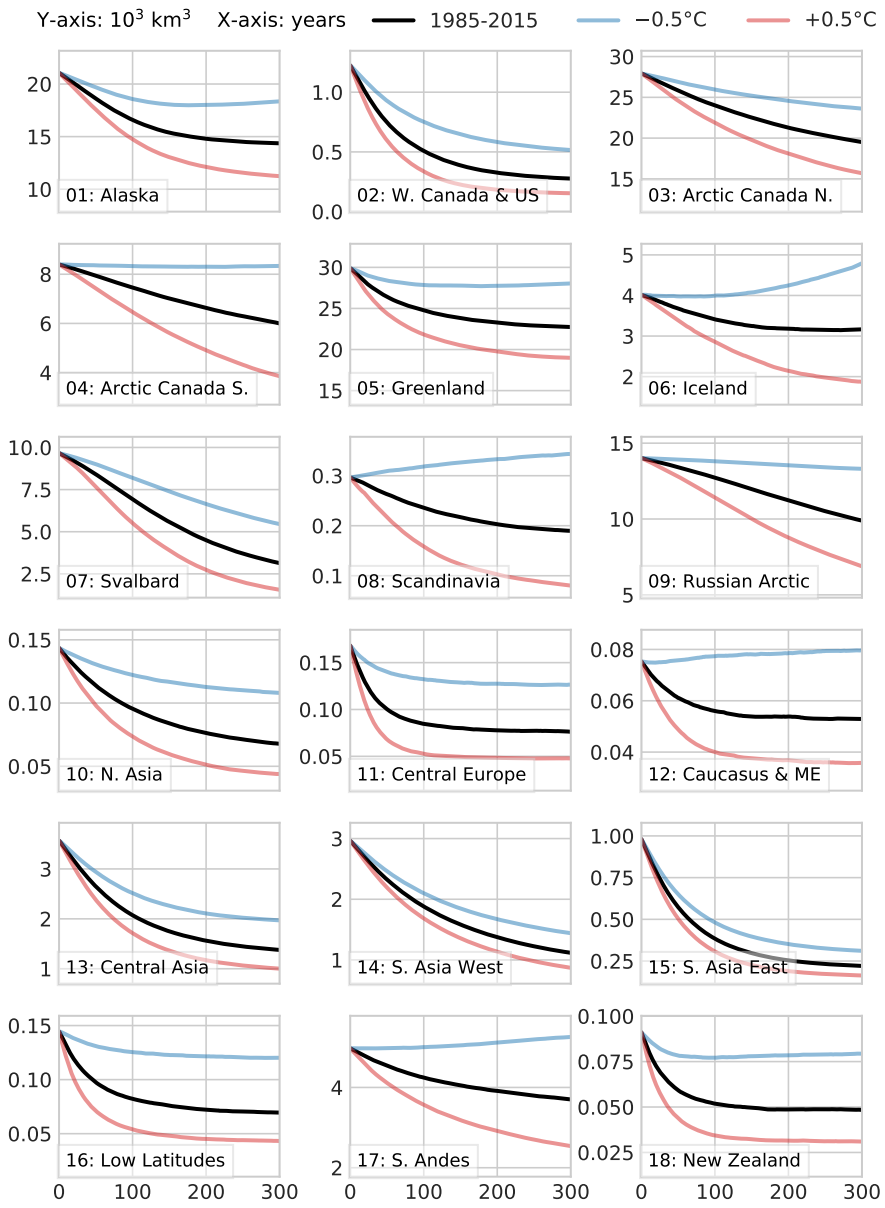

Fig. 2.11: Regional glacier volume change under the 1985-2015 climate (randomized) with three temperature biases ($-0.5°$, $0°$, $+0.5°$). Note the units of the y-axes (10^3 km^3) and the marked regional differences.

A further model test is presented in Fig. 2.12. Here, we apply a new climate scenario: the climate at t^* which, for each glacier individually, represents a theoretical equilibrium climate. In addition to the global response to these scenarios, we separate between the majority group of smaller glaciers and the much smaller group of very large glaciers. Both groups are selected so that they sum up to one quarter of the total glacier volume. A striking feature of the runs is that the glaciers tend to grow under the artificial t^* climate: the growth is slow at first and accelerates with time, hinting towards a positive feedback. This feedback is driven by two factors: first, a higher surface elevation leads to a positive change in mass balance (mass balance-elevation feedback); second, because of the parabolic and trapezoidal bed shapes, a larger ice thickness leads to a wider accumulation area above the ELA and to a wider ablation area below the ELA. It appears that the positive width-accumulation feedback is stronger than the negative width-ablation feedback. This can be explained by the larger accumulation area of glaciers in an equilibrium climate: the average accumulation area ratio at t^* in OGGM is 51%. In order to test which of these feedbacks is stronger, we run a simulation with rectangular bed shapes exclusively (dotted light purple line in Fig. 2.12), therefore eliminating the width-accumulation but keeping the mass balance-elevation feedback. The results show that for the vast majority of glaciers the feedback almost disappears, while the very large glaciers still show a weak and delayed altitude feedback.

It is unclear whether this is a bug or a feature. On the one hand, this behaviour is not really desirable since one would expect glaciers to remain constant under a theoretical equilibrium climate. On the other hand, t^* is just a vehicle to calibrate the model and was not supposed to yield a particular insight (for example, many glaciers can only have an equilibrium t^* climate after the application of a bias to the operational mass balance model). There are many reasons why small initial perturbations such as numerical noise or the differences between the bed inversion and forward model numerical schemes might lead to a different equilibrium. It must also be noted that this feedback is slow to appear, and will only have a notable influence on the largest glaciers for long term simulations in a cooler climate (the global volume change after 100 years due to the feedback is 2.4% for the default and 1% for the all rectangular cases). The very simple definition of an "equilibrium climate" for these very large glaciers is problematic anyway: large glaciers have a very slow but potentially large response to the smallest changes in climate. At the global scale, most of the 300-yr volume loss is due to the small glaciers, which respond faster and stronger than larger ones.

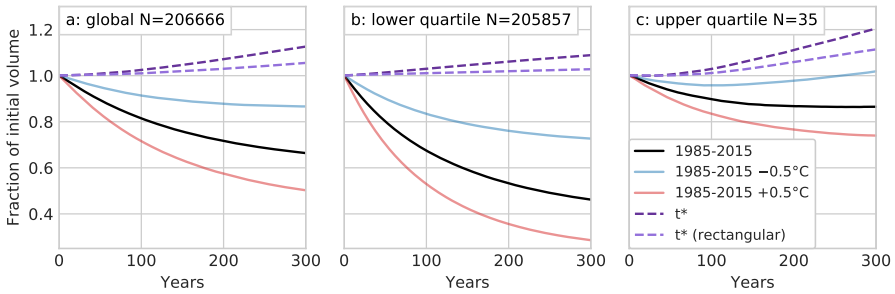

Fig. 2.12: **a**: global glacier volume change under various climate scenarios (1985-2015 climate with three temperature biases and climate at t* which, for each glacier individually, represents a theoretical equilibrium climate) and model configurations (rectangular bed instead of the mixed default), plotted as a fraction of the initial volume. **b** and **c**: volume changes of all glaciers making up for the first and last quartile of the sorted cumulative total volume.

2.5 Conclusions

We present a new model of global glacier evolution, the Open Global Glacier Model (OGGM, v1.1). The panoply of tools available to compute past and future glacier change range from simple box models (e.g. Harrison, 2013) to more complex, geometry aware models (Huss and Hock, 2015, to cite the most recent in date). OGGM undoubtedly belongs to the complex side of this scale. Different model complexities are justified by different problem settings, taking into account the model-specific merits and drawbacks. Instead of endorsing one approach over the other, OGGM aims to provide a framework which allows one to switch between models and allows objective intercomparisons. In fact, the ice dynamics module represents only a small fraction of the OGGM codebase: a huge amount of work has been invested to provide a series of tools which will help others in their own modelling endeavours. Any interested person can download, install, and run these tools at no cost. This includes the automated download of topographic and climate data for any location on the globe, the collation of glacier attributes, the automated computation of glacier centerlines, or the delineation of glacier dynamical entities. While some of these tools have been described elsewhere, the added value of OGGM is that they are now centralised, documented, and available for public review via the open-source model.

In the future, we will continue to encourage external contributions in several ways. First, it must be as easy as possible for a new user to detect where and how a contribution can be implemented: here, documentation is key. Then, the model must be able to cope with different ways to simulate a considered process: every single task in the OGGM workflow can be replaced or enhanced, as long as the format of the input and output files is agreed beforehand. Perfect modularity will be hard to achieve, but the recent implementation of alternative numerical solvers show

that modularity is possible. Finally, we need to ensure attribution to the original contribution (e.g. a scientific publication) in order to engage the wider community. For this purpose, we developed a template repository for external OGGM modules: `https://github.com/OGGM/oggmcontrib`. This development model will ensure that users importing OGGM extensions will be aware of the source of each module they are using and will be able to refer to the original contribution appropriately. We hope that this development model will foster new collaborations.

We cannot (and do not want to) demonstrate that OGGM will provide more accurate estimates of future sea-level rise than earlier attempts. However, OGGM allows new studies which weren't possible before. The dynamical representation of glacier advances and retreat enables studies of glacier evolution at long (paleo-) time scales, where ice dynamics and geometrical attributes such as the accumulation area ratio play an important role (e.g. Mackintosh et al., 2017). First OGGM simulations over the last millennium show very promising results (Goosse et al., 2018). The modular framework allows one to compare the performance of various parametrisations such as the mass balance and downscaling algorithms. It may be argued that the amount of available data is not enough to constrain modelling studies such as ours at the global scale: OGGM can now be used to test this argument by allowing simpler modules to be added to the codebase and test the added value of increased complexity.

Planned and envisioned future developments for the model follow the general guidelines of modularity and extendability. While some of the authors are working on adding even more complexity to the model (for example by improving the frontal ablation and mass balance parametrisations or by implementing a distributed ice dynamics module), it is part of our plans to implement simpler approaches such as the original Marzeion et al., 2012b model or the Huss and Farinotti, 2012 approach to ice thickness estimation. A considerable amount of work will be needed to correctly assess the uncertainties associated with the model chain: here, Monte Carlo and Bayesian approaches might be the way to follow.

The non-linear dynamical behaviour of glaciers raises a wide range of very interesting inverse problems. For example, how to deal with the transient climate issue in the ice thickness inversion algorithm? How much information about past climate can be extracted from moraine proxies and today's glacier extent? What are the uncertainties associated with global sea-level rise estimates, and where do they originate? How much complexity is just right? These are all questions the authors hope will be easier to address through the publication of OGGM.

2.6 Code Availability, Testing, and Software Requirements

The OGGM software is coded in the Python language and licensed under the GPLV3 free software license. The latest version of the code is available on Github (`https://github.com/OGGM/oggm`), the documentation is hosted on ReadTheDocs (`http://docs.oggm.org`), and the project webpage for communication and dissemination can be found at `http://oggm.org`. Past and intermediate versions are available in a permanent DOI repository (`https://zenodo.org/badge/latestdoi/43965645`). The software ships with an extensive test suite which can be used by the users to test their configuration. The tests are triggered automatically at each new code addition, reducing the risk of introducing new bugs (`https://travis-ci.org/OGGM/oggm`). The suite contains unit tests (for example for the numerical core) and integration tests based on sets of real glaciers. At the time of writing, 85% of all relevant lines of code are covered by the tests (i.e. called at least once by the test suite). The remaining 15% are challenging to monitor because they mostly concern the automated downloading tools which are used in production and cannot be tested automatically.

The following open-source libraries have to be installed in order to run OGGM: `numpy` / `scipy` (Walt et al., 2011), `scikit-image` (Walt et al., 2014), `shapely` (Gillies, 2007), `rasterio` (Gillies, 2013), `pandas` (McKinney, 2010), `geopandas`, `xarray` (Hoyer and Hamman, 2017), `pyproj`, `matplotlib` (Hunter, 2007), and `salem` (Maussion et al., 2017). OGGM runs on all major platforms (Windows, Mac, Linux) but we recommend using Linux as this is the platform it is most tested on. The code and data used to generate all figures and analyses of this paper can be found at `https://github.com/OGGM/gmd_paper_2018`.

2.7 Appendix

2.7.1 Climate Data

The default climate dataset used by OGGM is the Climatic Research Unit (CRU) TS v4.01 Dataset (Harris et al., 2014, released 20.09.2017). It is a gridded dataset at 0.5° resolution covering the period 1901-2016. The dataset is obtained by interpolating station measurements and therefore does not cover the oceans and Antarctica. The TS dataset is further downscaled to the resolution of 10' by applying the 1961-1990 anomalies to the CRU CL v2.0 gridded climatology (New et al., 2002). This step is necessary because the TS datasets do not contain an altitude information,

which is needed to compute the temperature at a given height on the glacier. To compute the annual mass balances we use the hydrological year convention (the year 2001 being October 2000 to September 2001 in the Northern Hemisphere, April 2000 to March 2001 in the Southern Hemisphere).

For each glacier, the monthly temperature and precipitation time series are extracted from the nearest CRU CL v2.0 grid point and then converted to the local temperature according to a temperature gradient (default: 6.5K km^{-1}). No vertical gradient is applied to precipitation, but we apply a correction factor p_f=2.5 to the original CRU time series (similar to Marzeion et al., 2012b). This correction factor can be seen as a global correction for orographic precipitation, avalanches, and wind-blown snow. It must be noted that this factor has few (if any) impact on the mass balance model performance in terms of bias. This is due to the automated calibration algorithm, which will adapt to a new factor by acting on the temperature sensitivity μ^*. To verify that the chosen precipitation factor is realistic, we use another metric: the standard deviation of the mass balance time-series. Comparisons between model and observations show that the model underestimates variability by about 10%: we could tune the precipitation factor towards higher values to reduce this discrepancy but refrain to do so, as we do not want to add an additional free parameter in the model.

2.7.2 WGMS Glaciers

To calibrate and validate the mass balance model, OGGM relies on mass-balance observations provided by the World Glacier Monitoring Service (WGMS, 2017). The Fluctuations of Glaciers (FoG) database contains annual mass-balance values for several hundreds of glaciers worldwide. We exclude water-terminating glaciers and the time series with less than five years of data. Not all of the remaining glaciers can be used by OGGM: we also need a corresponding RGI outline. Indeed, the WGMS and RGI databases have distinct glacier identifiers and it is not guaranteed that the glacier outline provided by the RGI fits the outline used by the local data providers to compute the specific mass balance. Since 2017, the WGMS provides a lookup table linking the two databases. We updated this list for the version 6 of the RGI, leaving us with 254 mass balance time series.

These data are not equally distributed over the glaciated regions (see e.g. Zemp et al., 2015, and Fig. 2.13), and their quality is highly variable. In the absence of a better data basis (at least for the 20th century), we have to rely on them for the calibration and validation of our model. Fortunately, these data play a relatively minor role in the model calibration as explained in Sect. 2.3.3. For future studies it

might be advisable to use independent, regional geodetic mass balance estimates for validation as well.

2.7.3 RGI Regions

A map of the RGI regions and some basic statistics are presented in Fig. 2.13.

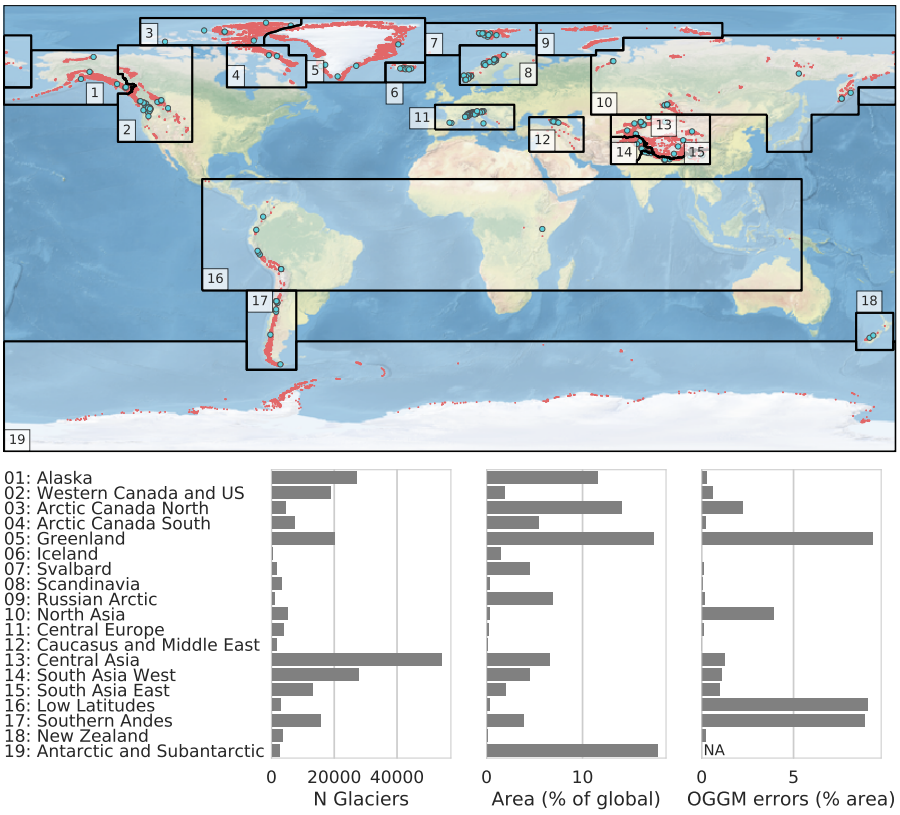

Fig. 2.13: **Upper panel**: map of the RGI regions; the red dots indicate the glacier locations and the blue circles the location of the 254 reference WGMS glaciers used by the OGGM calibration. **Lower panel**: region names and basic statistics of the database (number of glaciers per region, regional contribution to the global area in percent, and percentage of the regional area which cannot be modelled by OGGM).

Author contributions

BM and FM are the initiators of the OGGM project. FM is the main OGGM developer and wrote most of the paper. AB developed the downstream bedshape estimation algorithm. NC wrote parts of the documentation. MD wrote the cross-validation monitoring webpage. JE developed the glacier partitioning tool. KF wrote parts of the bed inversion and dynamical cores. PG wrote the lateral drag parameterization. AJ provided a robust implementation of the dynamical core used for testing and contributed to the development of the operational scheme. JL provided the WGMS

to RGI lookup table and contributed to the topographical data download tool. FO contributed to the AWS deployment tool. BR developed the frontal ablation parametrisation tool. TR developed the download and parallelisation tools and is largely responsible for the successful deployment of OGGM on supercomputing environments. AV contributed to the climate and mass balance tools. CW provided the first implementation of the centerline determination algorithm. All authors continuously discussed the model development and the results together.

3

Initialization of a Global Glacier Model Based on Present-Day Glacier Geometry and Past Climate Information: an Ensemble Approach

Published 2019 in *The Cryosphere*, **13**, pages 3317–3335

Authors and Affiliation

Julia Eis [1], Fabien Maussion [2] and Ben Marzeion [1,3]

[1] Institute of Geography, University of Bremen, Bremen, Germany
[2] Department of Atmospheric and Cryospheric Sciences, University of Innsbruck, Innsbruck, Austria
[3] MARUM - Center for Marine Environmental Sciences, University of Bremen, Bremen, Germany

Context

The Open Global Glacier Model (OGGM; presented in Chapt. 2) can be used to simulate past and present glacier mass change for each of the world's glaciers individually. But especially for the simulations in the past, OGGM is so far lacking an adequate initialization method. After the preprocessing, the only information available is the present day state, which is derived from the glacier outline and the underlying topography data. Initializing a past climate run (e.g. in 1850) with this state, would lead to large uncertainties and unrealistic glacier mass changes, as the present-day state in many cases is by far to small. With the increase in complexity (compared to the model in Marzeion et al. (2012b)), the initialization of OGGM requires the determination of the widths, the surface elevation and the bed topography for each grid point along the flowline. To this end, we present in this

Chapter a new initialization approach that relies on the only information given: the present day state of a glacier and information about past climate. First, a large set of plausible glacier states is generated using a random climate run. In the next step a subset of glacier candidates is selected and modeled forward to the present day by using past climate information. A fitness function that takes geometry differences from the present day states into account, is utilized to evaluate the selected glacier candidates. However, in many cases, the results are non-unique, viz. multiple glacier candidates converge to the present day state. We applied the method initially in a synthetic environment only, allowing us to determine the uncertainties of the method itself (under perfectly known boundary conditions). Additionally, we tested different fitness functions to determine the best evaluation criteria. Furthermore, we analyzed the reconstructablity of glaciers with regard to specific glacier characteristics (e.g. glacier size, slope, response time). Due to the synthetic environment it was not possible to compare the results with real glacier observations from the past. This aspect and the necessary changes to the model calibration will be considered in the next chapter (Chapt. 4).

Personal Contribution

J. Eis is the main developer of the initialization module. This includes the design, the implementation, the testing, as well as the documentation of this external OGGM module. J.Eis performed all simulations, created all graphics and mainly wrote the paper. The conceptual design of the study was done by J.Eis consulted by the co-authors F. Maussion and B. Marzeion. All authors continuously discussed the findings and earlier states of the manuscript. A detailed description of the contribution of all authors can be found in the author contribution section on page 80.

3.1 Abstract

To provide estimates of past glacier mass changes over the course of the 20th century, an adequate initial state is required. However, empirical evidence about past glacier states at regional or global scales is largely incomplete, both spatially and temporally, calling for the use of automated numerical methods. This study presents a new way to initialize the Open Global Glacier Model from past climate information and present-day glacier states. We use synthetic experiments to show that even with these perfectly known but incomplete boundary conditions, the problem of model initialization is an ill-posed inverse problem leading to nonunique solutions, and we propose an ensemble approach as a way forward. The method works as follows: we generate a large set of physically plausible glacier candidates for a given year

in the past (e.g., 1850 in the Alps), all of which are then modeled forward to the date of the observed glacier outline and evaluated by comparing the results of the forward runs to the present-day states. We test the approach on 2660 Alpine glaciers and determine error estimates of the method from the synthetic experiments. The results show that the solution is often nonunique, as many of the reconstructed initial states converge towards the observed state in the year of observation. We find that the median state of the best 5 % of all acceptable states is a reasonable best estimate. The accuracy of the method depends on the type of the considered observation for the evaluation (glacier length, area, or geometry). Trying to find past states from only present-day length instead of the full geometry leads to a sharp increase in uncertainty. Our study thus also provides quantitative information on how well the reconstructed initial glacier states are constrained through the limited information available to us. We analyze which glacier characteristics influence the reconstructability of a glacier, and we discuss ways to develop the method further for real-world applications.

3.2 Introduction

Glaciers contributed significantly to past sea-level rise (SLR; e.g., Gregory et al., 2013; Slangen et al., 2017a; WCRP Global Sea Level Budget Group, 2018; Wouters et al., 2019; Zemp et al., 2019), and they will continue to be a major contributor in the 21st century (e.g., Church et al., 2013; Slangen et al., 2017b; Hock et al., 2019). A large fraction of this contribution will be caused by the ongoing adjustment of glaciers to previous climate change (Marzeion et al., 2014a; Marzeion et al., 2018). Reconstructions of past glacier mass change are therefore not only necessary to determine the budget of past sea-level change (Gregory et al., 2013) and to increase the confidence in projections (by allowing the quantification of the agreement with observations; Marzeion et al., 2015); they also enable us to quantify the pattern of the ongoing adjustment of glaciers to present-day climate. Estimates of global glacier mass change are based on in situ measurements in mass and length changes (e.g., Zemp et al., 2015; Leclercq et al., 2011), on remote sensing techniques (e.g., Gardner et al., 2013; Jacob et al., 2012; Bamber et al., 2018; Wouters et al., 2019), or on mass balance modeling driven by climate observations (Marzeion et al., 2012b; Marzeion et al., 2015). Since observations of temperature, and to a smaller degree precipitation, are more ubiquitous (e.g., Harris et al., 2014) than glacier observations (WGMS, 2018), reconstructions of glacier change produced by forcing a glacier model with climate observations have the potential to increase the understanding of past glacier behavior. Finally, reconstructing glacier change based on climate model output allows us to test the skill of climate models (Goosse et al., 2018).

A number of global glacier models were developed in the past (e.g., Radić and Hock, 2011; Radić and Hock, 2014; Giesen and Oerlemans, 2012; Giesen and Oerlemans, 2013; Marzeion et al., 2012b; Marzeion et al., 2014a; Huss and Hock, 2015; Maussion et al., 2019). The more recent and complex of these models (e.g., Huss and Hock, 2015; Maussion et al., 2019) require digital elevation models (DEMs) and outlines from the Randolph Glacier Inventory (RGI; Pfeffer et al., 2014) to derive the initial surface hypsometry. Hence, their starting date of a glacier evolution simulation depends on the recording date of the DEM and the outline, which typically do not coincide with one another, nor with the required starting date of a projection. The model of Huss and Hock (2015) indicates a high sensitivity to the initial ice volume. Similarly, Maussion et al. (2019) remark that great uncertainties, especially on local and regional scales, derive from unknown initial conditions.

Despite the importance of glacier contribution to past sea-level rise, so far only one model was able to provide estimates of glacier mass changes over the course of the entire 20th century on the global scale (Marzeion et al., 2012b). All other global modeling studies limit their application to the recent past and future projections. The reconstruction by Marzeion et al. (2012b) was possible because of the highly parameterized representation of ice dynamics and glacier geometry change, applying a volume–area–time scaling to translate mass change into surface area and elevation range changes. Based on this approach, it was sufficient to iteratively optimize one variable (glacier size in the year of interest, e.g., 1850) such that when run forward to the year of the observed glacier outline, the modeled glacier area agreed with the observed glacier area.

An increase in model complexity impedes the process as more and more variables are required for initialization. Flow line models require input data along the coordinates of the flow line (e.g., bed topography, surface elevations, and/or widths), and thus more complex initialization methods are needed. For example, Pelt et al. (2013) developed an iterative inverse method to reconstruct distributed bedrock topography and simultaneously initialize an ice flow model. Zekollari et al. (2019) added an ice flow model to Huss and Hock (2015), which required an automated initialization for glaciers in 1990 (prior to the glacier inventory date) to avoid spin-up issues and so that the reconstructed initial states fit the glacier geometry at the inventory date after being modeled forward. By choosing a decade-long initialization, they avoid problems of nonuniqueness (as we discuss below), but they raise the question of how arbitrarily this date can be chosen. Similar approaches exist for the initialization of ice sheet models, where most work focuses on estimating the present-day state of ice sheets in order to make accurate projections of future ice sheet change (e.g., Heimbach and Bugnion, 2009; Lee et al., 2015; Mosbeux et al., 2016). Goelzer et al. (2018) divide the existing initialization approaches into three methods: spin-up, assimilation of velocity, and assimilation of surface elevation. Spin-up procedures

are typically used for long-term and paleoclimate simulations; the required spin-up time is unknown and can be relative long. Additionally, the reconstruction cannot be expected to represent effects from internal climate variability correctly. The data assimilation approaches typically determine model parameters (e.g., basal parameters like basal friction or bedrock topography) that reduce the mismatch between observed and modeled velocities or surface elevations.

In this study, we aim to identify fundamental limitations that narrow the reconstruction of past glacier states from present-day geometries, under the assumption of perfectly known boundary conditions and a perfect glacier model. Specific research questions are as follows.

- To which degree does the past evolution of a glacier constrain its present-day geometry?
- How much information does the present-day glacier geometry contain about its past states?
- Is it possible to reconstruct past glacier states from the partial information available to us?
- How far can we go back in time to have an initial geometry that still determines the present-day glacier geometry?
- Which glacier attributes influence the answers to the questions above?

To this aim, we present a new method estimating past glacier states and apply it to synthetic numerical experiments, and we show the obstacles that need to be overcome before applying our method to real-world problems. After introducing the relevant features of the Open Global Glacier Model (OGGM; Maussion et al., 2019) in Sect. 3.3.1, we describe the design of the synthetic experiments in Sect. 3.3.3. The synthetic framework serves to test the skill of our approach in a surrogate model world where everything is known, and it allows us to apply data denial experiments to address the questions listed above. The initialization method is presented in Sect. 3.3.4. The developed method consists of three steps: generation of plausible glacier states, identification of glacier state candidates, and their evaluation based on the misfit between the modeled and the observed geometry at the year of the observation. We applied our approach to 2660 Alpine glaciers and present the results for the reconstructed initial states in the year 1850 in Sect. 3.5.1. The influence of the considered type of observation (e.g., glacier length, area, or geometry) is shown in Sect. 3.5.2 and a statistical analysis of glacier attributes that influence the reconstructability of a glacier is presented in Sect. 3.5.3. Finally, we summarize the

results and discuss the limitations of the method and its applicability to real-case studies, as well as needed and possible future developments in Sect. 3.7.

3.3 Methods

3.3.1 The Open Global Glacier Model

The Open Global Glacier Model (OGGM; Maussion et al., 2019) is an open-source numerical framework that allows the modeling of past and future changes of any glacier in the world. Starting with a glacier outline, provided by the Randolph Glacier Inventory (RGIv6.0; Pfeffer et al., 2014), a suitable surface DEM is automatically downloaded and interpolated to a local grid. The size of the local grid is given by a border parameter, which is the number of grid points outside the glacier boundaries. We choose a border value of 200 grid points to ensure that large glacier states can also be generated. The resolution of the map topography $\mathrm{d}x$ depends on the size of the glacier ($\mathrm{d}x = a\sqrt{S}$, with $a = 14\,\mathrm{m\,km^{-1}}$ and S the area of the glacier in square kilometers) and is constrained to $10\,m \leq \mathrm{d}x \leq 200\,m$. After the preprocessing, glacier centerlines are computed using a geometrical routing algorithm (adapted from Kienholz et al., 2014). They are then considered to be glacier flow lines, and grid points are generated using a fixed, equidistant grid spacing, which is twice that of the underlying 2-D map topography. Surface elevations along the flow line coordinates are then obtained from the underlying topography file, and glacier section widths are computed by intersecting the normal of the flow line to the boundaries of the glacier. By making assumptions about the shape of the bed (parabolic, rectangular, or a mix of both), OGGM estimates the ice thickness with a mass-conservation approach (Farinotti et al., 2009; Farinotti et al., 2017; Farinotti et al., 2019). Information on bed topography at each grid point results from the calculated ice thickness and the surface elevation. From this, the glacier length, area, and volume can be determined. These values depend strongly on the surface topography and are based on the (often wrong) assumption that the recording date of DEM and that of the outline coincide. The dynamical flow line model of OGGM can then be used to determine the evolution of the glacier under any given climate forcing by solving the shallow ice approximation along the flow lines.

The mass balance is computed at each grid point using climate data (monthly temperature and precipitation). Climate data can be used from different sources, including gridded observations or reanalyses for past climate, projections for future climate, or randomized climate time series. The purpose of forcing the mass balance model with randomized climate is to easily produce a great number of realistic climate forcings representative of a given time period, characterized by a center year

y_0 and a window size h (typically 31 years). All climate years $\in [y_0 - \frac{h-1}{2}, y_0 + \frac{h-1}{2}]$ are then shuffled infinitely in the next step. Additionally, it is possible to set a temperature bias β, which shifts all values of the temperature series towards warmer or colder climates.

Identically to the study of Maussion et al. (2019), we only calibrate the mass balance model, while the creep parameter A and the sliding parameter f_s are the same for each glacier and set to their default values ($A = 2.4 \times 10^{-24}\,\mathrm{s}^{-1}\,\mathrm{Pa}^{-3}$, $f_s = 0$, no lateral drag). The following mass-balance-related parameter values were used in this study: $p_f = 1.75$, $T_{\mathrm{Melt}} = -1.5°C$, $T_{\mathrm{Liquid}} = 2.0°C$, and $\Gamma = -6.5\,\mathrm{K\,km}^{-1}$. This parameter set was determined with a cross-validation performed with the HISTALP data set and tested for the 41 Alpine glaciers with more than 5 years of mass balance observation. For more details concerning the glacier model (e.g., the mass balance calibration or sensitivities to the dynamical parameters of the model), please refer to Maussion et al. (2019) and `http://docs.oggm.org` (last access: 10 December 2019).

3.3.2 Problem Description

Here, we define a *glacier state* (hereinafter referred to as *state*) as follows.

Definition 1. Let $m \in \mathbb{N}$ be the total number of grid points of all flow lines of a glacier. Then $s_t = (z_t, w_t, b)$ is a glacier state at time t, with surface elevation $z_t \in \mathbb{R}_+^m$, widths $w_t \in \mathbb{R}_+^m$, and bed topography $b \in \mathbb{R}_+^m$. The set $\mathcal{S}_{t_i} = \{s_t | t = t_i\}$ contains all physically plausible glacier states at time t_i.

The construction of an initial state is an inverse problem and can be defined in opposition to the direct problem. The *direct problem* corresponds to a forward model run: given an initial state $s_{t_0} \in \mathcal{S}_{t_0}$ at time t_0, the state $s_t \in \mathcal{S}_t$ at time $t > t_0$ can be computed by

$$s_t = G_{\mathrm{past}}(s_{t_0}), \tag{3.1}$$

where $G_{\mathrm{past}} : \mathcal{S}_{t_0} \to \mathcal{S}_t$ is an operator representing the equations of OGGM, using known climate time series as the boundary condition.

For *inverse problems*, the solution is known by direct observations: $s_{t_e} = s_{t_e}^{\mathrm{obs}}$, whereas the desired initial state s_{t_0} is unknown. The inverse problem consists of finding the initial state $s_{t_0} \in \mathcal{S}_{t_0}$, such that the forward modeled solution at time t_e fits the observations from the same year t_e:

$$s_{t_0} = G_{\mathrm{past}}^{-1}(s_{t_e}^{\mathrm{obs}}). \tag{3.2}$$

Unfortunately, we do not have an explicit formulation for G_{past}^{-1} in our case. A backwards reconstruction is impeded by the nonlinear interaction between glacier geometry, ice flow, and mass balance. Optimization methods can be used to solve inverse problems. To this end, we introduce a minimization problem such that the forward modeled state is as close as possible to the observation:

$$\min_{s_{t_0} \in \mathcal{S}_{t_0}} j(s_{t_0}), \tag{3.3}$$

with

$$\begin{aligned} j(s_{t_0}) :&= \frac{1}{m} \parallel s_{t_e}^{\text{obs}} - \underbrace{G_{\text{past}}(s_{t_0})}_{s_{t_e}} \parallel_2^2 \\ &= \frac{1}{m} \left(\sum_{i=0}^{m} \left(\left(z_{t_e}^{\text{obs}}\right)_i - \left(z_{t_e}\right)_i \right)^2 \right. \\ &\quad \left. + \left(\left(w_{t_e}^{\text{obs}}\right)_i - \left(w_{t_e}\right)_i \right)^2 \right). \end{aligned} \tag{3.4}$$

This function calculates the averaged difference in surface elevation and width between the observed and forward modeled glacier states. Differences in bed topography can be neglected, as we assume the bed topography to remain the same over the inspected time period.

In many cases, however, OGGM forward integrations of different initial states result in very similar states at time t_e. This implies that there exist many local minima of the function $j(s_{t_0})$. As uncertainties of the model can safely be assumed to be larger than the differences between those states at time t_e, it is impossible to identify the global minimum of $j(s_{t_0})$. That is, the solution of our inverse problem is nonunique.

The objective of our approach is therefore to identify the set $\mathcal{S}_{t_0}^{\epsilon}$ of all states, which correspond to the observed state $s_{t_e}^{\text{obs}}$ within a given uncertainty ϵ after being modeled forward. We call this condition the *acceptance criterion*:

$$J(s_{t_0}) := \frac{j(s_{t_0})}{\epsilon} < 1. \tag{3.5}$$

The function $J(s_{t_0})$ is called the *fitness function* in the following. Assuming a vertical error of 5 m in x and a horizontal error of 10 m in w, we propose setting $\epsilon = (5\,m)^2 + (10\,m)^2 = 125\,m^2$. These numbers can be changed easily, and in a real-world application they should be based on the vertical uncertainty of the reconstructed ice thickness and the horizontal uncertainty of the used outline. All states $s_{t_0} \in \mathcal{S}_{t_0}^{125}$ that have a fitness value smaller than 1 are called *acceptable states*. The first expectation would be that the glacier candidate with the smallest fitness value is also the best solution. However, due to uncertainties that derive from the model integration itself, this is not always the case. As an alternative, we

determine the 5th quantile of all states in $\mathcal{S}_{t_0}^{\epsilon}$. This set contains the best solutions of all acceptable states referring to their fitness values. We choose the median state as a representative of this set and compare the state with the minimal fitness value and the median state in Sect. 3.5.1.

3.3.3 Synthetic Experiments

3.3.3.1 Design

We create a time series of glacier states, which range from the target year of initialization t_0 (e.g., 1850) to the present date t_e (see Fig. 3.1 for an example). These are the glacier states that we aim to reconstruct with our initialization method, using only partial information (here the observed state at present day). This type of experiment is sometimes called "inverse crime" in the inverse problem literature (e.g., Colton and Kress, 1992; Henderson and Subbarao, 2017), and we explain this rationale below. To generate the synthetic experiments, we apply a random climate scenario (window size $h = 31$ years and center year $y_0 = t_0 = 1850$) and run the model 600 years forward (see Fig. 3.1c). The temperature bias is set to $\beta = -1\,\mathrm{K}$ to ensure that a relatively large 1850 glacier state is created (as expected for most real glaciers at the end of the Little Ice Age). The resulting state is defined to be the synthetic experiment state in year t_0 (see Fig. 3.1a). We model this state forward, applying the past climate time series from t_0 until t_e (here 2000) (see Fig. 3.1d) and obtain the observed state of the synthetic experiment (see Fig. 3.1b). Thanks to the initial temperature bias of $\beta = -1\,\mathrm{K}$, these synthetic states in t_e are very close to the real observed states in 2000 on average (total area difference for the Alps of about 1 %, but individual glaciers can vary), and the total synthetic glacierized area in 1850 fits well to an estimate of Zemp et al. (2006) (see Appendix 3.9.1 for more details). We call the states derived from the synthetic experiment s_t^{exp}.

3.3.3.2 Rationale

These synthetic states therefore provide a realistic setting with a strong advantage over actual observations: they are perfectly known. As stated in the introduction, reconstructing past glacier states is a complex inverse problem, the accuracy of which will depend on (i) the uncertainties in the boundary conditions (climate, glacier bed, etc.), (ii) the uncertainties in the glacier model itself, and (iii) a theoretical lower bound (termed "reconstructability" in this study) tied to the characteristics of the glacier itself (slope, size, the past climate, etc.). The main objective of the synthetic experiments is to separate these issues from one another and to focus on point (iii) only. This allows us to isolate and understand the limitations and

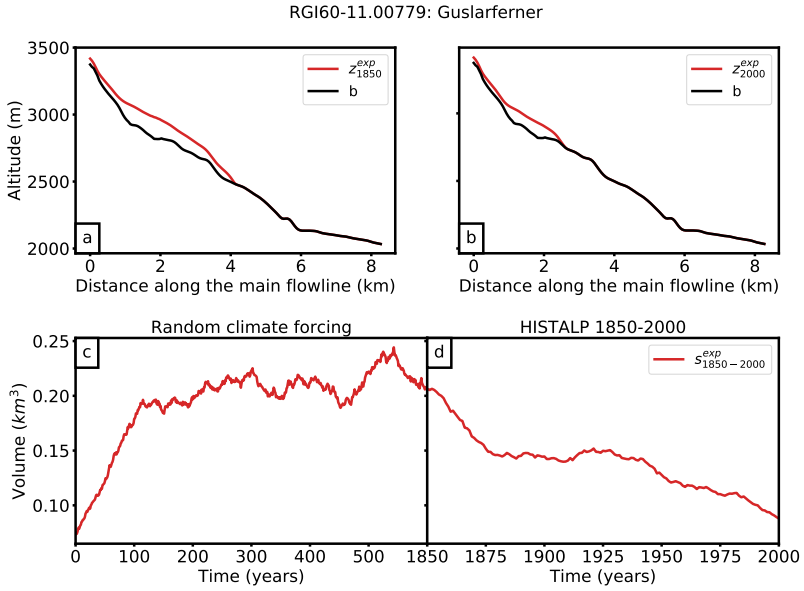

Fig. 3.1: Illustration of the generation of the synthetic experiment with the example of Guslarferner (Oetztal, Austria). Glacier thickness along the main flow line at **(a)** $t_0 = 1850$ and **(b)** $t_e = 2000$ is shown. The black line indicates the bed rock and the red line the ice surface of the synthetic experiment. **(c)** Generation of s^{exp}_{1850}, which is the state at $t = 600$ (the end of the trajectory), and **(d)** the volume of the glacier states s^{exp}_t from 1850 to 2000. Note that the synthetic year 2000 glacier does not necessarily correspond to the "true" year 2000 glacier.

errors of the developed method itself, as opposed to uncertainties that derive from unknown boundary conditions and model parameters. They also allow us to realize data denial experiments and detect which kinds of observations are necessary to reduce the uncertainties of our reconstruction (Sect. 3.5.2) and to determine which glacier characteristics affect the reconstructability of a glacier (Sect. 3.5.3).

3.3.4 Reconstruction of Initial Glacier States

Our initialization method consists of three main steps: generation of a set of physically plausible glacier states $\mathcal{S}_{t_0}$, identification of glacier candidates $s_{t_0} \in \mathcal{S}_{t_0}$, and their evaluation based on the fitness function $J(s_{t_0})$ (see Sect. 3.3.2).

3.3.4.1 Generation of Potential Glacier Candidates

In a first step, we generate a set of different, physically plausible states from which we will pool our candidates (Fig. 3.2a). For this purpose, we utilize a random mass balance model with a window size of $h = 31$ years and the center year $y_0 = t_0$ to create different climate conditions. Obviously, we do not use the same permutation as for the creation of the synthetic experiments (Sect. 3.3.3). This procedure generates a climate representative of a given time period with an interannual variability

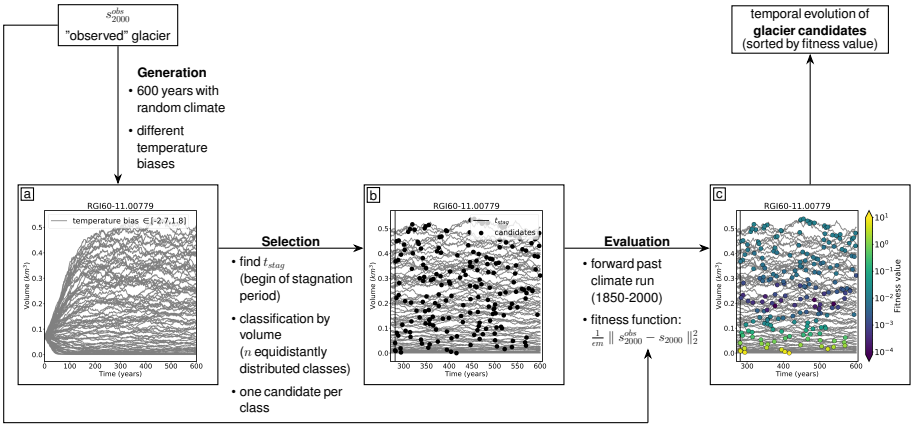

Fig. 3.2: Workflow of the candidate generation, selection, and ranking method, using Guslarferner (Oetztal, Austria) as an example. **(a)** Generation of potential glacier candidates. The grey lines indicate the glacier volume evolution for a set of different random climate scenarios over 600 years each. The temperature biases vary between -2.7 and 1.8 K. **(b)** Selection of candidates. The black vertical line indicates t_{stag} and the black points show 200 candidates. **(c)** Glacier candidates colored by their fitness value. Violet marks candidates with a small misfit, whereas yellow marks states that do not meet the acceptance criterion (Eq. 3.5).

uncorrelated to that of the original period. For each random climate a different way of permutation is used. This ensures that all generated climate time series differ from each other, but at the same time all represent the climate conditions around t_0 (and an associated temperature bias β). The infinite permutation is necessary to obtain a time series that is long enough for the glaciers to reach an equilibrium (while maintaining the impact of interannual climate variability) with the forcing climate (here 600 years). To create a large set of states, we additionally vary the temperature bias β. Glaciers respond differently to changes in climate, and thus the required temperature biases vary from glacier to glacier and have to be inferred. We start with temperature biases $\beta \in [-2, 2]$ K. If $\beta = 2$ K is not large enough to result in a present-day glacier with zero ice thickness, higher values will be used. If $\beta = -2$ K is not small enough to result in a glacier that reaches the boundary of the local grid (200 grid points outside of the glacier outline), smaller values will be used.

3.3.4.2 Selection of Candidates

Figure 3.2a shows the evolution of the volume of the generated glacier states over time. In the first years, the time series clearly diverge (mostly caused by the temperature bias β), but after a certain time all time series begin to fluctuate around an equilibrium value. We refer to the period of fluctuations around the assumed equilibrium as the *stagnation period*. During the stagnation period the glacier volume does not increase or decrease strongly in comparison to the total volume change since the beginning of the simulation. We define t_{stag} as the point in time when all trajectories have reached this stagnation period and choose the upper 10 volume

trajectories, corresponding to the lowest temperature biases, to determine t_{stag}. To this end, we smooth each of the 10 curves with a 10-year rolling window and calculate the time point of their first maximum. t_{stag} is defined as the latest of all previously determined time points (see Fig. 3.2b).

Defining t_{stag} is necessary because we determine initial glacier states at $t_0 = 1850$ and the searched glaciers are assumed to be in equilibrium with the climate around 1850. Hence, each state that fluctuates around an equilibrium value is a potential glacier state candidate (in the following referred to as "candidate"). This holds true for all states s_t with $t > t_{\mathrm{stag}}$. Depending on t_{stag} and the number of successfully completed random climate runs n_{r} (number of grey lines in Fig. 3.2), the sample size is $n_{\mathrm{r}}(600 - t_{\mathrm{stag}})$ (glacier states are stored yearly). The sample size is sufficiently large for all cases, e.g., in the case of the Guslarferner (Fig. 3.2) the sample contains approximately 44 500 members. In order to avoid testing very similar states, we classify all states by their volume and select one candidate per class. We choose n equidistantly and approximately uniform distributed classes, where n (default $n = 200$) is the number of candidates to evaluate in step three.

3.3.4.3 Evaluation

The last step evaluates all previously selected candidates. Each candidate is used as the initial condition for a forward run, using observed past climate time series, e.g., from $t_0 = 1850$ until $t_e = 2000$. All runs use the same model parameter set, except for the initial condition and exactly the same climate time series (e.g., no temperature bias β is applied for the past climate runs). Afterwards, we compare the resulting modeled states s_{t_e} with an observed state $s_{t_e}^{\mathrm{obs}}$ (here taken from the synthetic experiment) by applying the fitness function $J(s_{t_0})$ (Eq. 3.5). This function calculates the averaged difference between the glacier geometries at the grid points, more specifically between the surface elevations z_{t_e} and the widths w_{t_e}, of the observed and the modeled glacier. In Fig. 3.2c the candidates are colored by their fitness value.

3.4 Test Site and Input Data

We tested our approach on Alpine glaciers. The glacier outlines are taken from the Randolph Glacier Inventory (RGI v6.0, region 11; Pfeffer et al., 2014). We use topographical data from the Shuttle Radar Topography Mission (SRTM) 90 m Digital Elevation Database v4.1 (Jarvis et al., 2008). The SRTM acquisition date (2000) matches that of the RGI well (2003 for most glaciers). The climate data set we use for this approach is the HISTALP database (Auer et al., 2007, `http://www.zamg.ac.`

at/histalp, last access: 10 December 2019). The temperature time series covers the period 1780 to 2014 and the precipitation time series 1801 to 2014. Both data sets are available on a regular grid of 5 min resolution (approximately 9.3 km in the Alps).

We generate synthetic experiments (see Sect. 3.3.3) for all glaciers in the Alps, and we determine their glacier states in 1850 if the area of the observed synthetic state s^{exp}_{2000} is larger than $0.01\,\text{km}^2$. This value is consistent with the minimum-area threshold of the RGI. The condition is satisfied for 2660 synthetic experiments of the 3927 glaciers included in the Randolph Glacier Inventory in central Europe (region 11).

3.5 Results

Here we show the results for two example glaciers in 1850 as well as an error analysis for all tested glaciers (Sect. 3.5.1), the influence of the choice of the fitness function on the quality of our results (Sect. 3.5.2), and a statistical analysis of glacier attributes (including glacier response time) that influence the reconstructability of a glacier (Sect. 3.5.3).

3.5.1 Initial Glacier States in 1850

Following the method described in Sect. 3.3.4, we determine reconstructed initial glacier states in $t_0 = 1850$. Figures 3.3 and 3.4 show the results of Guslarferner, as an example glacier with a large set of accepted candidates. A second case with a more narrow set of acceptable states, Hintereisferner, is shown in Figs. 3.5 and 3.6. More examples can be found in the Supplement.

In particular the result of Guslarferner shows clearly that the determination of past states is not unique (see Fig. 3.3). Multiple initial states (violet and blue) merge to the observed state in the year of observation. The fitness values, which means the averaged difference between the forward modeled states and the observation at $t_e = 2000$, are extremely small for most candidates. The fitness values of all candidates range from 1.08 $\times 10^{-6}$ to 7.98. Only 16 of the 200 candidates have a fitness value higher than 1 and thus do not fulfill the acceptance criterion (Eq. 3.5); for these states, the glacier in 1850 is too small to reach the volume of the observed glacier within 150 years. Also, Fig. 3.4 illustrates the diversity of the different acceptable solutions (grey, shadowed area). The length of all states in S^{125}_{1850} varies between 0.98 and 8.1 km. The acceptance criterion in this example is not strong enough to provide any information about the searched state in $t_0 = 1850$, as any of

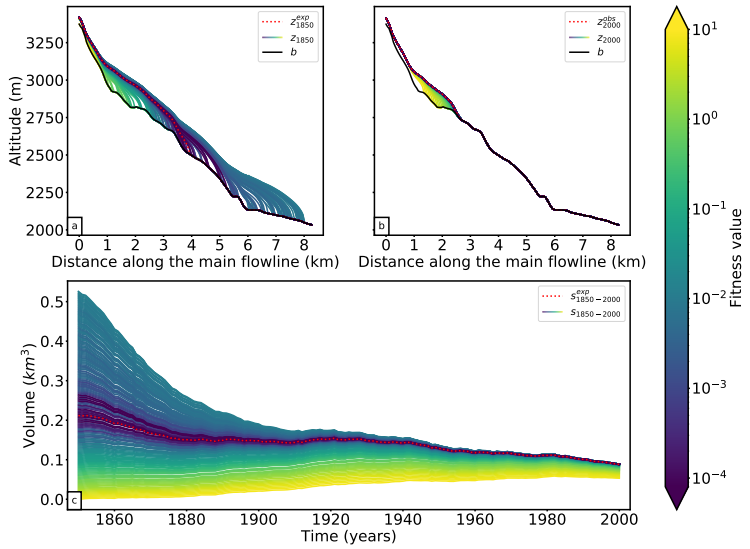

Fig. 3.3: Results for Guslarferner (Oetztal, Austria). Cross sections along the main flow line in **(a)** 1850 and **(b)** 2000 are shown. The black line indicates the bedrock, the red dotted line the surface elevation from the synthetic experiment, and the remaining lines the modeled ice surfaces of all candidates, colored by their fitness value. The synthetic experiment state in 2000 has a length of 2.7 km, an area of 1.71 km^2, a volume of 0.09 km^3, and a mean thickness of 62.8 m. **(c)** Volume changes from 1850 to 2000, colored by their fitness values.

the candidates would lead to an acceptable result. Figure 3.4 also shows the 5th percentile of all acceptable states (blue shadowed area). This set contains the 5 % best solutions, based on the fitness value. All candidates of the 5th percentile are in close proximity to the synthetic experiment. The range of fitness values of all candidates of the 5th percentile is $[1.08 \times 10^{-6}, 7.95 \times 10^{-5}]$, and the length of the states in 1850 only varies from about 3.6 to 5.3 km. All these candidates match the synthetic experiment in $t_e = 2000$ very well and converge to the synthetic experiment by 1900 at the latest, which can be seen in Fig. 3.4c. As a representative of this set, we choose the median state of the 5th percentile of S_t^{125} (in the following referred to as s_t^{med}). Figure 3.4a shows that the surface elevation of s_{1850}^{med} in 1850 corresponds very well to the synthetic experiment, whereas the state with the minimum fitness value (in the following referred to as s_t^{min}) mismatches the synthetic experiment at the tongue of the glacier. Regarding the volumes, s_t^{med} exactly matches the volume of the synthetic experiment in 1850, whereas the volume of s_t^{min} differs by 0.4 km^3.

In the case of Hintereisferner (see Fig. 3.5) the fitness values of most candidates are large compared to those of Guslarferner. Only a few candidates have extremely small fitness values and the past state is thus much more narrowly confined. The different states need more time to adapt to the climate conditions and therefore they do not converge as quickly to one state. As a result, the differences between the

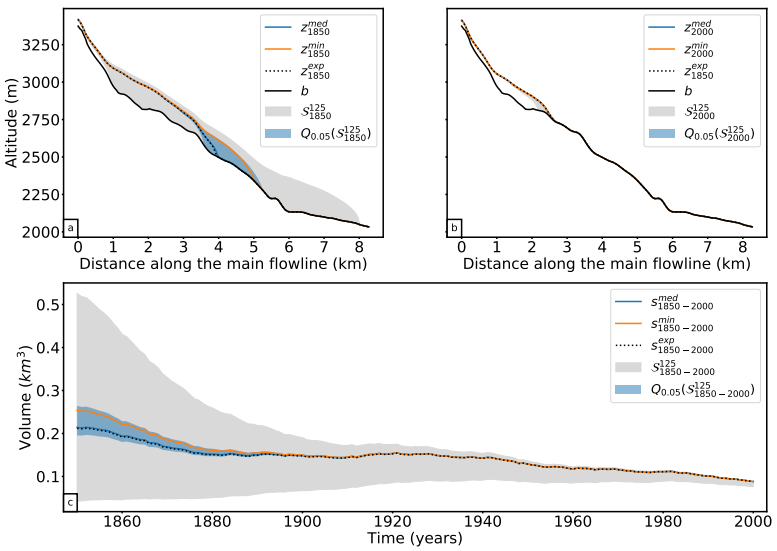

Fig. 3.4: Results for Guslarferner (Oetztal, Austria). Cross sections along the main flow line in **(a)** 1850 and **(b)** 2000 are shown. **(c)** Volume changes from 1850 to 2000. The grey shaded area indicates the range of all solutions with a fitness value smaller than 1 ($\mathcal{S}_t^{125}$). The blue shaded area shows the range of the 5th quantile of $\mathcal{S}_t^{125}$, the blue line s_t^{med}, and the orange line s_t^{min}.

forward modeled states and the observed state in 2000 are larger. The fitness values of all candidates range between 2.8×10^{-5} and 43.

A total of 36 candidates fulfill the acceptance criterion (Eq. 3.5). Figure 3.6 shows that the acceptance criterion in this case confines the result better than in the case of Guslarferner. The length of all glaciers in S_{1850}^{125} ranges from 8.4 to 12.3 km. In this case the 5th quantile of S_t^{125} is again in close proximity to the synthetic experiment, and all candidates of the 5th quantile have extremely small fitness values (between 2.8×10^{-5} and 5.4×10^{-4}). The length of the candidates of the 5th quantile in 1850 only varies from 9.1 to 10.3 km and is thus more precise than in the Guslarferner example. In this example, all candidates of the 5th percentile converge no later than 1920 to the state of the synthetic experiment. Here s_t^{min} matches the surface elevation of the synthetic experiment in 1850, as well as the volume trajectory over time, slightly better than s_t^{med}, but the volume differences to the synthetic experiments in 1850 are also very small in this example (0.004 km^3 for s_t^{min} and $-0.08\,\text{km}^3$ for s_t^{med}).

For both examples we were able to show that our method is able to recover the state in $t_0 = 1850$ of the synthetic experiment by only using information about the observed state of the synthetic experiment in $t_e = 2000$ and combining it with information about the past climate evolution. s_t^{med} as well as s_t^{min} match the

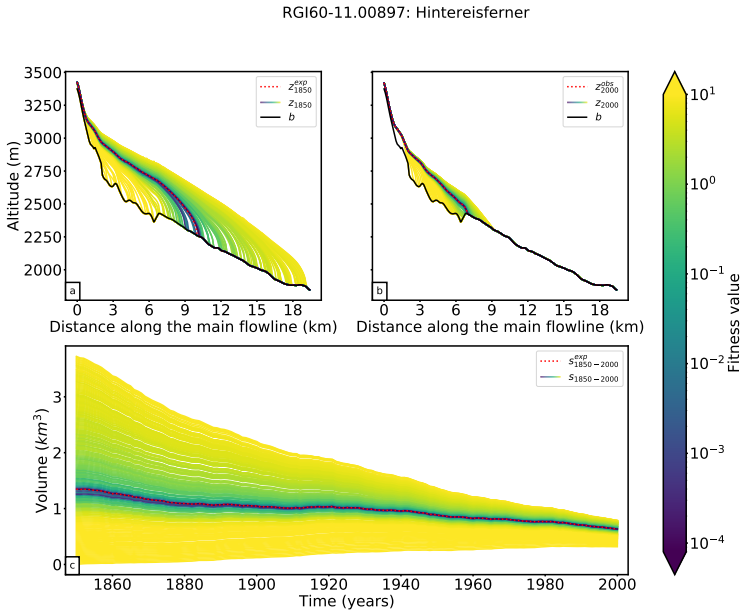

Fig. 3.5: Results for Hintereisferner (Oetztal, Austria). Cross sections along the main flow line in **(a)** 1850 and **(b)** 2000 are shown. Black line indicates the bedrock, the red dotted line the surface elevation from the synthetic experiment, and the remaining lines the modeled ice surfaces of all candidates, colored by their fitness value. The synthetic experiment state in 2000 has a length of 7.3 km, an area of 7.76 km^2, a volume of 0.63 km^3, and a mean thickness of 105.5 m. **(c)** Volume changes from 1850 to 2000, colored by their fitness values. All violet and blue glacier states merge to the observed glacier in 2000.

synthetic experiment in $t_0 = 1850$ extremely well. In the following, we provide an error analysis including all glaciers in the Alps to which we applied our method. For each of the 2660 glaciers we have calculated the absolute volume error to the synthetic experiment:

$$e_{\text{abs}}^{\text{med/min}}(t) = v^{\text{med/min}}(t) - v^{\text{exp}}(t), \tag{3.6}$$

where $v^{\text{exp}}(t)$ is the volume of the synthetic experiment in year t, and $v^{\text{med/min}}(t)$ is the volume of s_t^{med} or s_t^{min} in the same year t. Figure 3.7a shows the absolute volume errors in cubic kilometers for s_t^{med}, as well as for s_t^{min}.

Whereas the absolute volume errors in 1850 vary widely from approximately -1.1 to 2.9 km^3, they reduce rapidly within 60 years. In 1910, the errors range from approximately -0.25 to 0.17 km^3. The range of errors in the first 60 years is largely influenced by a few single outliers. Differences between s_t^{min} and s_t^{med} are small. Figure 3.7b shows the median and the range of the 5th–95th percentiles of $e_{\text{abs}}^{\text{med}}$ and $e_{\text{abs}}^{\text{min}}$ over time, indicating the robustness of our method. The median of e_{abs} of both analyzed states is very small; 0.00028 km^3 for s_t^{min} and 0.00076 km^3 for s_t^{med} in

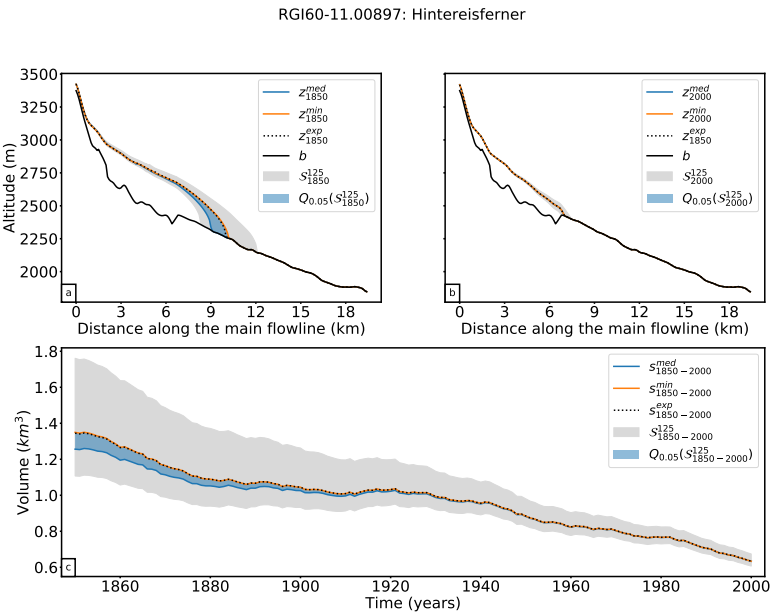

Fig. 3.6: Results for Hintereisferner (Oetztal, Austria). Cross sections along the main flow line in **(a)** 1850 and **(b)** 2000 are shown. **(c)** Volume changes from 1850 to 2000. The grey shaded area indicates the range of all solutions with a fitness value smaller than 1 ($\mathcal{S}^{125}_{1850}$). The blue shaded area shows the range of the 5th quantile of $\mathcal{S}^{125}_{t}$, the blue line s^{med}_{t}, and the orange line s^{min}_{t}.

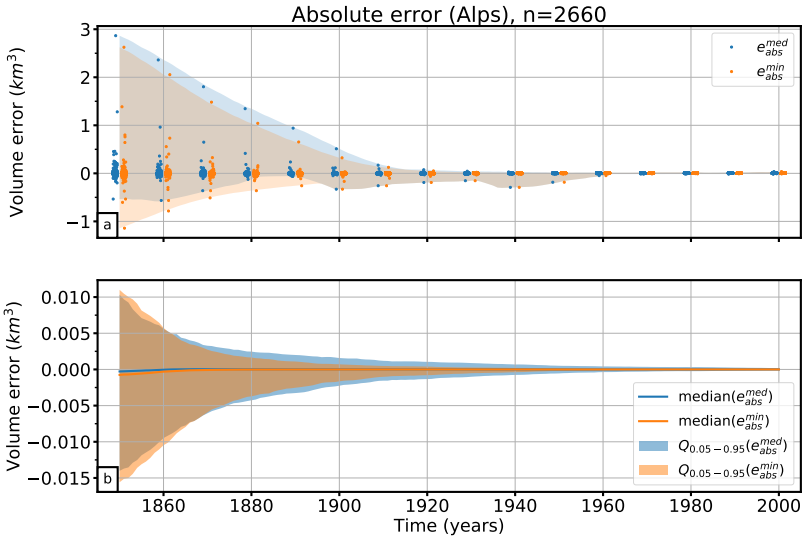

Fig. 3.7: Absolute volume errors in cubic kilometers over time of s^{min}_{t} and s^{med}_{t} of all tested glaciers. **(a)** The blue points mark all individual errors $e^{\text{med}}_{\text{abs}}$ of s^{med}_{t} and the orange points mark all individual errors $e^{\text{min}}_{\text{abs}}$ of s^{min}_{t}. The blue shadowed area shows the total range of the errors $e^{\text{med}}_{\text{abs}}$ and the orange shadowed area the total range of errors $e^{\text{min}}_{\text{abs}}$ over time. **(b)** The shadowed areas show the 5th and 95th percentiles ($Q_{0.05\text{–}0.95}$) of the absolute volume errors $e^{\text{med}}_{\text{abs}}$ (blue) and $e^{\text{min}}_{\text{abs}}$ (orange) over time, as well as the median of $e^{\text{med}}_{\text{abs}}$ (blue line) and $e^{\text{min}}_{\text{abs}}$ (orange line).

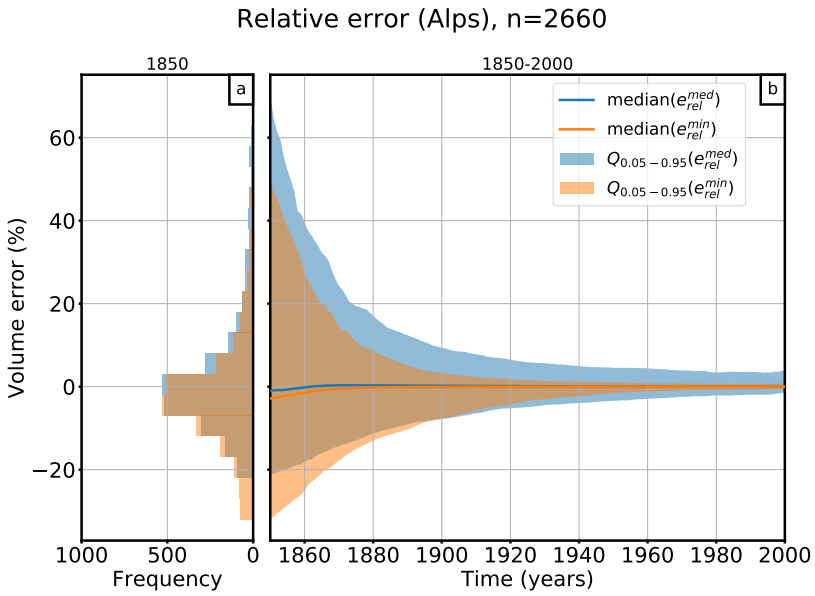

Fig. 3.8: Relative volume errors of s_t^{med} (blue colored) and s_t^{min} (orange colored). Panel **(a)** shows a histogram of all errors in the 5th–95th percentiles in the year 1850 and **(b)** the evolution of the relative errors from 1850 to 2000. The line indicates the median error and the shadowed area the 5th–95th percentile range $Q_{0.05\text{–}0.95}$.

1850. The improvement with time can also be seen here: the median of $e_{\text{abs}}^{\text{med}}(1910)$ is of the order of $10^{-5}\,\text{km}^3$, and that of $e_{\text{abs}}^{\text{min}}(1910)$ is of the order of $10^{-6}\,\text{km}^3$.

As our test site contains large and small sized glaciers, we also evaluate relative errors (%):

$$e_{\text{rel}}^{\text{med/min}}(t) = \frac{e_{\text{abs}}^{\text{med/min}}(t)}{v^{\text{exp}}(t)} \times 100. \tag{3.7}$$

Figure 3.8a shows the histogram of the relative errors in 1850, whereas the evolution from 1850 to 2000 of the median and the 5th–95th percentiles of the relative errors is shown in Fig. 3.8b.

The median of the relative volume errors in 1850 is $-0.97\,\%$ for s_t^{med} and $-2.69\,\%$ for s_t^{min}. The 95th percentile value of $e_{\text{rel}}^{\text{med}}$ is 70 %. With 48 % the value of $e_{\text{rel}}^{\text{min}}$ is smaller for s_t^{min}. Whereas s_t^{min} has a slightly smaller 5th–95th percentile range than s_t^{med} in 1850, the median error of s_t^{med} is slightly smaller than that of s_t^{min}. Both states fit the synthetic experiment well. In many cases, s_t^{med} is equal to s_t^{min}, but for some glaciers either s_t^{min} or s_t^{med} has a clearly better performance. In all cases, the uncertainties quickly decrease after around 1900 to 1930.

Figure 3.8a also shows that the error distribution is skewed, and our method has a slight tendency to underestimate the glacier volume. Although 64 % of the relative errors have a negative sign, a few large positive outliers influence the mean error

and shift it to a positive value of 16 % (in 1850) for the minimum states or 23 % (in 1850) in the case of the median states.

3.5.2 Impact of the Fitness Function

For the evaluation of the glacier candidates we used a fitness function based on differences in the geometry of the glacier (see Eq. 3.5). In this section we want to test the influence of limited information on glacier geometry on the reconstructability of past glacier states. Thus, we additionally evaluate the candidates by only using information about the glacier area or length.

For the glacier-area-based evaluation, we used the following fitness function:

$$J_A(A_{t_e}) = (A_{t_e}^{\mathrm{obs}} - A_{t_e})^2, \tag{3.8}$$

where A_{t_e} is the glacier area at time t_e. The fitness function that takes only information about the glacier length $l(t_e)$ at time t_e into account is similar:

$$J_l(l_{t_e}) = (l_{t_e}^{\mathrm{obs}} - l_{t_e})^2. \tag{3.9}$$

For each glacier at our test site, we also evaluate the 200 candidates with the fitness functions J_A and J_l. For each evaluation method (geometry, area and length based), we determine the state with the minimal fitness function[1]and calculate the relative volume error between it and the synthetic experiment.

Figure 3.9 shows the relative errors of all three evaluation methods. Figure 3.8a shows the distribution of the relative errors of the 5th–95th percentiles in 1850, whereas the evolution from 1850 to 2000 of the median and the 5th–95th percentiles of the relative errors is shown in Fig. 3.8b. The more information taken into account for the evaluation, the smaller the errors. The greatest uncertainties are associated with using the glacier-length-based fitness function (Eq. 3.9), whereas the differences between the area-based evaluation (Eq. 3.8) and the geometry-based evaluation (Eq. 3.5) are small. While the median errors in 1850 of the geometry- and the area-based evaluations are close (-2.69 % for the geometry and -2.83 % for the area approach), the median error in 1850 of the glacier length evaluation has, with 107 %, the worst performance. This also applies for the values of the 95th percentile; 95 % of the tested cases have a relative volume error smaller than 1043 % in 1850 if the length-based fitness function is used for the evaluation. In contrast to the other two evaluations, this approach overestimates the volume. For the area-based

[1]Instead, it is also possible to choose s_t^{med} for the uncertainty analyses, but this would require acceptance criteria for the fitness functions J_A and J_l, which would influence the state. For simplification, we choose the state with the minimal fitness function.

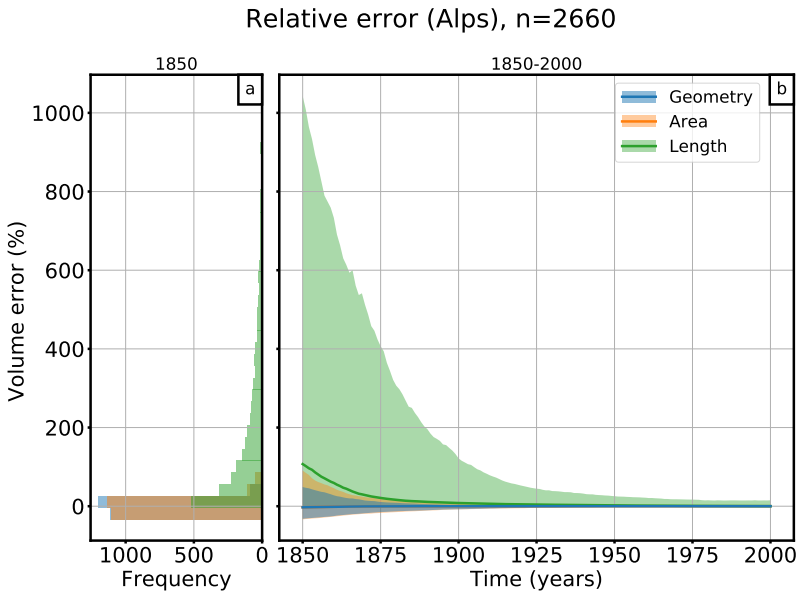

Fig. 3.9: Relative volume errors of $s_t^{\min}$ derived from different fitness functions based on the geometry (blue), glacier area (orange), and glacier length (green). Panel **(a)** shows a histogram of all relative errors in the 5th–95th percentiles in the year 1850 and **(b)** the evolution of the relative errors from 1850 to 2000. The line shows the median error and the shadowed area the 5th–95th percentile range.

evaluation, 95 % of the tested glaciers have an error smaller than 90 %, and for the geometry-based fitness function the error is smaller than 49 %. This shows that the advantage of using the geometry instead of the glacier area to evaluate the candidates is not very high; both evaluations show a very good performance. Especially if the states are modeled forward (e.g., to 1900), both approaches perform well. However, it is not advisable to use the glacier-length-based evaluation.

3.5.3 Reconstructability

The examples from Sect. 3.5.1 as well as in the Supplement indicate a high variation in the number of viable reconstructed candidates between glaciers. This number can range from a few viable solutions in a well-defined range to many solutions without any constraints (all tested candidates have the same fitness value). In other words, some glaciers can be reconstructed easily, and some cannot.

We define a new measure of reconstructability r, where we set the volume range of the 5th percentile in relation to the volume range of all acceptable states of the glacier:

$$r = 1 - \frac{\text{range}(Q_{0.05})}{\text{range}(S^{125})}. \tag{3.10}$$

For a glacier with a unique solution, this measure is equal to 1. If all accepted candidates have exactly the same fitness value, the measure will be zero (this occurs

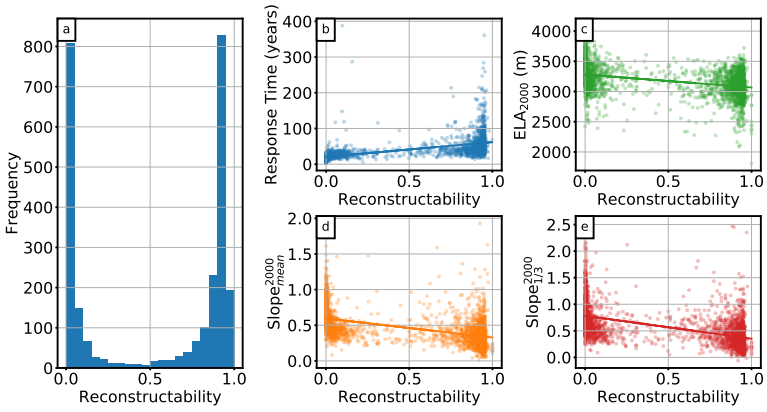

Fig. 3.10: Reconstructability measure. **(a)** Histogram of the reconstructability measure of all 2660 glaciers. **(b–e)** Scatter plots with linear regression. The x axis always shows the reconstructability measure. The y axis shows **(b)** the e-folding response time ($n = 2149$), **(c)** the equilibrium line altitude in 2000 ($n = 2660$), **(d)** the mean surface slope in 2000 ($n = 2660$), and **(e)** the mean surface slope of the last third of the glacier in 2000 ($n = 2660$).

if all candidates converge to exactly the same state before the year 2000). Thus, a small measure represents a glacier with low reconstructability, and a measure close to 1 implies a higher reconstructability of the glacier. For example, r is equal to 0.857 for Hintereisferner and 0.879 for Guslarferner. The similarity of the two values can be explained by the similar proportion of the range of the 5th percentile to the range of all acceptable states in both cases (see Figs. 3.3 and 3.6). A histogram of the reconstructability values of all 2660 tested glaciers in the Alps is shown in Fig. 3.10a. The distribution is bimodal and slightly skewed towards a high reconstructability. Values in the middle range are rare.

What glacier characteristics will influence this reconstructability? The working hypothesis is that it is likely to be associated with the concept of glacier "response time" (here formulated qualitatively). Glaciers with a short response time tend to be less sensitive to initial conditions and will "forget" their initial state after a short period of time. This will probably lead to low reconstructability values. Inversely, glaciers with a long response time will be easier to reconstruct.

To test this hypothesis, we used the e-folding approach (as defined in Oerlemans, 1997b; Oerlemans, 2001) and calculated the time response to a step function. To this end, we first run the 1850 state of the synthetic experiment glacier into an equilibrium state by using a constant climate (mean climate of the years 1835–1865, temperature bias $= -1\,\mathrm{K}$). We choose the same settings that were used for the generation of the synthetic experiments in order to obtain an equilibrium state s_{eq1} close to our synthetic experiment in 1850. Next, we apply to s_{eq1} a constant climate obtained by the mean climate of the years 1850–1880 using no temperature bias

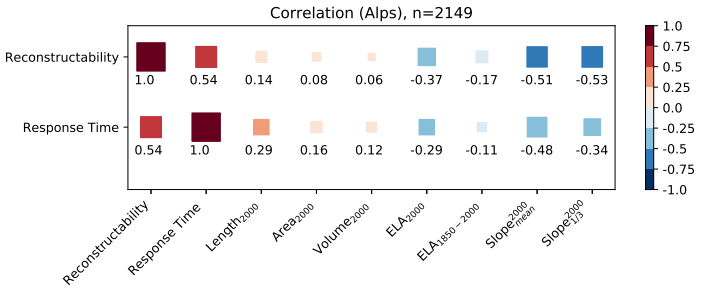

Fig. 3.11: Correlation of the reconstructability measure and the e-folding response time to various glacier characteristics. Correlation values are represented by the square color and size.

and receive the corresponding equilibrium state s_{eq2} (i.e., a step change of 1 K). We calculate the e-folding time of these two states for each glacier, but we exclude the glaciers where the volume of s_{eq2} reaches zero (which was the case for approximately 500 glaciers out of 2660[2]).

The scatter plot in Fig. 3.10b indicates a relation between the reconstructability measure and response time. The variance of the response time increases for reconstructability values close to 1. Dependencies with the reconstructability could also be detected for the position of the equilibrium line altitude (ELA) (Fig. 3.10c), the mean surface slope in 2000 (Fig. 3.10d), and the mean surface slope in 2000 of the last third of the glacier (Fig. 3.10e).

Furthermore, we calculated correlations of both reconstructability and response time with the following variables: glacier length (in 2000), area (in 2000), volume (in 2000), equilibrium line altitude (ELA) in 2000, equilibrium line altitude change from 1850 to 2000, mean surface slope (in 2000), and mean surface slope over the lowest third of the glacier (in 2000) (Fig. 3.11).

The variable explaining reconstructability best is the glacier response time (correlation of 0.54). Both values correlate with the same glacier characteristics. Contrary to a common misunderstanding, glacier length, area, and volume do not correlate well with the reconstructability measure or with the response time. The variable having the main influence is slope: generally, the larger the slope, the lower the reconstructability measure or the response time of a glacier. These findings coincide with results from Lüthi (2009), Zekollari and Huybrechts (2015), and Bach et al. (2018), who concluded that response times depend more on the steepness of the surface than on the glacier size. The correlation of the mean surface slope can be

[2]We also tested a step of 0.5 K, leading to a larger sample size but no significant change to the correlation analysis and our results. Thus, we kept the 1 K step change here.

further increased by taking the lowest third of the glacier. In addition, the position of the ELA in 2000 also influences the reconstructability, whereas the ELA change from 1850 to 2000 only plays a minor role.

Taken alone, these correlation values remain quite low and do not provide enough predictive power to create a statistical model of reconstructability. However, they provide a good indication about which factors should be taken into account for future applications.

3.6 Hardware Requirements and Performance

For this study we used a small cluster comprising two nodes with two 14-core CPUs each, resulting in 112 parallel threads (two threads per core). Our method requires running hundreds of dynamical model runs for each single glacier, and, as described in Maussion et al. (2019), the dynamical runs are the most expensive computations. The size of the glacier and the required time stepping to ensure a numerical stability strongly influence the required computation time. The computation time needed to apply our initialization procedure to one glacier varies from 30 s to 26 min. In total, initializing the 2660 glaciers in 1850 takes about 3.75 d on our small cluster.

3.7 Discussion and Conclusions

In this study, a new method to initialize past glacier states is presented and applied to synthetic experiments. Assuming a perfectly known world allows us to identify the errors of our method alone and to separate them from uncertainties in observations and errors introduced by model approximations, a task impossible to realize in real-world applications. However, the synthetic experiments do not allow external validation, e.g against past outlines derived from moraines, historical maps, or remote sensing (such as provided by GLIMS; Raup et al., 2007). Model uncertainties will have to be accounted for and will have to be compared to and added to the theoretical lower bound discussed in this study. Similarly, our results do not provide information about actual past glacier mass change. Since in our synthetic experiments glaciers states in 2000 may be different from the real ones, the modeled initial glacier states in 1850 do not correspond to reality either. The past states determined in this study can only serve to verify the functionality of the developed method.

Our results have shown that the solutions are not unique. Multiple candidates match the observation in $t_e = 2000$, sometimes with a large spread. This raises interesting

questions about the use of past glacier change information to reconstruct climate variations, which we do not address here. In the context of model initialization, this nonuniqueness impedes the reconstruction. We evaluated the candidates with a fitness function based on averaged geometry differences between the forward modeled and the observed state in $t_e = 2000$. The threshold value $\epsilon = 125\,\mathrm{m}^2$ was derived by assuming a typical error of 5 m in surface elevations and 10 m in glacier width, but how these values should be chosen depends on the specific glacier setting. Especially in cases where many of the candidate states have extremely small fitness values, a more strict acceptance criterion can help to narrow the results. On the other hand, an ϵ that is too strict could lead to none of the candidates fulfilling the criterion.

Due to uncertainties that derive from the model integration, the glacier state with the minimal fitness value is not always close to the synthetic experiment. As a more robust alternative, we propose using s_t^{med}, the median state of the 5th percentile of all acceptable states as the best estimate. In Sect. 3.5.1 we compared the errors of both approaches. The median error of s_t^{med} is slightly smaller than that of s_t^{min}, and the total range of absolute errors is smaller for s_t^{med} in 1850, too. Modeling the reconstructed initial states forward in time approximately 60 years leads to a rapid reduction of the error, and s_t^{min} performs a bit better than s_t^{med}. By making use of the knowledge about the past climate, the number of candidates at later stages is, through this forward run, more constrained than by initializing them directly at a later time (see Appendix 3.9.2 for a more detailed description of the inverted approach at different times).

By comparing different fitness functions for the candidate evaluation, we showed that using limited information only (glacier area and glacier length) leads to an increase in the errors in 1850. This indicates what kind of observation is needed to be able to reconstruct past glacier states from today's state. The differences between the geometry-based evaluation and the area-based evaluation are small, but the differences to the length-based evaluation are significant. But this effect is also influenced by the spatial resolution of the model grid: a higher resolution of the grid would lead to more variability in fitness values and hence to a more precise initialization. At the same time, a higher resolution would increase the computational demands of the initialization method. We strongly recommend using either the geometry- or the area-based fitness function for the evaluation. In this study, we only take the observation of the year t_e into account. Multi-temporal outlines are likely to greatly reduce uncertainties at prior times.

Our results are relevant for future glacier evolution modeling studies, as they indicate that at least for some glaciers the time needed to converge to a similar evolution regardless of the 1850 state is comparatively short. Our study might also be useful to

determine a good starting point of a past simulation, e.g., to improve the initialization date in Zekollari et al. (2019). A correlation analysis of the reconstructability and glacier characteristics showed the position of the ELA as well as the slope (especially in the lower part of the glacier) influence the reconstructability, whereas attributes like the glacier size do not have a strong impact. We could also show that the reconstructability measure correlates well with a separately obtained response time of the glacier.

Future work will include the application of the method to real-world cases, which will come with additional challenges. For example, we will have to consider the merging of neighboring glaciers when growing. Importantly, the effect of uncertainties in the boundary conditions (in particular the glacier bed and its outlines and uncertainties in the climate forcing) will have to be quantified. This also includes testing the influence of the choice of climate conditions on the accuracy of our method. Here again, the synthetic framework will be useful by allowing data denial and data alteration experiments. To ensure the robust reconstruction of real-world glacier states, additional changes and model developments are necessary. This includes the development of a glacier-individual calibration method for dynamical parameters (e.g., sliding parameter, creep parameter) as well as of the mass balance model.

3.8 Code Availability

The OGGM software together with initialization method are coded in the Python language and licensed under the GPLV3 free software license. The latest version of the OGGM code is available on GitHub (`https://github.com/OGGM/oggm`), the documentation is hosted on Read the Docs (`http://oggm.readthedocs.io`, last access: 10 December 2019), and the project web page for communication and dissemination can be found at `http://oggm.org` (last access: 10 December 2019). The OGGM version used in this study is v1.1. The code for the initialization module is available on GitHub (`https://github.com/OGGM/initialization`). The OGGM version used for this study is available in a permanent DOI repostiory (doi:10.5281/zenodo.2580277).

3.9 Appendix

3.9.1 Temperature Bias for the Synthetic Experiments

For the generation of the synthetic experiment state in 1850, we use a temperature bias of $-1\,\mathrm{K}$ in order to create a relatively big glacier state. To justify the choice of

this value, we have tested different temperature biases: the results are summarized in Fig. 3.12. This figure shows that applying positive or small negative temperature biases to the synthetic experiments results in large area differences to the RGI in 2000, and the total glacierized area in 1850 is also too small. The sample size is reduced because fewer glaciers fulfill the area threshold criteria of 0.01 km^2. Negative temperature biases that are too large also reduce the sample size because some runs fail (the glacier becomes larger than the underlying grid). The experiments with a temperature bias of -1, -1.25, or -1.5 K perform best regarding the area difference to the RGI in 2000. But only the experiment with the temperature bias of -1 K performs well regarding the estimation in 1850 of Zemp et al. (2006), where however it needs to be taken into account that the dots only represent a subset (the small glaciers in 2000 are missing) of the glaciers considered in Zemp et al. (2006).

3.9.2 Initialization at Different Starting Times

We applied our method to different starting times (1850, 1855, . . . , 1965) to test how far one can go back in time to obtain a good initial state for this glacier. While this inverted setup is computationally very expensive, unfortunately it does not lead to improved results. See Fig. 3.13 for two different examples.

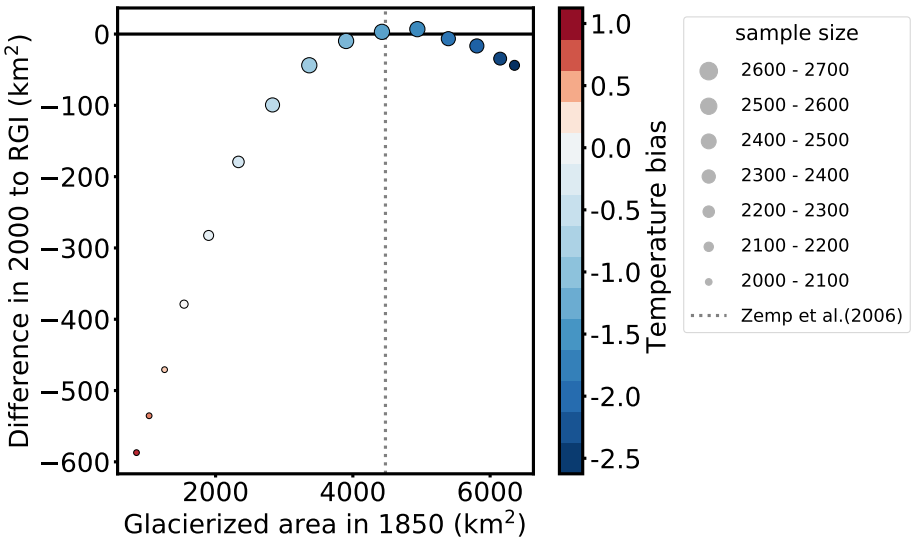

Fig. 3.12: Difference between the total area in 2000 and the total area from the RGI plotted as a function of total area in 1850. Colors mark the applied temperature bias to create the synthetic experiments, and the size of the points mark the sample size (number of glaciers with an area larger than 0.01 km^2 in 2000). The dashed grey line marks the estimated total area of all Alpine glaciers in 1850 from Zemp et al. (2006).

For each tested starting year, we determined the median state and conducted an uncertainty analysis (similar to the one in Sect. 3.5.1). We find that the uncertainties of the median states at the different starting points are higher than when performing the initialization for the year 1850 (only) and running this state forward in time. While this is counterintuitive, the main reason is that by starting in 1850 even with a very large number and range of candidates, the very unrealistic ones are quickly forced to converge by the boundary conditions (i.e., by climate), effectively reducing the number of potential candidates for a later date. In other words, we make use of our knowledge about past climate to reduce the number of candidates at each later stage. In real-world applications, results might be different since uncertainties in past climate are large. While this should be explored further, because of the computational cost it is hard to imagine an eventual applicability on the global or even large regional scale.

Author Contributions

JE is the main developer of the initialization module and wrote most of the paper. BM and FM are the initiators of the OGGM project and helped to conceive this study. FM is the main OGGM developer and participated in the development of the initialization module.

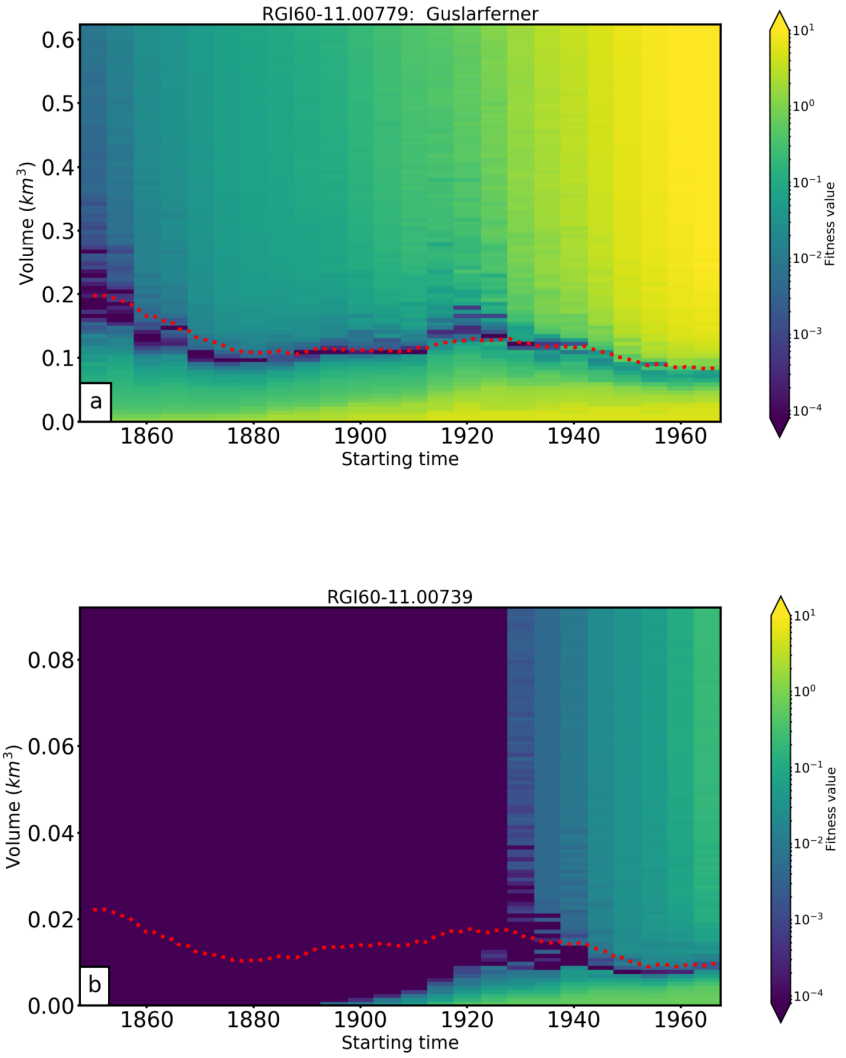

Fig. 3.13: Reconstructability for different starting times. Colors indicate the fitness value of a simulation initialized with a glacier volume indicated by the vertical axis at a time indicated by the horizontal axis. Red dotted line shows the synthetic experiment. **(a)** Example for a glacier with ordinary reconstructive power; the "observed" glacier state in 2000 constrains the past evolution well in the 20th century, and the reconstruction is close to the goal. **(b)** Example for a glacier with very low reconstructive power; the "observed" glacier state does not constrain the past glacier evolution before approximately 1930.

4

Reconstruction of past glacier changes using a glacier model: validation with observations

Submitted to *Frontiers in Earth Science*

Authors and Affiliation

Julia Eis [1], Larissa van der Laan[2], Fabien Maussion [3] and Ben Marzeion [1,4]

[1] Institute of Geography, University of Bremen, Bremen, Germany
[2] Institute of Hydrology and Water Resources Management, Leibniz Universität Hannover, Hannover, Germany
[3] Department of Atmospheric and Cryospheric Sciences, University of Innsbruck, Innsbruck, Austria
[4] MARUM - Center for Marine Environmental Sciences, University of Bremen, Bremen, Germany

Context

The Open Global Glacier Model (see Chapt. 2) can be used to provide information about glacier mass change over the course of the entire 20th century, but an adequate initial state is required. To this end, a new initialization approach was developed and presented in Chapter 3. The method relies on glacier information about the present day, because this is the only information available for each of the approx. 200 000 glaciers worldwide. But the reconstruction of glacier states comes along with many complications. Even under perfectly known conditions (synthetic experiments) the solution for many tested glaciers is not unique. Multiple states, converge to the same present day-state and a clear reconstruction is not possible. We showed that the median state of the 5th percentile gives a best estimate and fits well the synthetic experiment. Thanks to the synthetic environment, we determined the uncertainty of the method itself, as uncertainties from the model, climate data or from glacier observations (used for the model calibration) could be excluded. The

main disadvantage of the synthetic environment is that the reconstructed glaciers states do not represent real glacier changes and thus an evaluation with glacier observations was not possible. However, this Chapter presents a further development which allows the validation of our initialization method with glacier observations. To this end, we introduce a glacier-specific calibration of the mass balance model, which ensures that the reconstructed glacier evolution ends in a state as close as possible to the RGI state (the state obtained from the RGI outline). We evaluate the proposed initialization method based on differences to observed mass balance changes (see Sect. 1.5.2) and to glacier length changes (see Sect. 1.5.1).

Personal Contribution

J. Eis developed and designed the study and all associated methods. This includes the implementation of glacier-specific calibration of the mass balance model. J. Eis performed all simulations and the resulting error calculations, created all figures and primary wrote the paper. All authors continuously discussed the new findings and earlier states of the manuscript. A more detailed description of the contribution of all authors, can be found in the author contribution section on page 107.

Abstract

Estimations of global glacier mass changes over the course of the 20th century require automated initialization methods, allowing the reconstruction of past glacier states from limited information. In a previous study, we developed a method to initialize the Open Global Glacier Model (OGGM) from past climate information and present day geometry alone. Tested in an idealized framework, this method aimed to quantify how much information present-day glacier geometry carries about past glacier states. The method was not applied to real world cases and therefore the results were not comparable with observations. This study closes the gap to real world cases by introducing a glacier-specific calibration of the mass balance model. This procedure ensures that the modeled present day geometry matches the observed area and that the past glacier evolution is consistent with bias-corrected past climate time series. We apply the method to 517 glaciers, spread globally, for which either mass balance observations or length records are available, and compare the observations to the modeled reconstructed glacier changes. For the evaluation of the initialization method we use multiple measures of reconstruction skill (e.g. MBE, RMSE, correlation). We found that the modeled mass balances and glacier lengths are in good agreement with the observations, especially for glaciers with many observation years. These results open the door to a future global application.

4.1 Introduction

Compared to the Greenland and Antarctic ice sheets, the ice mass stored in glaciers seems negligibly small (<1%) (e.g. Oppenheimer et al., 2019), but glaciers contributed between 25% and 30% of the observed global mean sea-level rise during 1993-2015 (Zemp et al., 2019). Along with ice sheet mass loss and thermal expansion of sea water, glaciers will continue to be a major sea-level rise contributor in the 21st century (Church et al., 2013; Slangen et al., 2017b; Hock et al., 2019). Independent from the Representative Concentration Pathway (RCP), glaciers mass loss is projected to exceed the contributions from Greenland or Antarctica ice sheets until 2100 (Oppenheimer et al., 2019). However, glacier changes also have an impact on local and regional scales: mountain glaciers affect the water availability in many regions of the world (e.g. Kaser et al., 2010; Immerzeel et al., 2012; Huss and Hock, 2018) and both retreating and advancing glaciers can lead to increased geohazards (see Kääb et al., 2005, for an overview). It is consequently relevant to improve the knowledge of past and future glacier mass change (Marzeion et al., 2012b).

To estimate glacier mass change on a global scale, in situ measurements in mass and length changes (e.g. Zemp et al., 2015; Leclercq et al., 2014), remote sensing techniques (Gardner et al., 2013; Jacob et al., 2012; Bamber et al., 2018; Wouters et al., 2019) or mass balance modeling driven by climate observations (e.g. Radić and Hock, 2011; Radić and Hock, 2014; Giesen and Oerlemans, 2012; Giesen and Oerlemans, 2013; Marzeion et al., 2012b; Marzeion et al., 2014a; Huss and Hock, 2015; Maussion et al., 2019) can be used. However, most of these model based studies limit their application to the recent past (ignoring past glacier geometry change) or to the future. Nevertheless, glacier mass change in the past should not be neglected: a large fraction of future glacier mass loss ($36 \pm 8\%$) is caused by the future adjustment of glaciers to past climate change (Marzeion et al., 2014a; Marzeion et al., 2018). As a result, reconstructions of past glacier change are important to quantify the ongoing adjustment of glaciers to past and present-day climate. In addition, reconstructions can be used to determine the budget of past sea-level change (Gregory et al., 2013). By allowing the quantification of the agreement with observations (Marzeion et al., 2015), reconstructions increase the confidence in projections.

So far, only one model was able to provide global estimates of glacier mass changes over the course of the entire 20th century, including a simple representation of glacier geometry change (Marzeion et al., 2012b). For more complex models (e.g. Huss and Hock, 2015; Maussion et al., 2019) this process is impeded by initialization issues, as more and more variables need to be initialized. I.e., flow line models

require input data along the coordinates of the flow lines (e.g. bed topography, surface elevations, and/or widths) and thus more complex initialization methods are required. Zekollari et al. (2019) added an ice flow model to Huss and Hock, 2015 and developed an automated initialization for glaciers in 1990 (i.e., prior to the inventory date) in order to avoid spin-up issues. The ensemble approach from Eis et al. (2019) can be used for an initialization further back in time (e.g. 1850), but the larger time difference to the inventory date lead to non-unique solutions of the initial glacier geometry. We now call glacier geometry (i.e. glacier outlines and surface elevation of a glacier at a given point in time) the "state" of the glacier.

The approach from Eis et al. (2019) works as follows: first, a large number of physically plausible glacier states for a given year in the past is generated, using a spin-up run of the model forced by random climate representatives of the conditions around the year of initialization. From this set of possible past glacier states a subset of equidistant and approximately uniformly distributed states is selected and called “glacier candidate states”. All these candidate states are then modeled forward to the present-day and evaluated by comparing the result of the forward runs to the present-day glacier states. In order to separate uncertainties of the initialization method alone from all other sources of uncertainty, Eis et al. (2019) relied on synthetic experiments. These synthetic experiments were generated by running the same glacier model forward such that a perfectly known glacier evolution until present-day was produced (including boundary conditions). The synthetic experiment state at the present-day was then used to reconstruct the synthetic experiment state in 1850.

While this procedure allows an exact evaluation of the uncertainties of the method alone, it does not allow an external validation, e.g. against in-situ measurements of glacier mass balance or length changes. The results from Eis et al. (2019) thus do not provide information about actual past glacier changes, because the synthetic experiment states in 2000 can be different to real states. Consequently, the reconstructed evolution from 1850 onward do not necessarily correspond to reality either, and uncertainties in a real-world application will necessarily be larger than in the synthetic experiments.

In this study we present a new way to calibrate the mass balance model, which will allow a validation of Eis et al. (2019) based on real glacier observations. To this end, we first introduce all relevant features of the Open Global Glacier Model (OGGM) in Sect. 4.2.1. We describe the set-up of calibration runs in Sect. 4.2.3. These preliminary runs allow a glacier-specific calibration of the mass balance model, which enables the comparison with glacier observations. We apply the initialization method from Eis et al. (2019) by using the results of the calibration runs to 517 glaciers with mass balance observations or length records. The calibration is evaluated in Sect.

4.3.1 and the results of the initialization are shown in Sect. 4.3.2. One focus of this study is the validation of the initialization method from Eis et al. (2019) by using glacier observations (see Sect. 4.3.3). A statistical analysis based on mass-balance observations provided by the World Glacier Monitoring Service (WGMS, 2018) can be found in Sect. 4.3.3.1. Additionally our method is evaluated based on glacier length change observations from Leclercq et al. (2014) in Sect. 4.3.3.2. Finally, we summarize the results and discuss the limitations of the method, as well as future applications in Sect. 4.5.

4.2 Methods

4.2.1 The Open Global Glacier Model

The open source numerical framework Open Global Glacier Model (OGGM; Maussion et al., 2019) is able to model the evolution of all glaciers worldwide. OGGM utilizes the outline of any glacier, which can, e.g. be obtained from the Randolph Glacier Inventory (RGIv6.0; Pfeffer et al., 2014). A digital elevation model (DEM), covering the glacier outlines, is automatically downloaded and subsequently interpolated to a local grid. The resolution dx of the local grid depends on the size of the glacier by following the equation $dx = a\sqrt{S}$, using a parameter value $a = 14$ m km^{-1} and S the surface area of the glacier in km^2. It is bound by a highest resolution of $dx = 10$ m and an lowest of $dx =$200 m. The extent of the grid is set using a border parameter which defines the number of grid points to be included outside of the outline of the glacier. This parameter thus determines how large a glacier can grow in the model beyond its current outline. In Eis et al., 2019, we chose a border parameter of 200 grid points in order to allow glaciers to grow considerably beyond their present-day extent. The DEM serves as input for a geometrical routing algorithm (adapted from Kienholz et al., 2014) to calculate the centerlines of the glacier. They are considered as flowlines and composed of equidistantly distributed grid points with a distance twice that of the local grid resolution dx. From the topography, surface elevations along the flowline coordinates are calculated. The width of the glacier at a flow line grid point is taken as the length of the normal to the flowline. It is then corrected to ensure the glacier's hypsometry is correctly represented in the model. Additionally, the ice thickness is estimated by assuming a certain bed shape (parabolic, rectangular or mixed) and using a mass-conservation approach (Farinotti et al., 2009; Recinos et al., 2019; Farinotti et al., 2019). The bed topography is calculated from ice thickness and surface elevation, and length, area, and volume of the glacier are derived. These values are obtained using the assumption that the glacier outline and the DEM originate from the same date. Utilizing monthly temperature and precipitation data, mass balances at the flowline grid points are

calculated. A number of different sources of climate data can be used as forcing of the mass balance model, e.g., past climate observations (gridded), reanalyses, projections or randomized time series. The evolution of the glacier geometry under the specific climate forcing is calculated by a dynamical flowline model, which solves the shallow ice approximation. More information about OGGM can be found under `http://docs.oggm.org` and in Maussion et al. (2019).

4.2.2 Input Data and default model parameters

The glacier outlines used in this study are taken from the Randolph Glacier Inventory (RGI v6.0, region 11; Pfeffer et al., 2014). For each of the glacier outlines, a transverse Mercator projection, centered on the glacier, is defined in order to preserve map projection properties (e.g. area, distances, angles). Next, the topographical data is automatically downloaded by OGGM. The acquisition dates of the DEMs vary from 2000 (for SRTM) to 2009 and roughly match that of the RGI. The climate data set we use for this approach is the Climatic Research Unit (CRU) TS v4.01 data set (Harris et al., 2014, released 20 September 2017). It is a gridded dataset at 0.5° resolution and covers the period from 1901 to 2016. Further downscaling to a resolution of 10′ is achieved by applying the 1961-1990 anomalies to the CRU v2.0 gridded climatology (New et al., 2002). Monthly temperature and precipitation time series are extracted for each glacier from the nearest CRU CL v2.0 grid point and then converted to the local temperature according to a temperature gradient (default: -6.5 K km^{-1}). As the initialization procedure requires climate data of the 15 preceding years of the initialization year t_0, an earlier initialization than $t_0 = 1917$ is not possible.

Identical to the study of Maussion et al. (2019) and Eis et al. (2019), only the the mass-balance model is calibrated while the creep parameter A and the sliding parameter f_s are the same for each glacier and set to their default values ($A = 2.4 \times 10^{-24} s^{-1}$ Pa^{-3}, $f_s = 0$, no lateral drag). For parameters values related to the mass balance model, in this study we use the precipitation correction factor $p_f = 2.5$, the melt temperature $T_{Melt} = -1.0$°C, the liquid precipitation temperature $T_{Liquid} = 2.0$°C and the temperature lapse rate $\Gamma = -6.5\ K$ km^{-1}. This parameter set was determined through a cross-validation, done with the CRU4 TS v4.01 data set (Harris et al., 2014) for the 254 glaciers worldwide that have more than 5 years of mass-balance observations in WGMS (2018).

4.2.3 Glacier-specific calibration of the mass balance model

Eis et al. (2019) showed that the use of synthetic experiments provides many advantages, but it also causes one main disadvantage. The geometry of synthetic experiment states at the inventory date usually does not coincide with the geometry of the observed states. Thus, the reconstructed time series does not correspond to real past glacier states, which implies that an evaluation of the method with glacier observations is not possible.

In this study, we aim to reduce the geometry mismatch of the result to the observation by introducing so called calibration runs. This improvement allows the application of the initialization method from Eis et al. (2019) to real-world cases and evaluating the reconstructed time series with glacier observations. To this end, we introduce a mass balance offset β_{mb} to the mass balance equation which will be applied to every forward run. With the help of the calibration runs, we identify an optimal value of β_{mb}, such that the area of the observed state is matched. The observed state is obtained from the RGI glacier outline and the underlying topography file and hereinafter referred to as RGI state s^{RGI}. In contrast to Eis et al., 2019, the calibration run with the optimal β_{mb} therefore coincides with the RGI state s^{RGI} at the inventory date t_{RGI}.

4.2.3.1 Rationale

Before motivating the choice to introduce and optimize the mass balance offset β_{mb}, we describe the general procedure of its determination. The mass balance offset is typically determined as a diagnostic of model performance during the calibration of the mass balance model, for which OGGM adapted the method from Marzeion et al. (2012b). For all 254 reference glaciers (with more than 5 years of mass balance observation) the mass balance offset is determined during the calibration of the temperature sensitivity parameter μ^*. $\mu^* = \mu(t^*)$ is identified such that the smallest possible offset $\beta^*_{mb} = \beta_{mb}(t^*)$ is produced. The offset $\beta_{mb}(t)$ is defined as the difference between the mean of the modeled mass balances during the years of observations $\overline{B(t)_{\text{modeled}}}$ and the mean of the observed mass balances $\overline{B(t)_{\text{observed}}}$:

$$\left|\overline{B(t)_{\text{modeled}}} - \overline{B(t)_{\text{observed}}}\right| = |\beta_{mb}(t)| \tag{4.1}$$

The mass balance offset β_{mb} is then subtracted from the modeled mass balances. Thus, β_{mb} compensates for errors in the climate time series, as well as errors from the mass balance model (corresponding to errors in $\overline{B(t)_{\text{modelled}}}$). The derived offsets cannot be neglected and thus a bias correction of the mass balance model becomes

necessary. To this end, Marzeion et al. (2012b) suggests an interpolation of the mass balance offset using the offset of the 10 closest reference glaciers (weighted by distance) for all glaciers without mass balance observations. But this assumes that neighboring glaciers display similar mass balance offsets, which is not necessarily the case, as other characteristics - e.g. glacier size - could have an influence as well. To avoid these assumptions, in this study, we suggest the use of a different method of determining the mass balance offset for all glaciers.

4.2.3.2 Design

With the help of the calibration runs, we iteratively obtain an optimal mass balance offset β^*_{mb}, for which the area of the glacier state at the inventory date t_{RGI} is closest to the area of the RGI state. For this purpose, a bisection method, starting with the boundary values $a = -2000$ mm w.e. and $b = 2000$ mm w.e. is used. Thanks to the quick convergence of the bisection method, $n_{max} = 12$ is sufficient to determine the mass balance offset with an accuracy of $\varepsilon_{\beta_{mb}} = 1$ mm w.e. Additionally, the iteration is stopped in case the area difference is smaller than $1e^{-4}$ km^2. First, the midpoint $c = 0$ mm w.e. is evaluated. To this end, we generate a glacier state for the year of the initialization $t_0 = 1917$ (hereinafter referred to as s^{OGGM}_{1917}), using the mass balance offset $\beta_{mb} = c = 0$ mm w.e. The generation of s^{OGGM}_{1917} is oriented on the generation of the synthetic experiments in Eis et al. (2019): we use a 600 year long random climate scenario, which results from shuffling the climate years from 1901 to 1932 (the years around t_0) infinitely. Thereby a realistic climate forcing, representative of the time period of the initialization, is created. The RGI state, which is the only known state, is used as initial condition for this run (see Fig. 4.1A). The state at the end of the random climate run ($t = 600$) is s^{OGGM}_{1917} (marked as red point in Fig. 4.1A). We then use the past climate from 1917-t_{RGI} and run s^{OGGM}_{1917} forward until the inventory date t_{RGI}. The same mass balance offset $\beta_{mb} = c$ as in the random climate run is used. The glacier state at the inventory date t_{RGI} is then compared to the RGI state. If the RGI state is not matched, another mass balance offset β_{mb} will be tested. As in OGGM the mass balance offset will be subtracted from the modeled mass balance, the mass balance offset is increased if the area of s^{OGGM} is larger than the area of the RGI state. For this purpose, the lower bound a will be set equal to the midpoint c. Inversely, a smaller mass balance offset β_{mb} is tested when the area of s^{OGGM} is smaller. Here, the upper bound b is set equal to c. The new midpoint $c = \frac{a+b}{2}$ is calculated and a new OGGM state is generated with the mass balance offset $\beta_{mb} = c$. This procedure is repeated until the maximum number of iterations $n_{max} = 12$ is reached or the area difference falls below the threshold of $1e^{-4}$ km^2. The optimal mass balance offset β^*_{mb}, which produced the OGGM state with the smallest area difference to the RGI state, and the corresponding

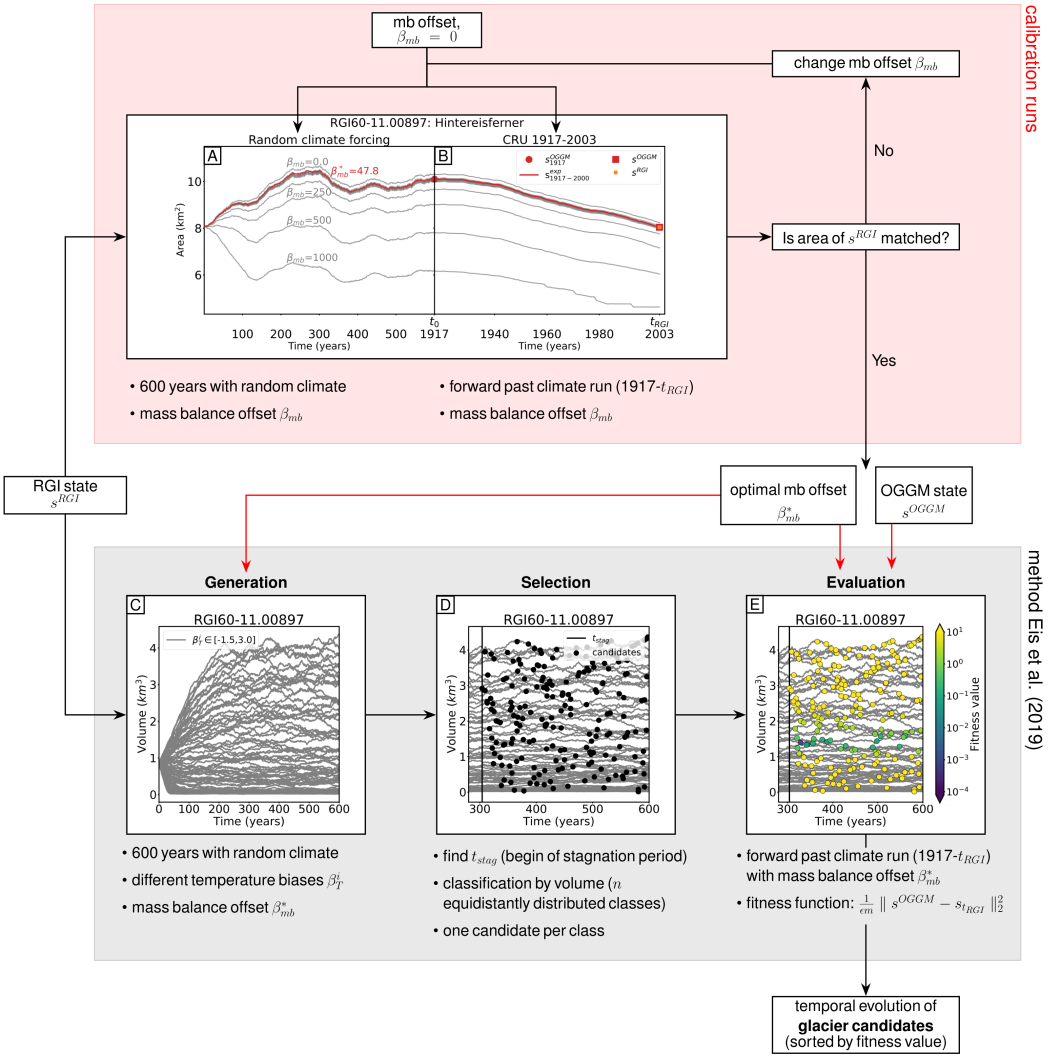

Fig. 4.1: Workflow of the calibration runs and the ensemble approach from Eis et al. (2019). **A-B:** Calibration runs, the grey lines indicate the iteration procedure and the brown line the result obtained with the optimal mass balance offset β^*_{mb}. **A:** The generation of s^{OGGM}_{1917} (marked as red point) using a run forced by random climate with the iteratively chosen mass balance offset β_{mb}. s^{OGGM}_{1917} is then used as starting point of the run in **B**. **B:** Past climate run with β_{mb} from $t_0 = 1917$ to the inventory date t_{RGI}. Different β_{mb} will be tested until the area of the RGI state (s^{RGI}, marked as orange square) is matched in t_{RGI}. s^{OGGM} (marked as red square), according to the optimal mass balance offset β^*_{mb}, is the closest to s^{RGI}. **C-E:** Ensemble approach from Eis et al. (2019). **C:** Generation of potential glacier candidates. The grey lines indicate the glacier volume evolution for a set of different random climate scenarios over 600 years each. The temperature biases vary between -1.5 and 3.0 K. **D:** Selection of candidates. The black vertical line indicates t_{stag} and the black points show 200 candidates. **E:** Glacier candidates colored by their fitness value. Violet marks candidates with a small misfit, whereas yellow marks states that do not meet the acceptance criterion.

OGGM state s^{OGGM} are then used for an initialization with the method from Eis et al. (2019).

4.3 Results

We apply our method to all glacier outlines from the RGI (version 6) that can either be linked to mass balance observations provided by the World Glacier Monitoring Service (WGMS, 2017) or to the glacier length records from Leclercq et al. (2014). We exclude all Antarctic and Subantarctic glaciers (RGI region 19), because no CRU data is available for this region. Additionally, we exclude glaciers that are strongly connected to the Greenland ice sheet (connectivity Level 2 in Rastner et al., 2012). Because of the complex dynamical response of water-terminating glaciers, they are excluded as well.
This leads to a total sample size of 519 glaciers. For 253 glaciers, there are mass balance time series and for 317 glaciers there are length records (51 glaciers have both). The identification of glaciers in the Leclercq data set in the RGI is done as in Parkes and Goosse (2019).
During the calibration runs, two glaciers failed due to processing errors and thus we were able to initialize the glacier states in $t_0 = 1917$ for 517 glaciers. The end of the past climate run t_e is set to the acquisition date of the RGI outline t_{RGI} and thus it can vary between individual glaciers.

4.3.1 Optimized mass balance offsets

We perform the calibration runs for all tested glaciers as described in Sect. 4.2.3 and obtain for each of the glaciers an optimal mass balance offset β^*_{mb}. In Fig. 4.2A the distribution of the derived mass balance offsets β^*_{mb} of all glaciers is shown. It is a leptokurtic distribution (positive kurtosis), which is slightly skewed to the right. The values are centered at a mean value of $\mu = 5.8$ mm w.e. and the standard deviation is $\sigma = 267.9$ mm w.e.. The mass balance offsets β^*_{mb} obtained by the calibration runs are of similar magnitude and distribution as the mass balance offsets obtained by the method from Marzeion et al. (2012b). . Figure 4.2B demonstrates that s^{OGGM} matches the area of s^{RGI} very well in all cases. The mean relative area difference across all glaciers is 1.2×10^{-4} % and also the 5th and 95th percentiles of the relative area error are with values of $Q_{0.05} = -6 \times 10^{-4}$ % and $Q_{0.95} = 9 \times 10^{-4}$ very small. The outliers stem from very small glaciers, e.g. the largest relative error (-0.05%) occurs for the Northern Schneeferner (Central Europe, Alps), which has a small RGI area of 0.351 km^2. The absolute area difference to the RGI state is for this glacier -0.02 km^2. The largest absolute area difference with 2.9 km^2 occurs for the Breiðamerkurjökull (Iceland, RGI region 06), which had an area of 1067.7 km^2 in the year $t_{RGI} = 2000$.

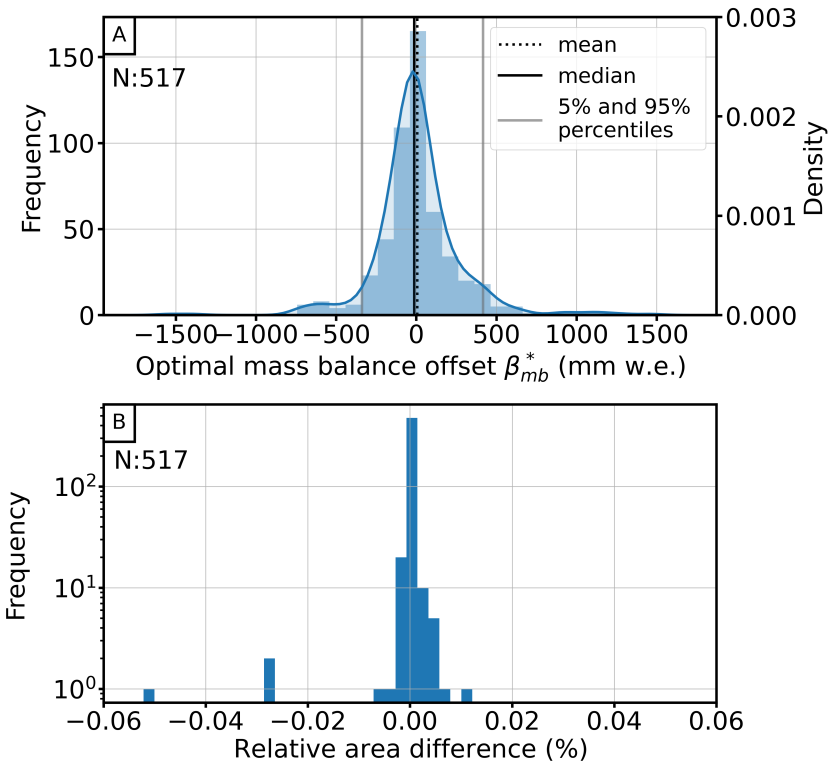

Fig. 4.2: **A:** Distribution of the derived optimal mass balance offsets β^*_{mb}. Vertical lines indicate the mean (dashed line), median (black line) and the 5% and 95% percentiles (grey lines) . The sample size is $n = 517$. **B:** Histogram of all relative area differences (%) of the OGGM state s^{OGGM} and RGI state s^{RGI}. The sample size is $n = 517$. Note that the y-axis is logarithmic.

4.3.2 Reconstructions in year 1917

We use the calibration runs to identify optimal mass balance offsets for each of the glaciers and apply the initialization method from Eis et al. (2019) to reconstruct their states in year 1917. The derived mass balance offsets β^*_{mb} are applied to all model runs during the initialization (the random climate runs and the past climate runs). This ensures that the reconstructed state at the inventory date is in close proximity to the RGI state s^{RGI} and thus allows a comparison with glacier observations. For the optimization, we use a fitness function based on geometry differences see Eis et al., 2019, for more details:

$$J(s_{t_0}) = \frac{1}{\epsilon m}\left(\sum_{i=0}^{m}\left((z^{OGGM}_{t_{RGI}})_i - (z_{t_{RGI}})_i\right)^2 + \left((w^{OGGM}_{t_{RGI}})_i - (w_{t_{RGI}})_i\right)^2\right), \quad (4.2)$$

with the uncertainty $\epsilon = 125$ and m the total number of grid points of all flow lines of a glacier. The fitness function $J(s_{t_0})$ calculates the averaged difference in surface

elevation z_t and width w_t between the OGGM state (s_t^{OGGM}, obtained from the calibration runs) and the forward modeled glacier states. Each glacier candidate is evaluated based on the difference to the OGGM state at the inventory date t_{RGI}. All states that have a fitness value smaller than 1 are called acceptable states and Eis et al. (2019) suggested the median state (in the following referred to as s^{med}) of the 5th percentile of all acceptable states as the best representative of this set. Figure 4.3 demonstrates the advantages compared to an evaluation based on the RGI state s^{RGI}. Indeed, the range of acceptable candidates (with fitness values smaller than one) is similar for both evaluations, but a clear distinction between the best candidates is missing when using s^{RGI}. This occurs because the geometry of s^{RGI} is not matched perfectly for any of the tested glacier candidates. As s^{RGI} results from observational data (RGI outline and DEM with different inventory dates) directly, the shape cannot be reproduced exactly by a transient sate of the model. The poor distinction between the best candidates would impede the selection of the median state and thus an evaluation based on s^{RGI} could lead to false results. Figure 4.3A and C ,as well as Tab. 4.1, demonstrate that the difference between s^{RGI} and s^{OGGM} are very small and s^{RGI} is well represented by s^{OGGM}.

Tab. 4.1: Glacier length, area and volume of the median state in 1917 and 2003 of Hintereisferner (Ötztal, Austria). The last row contains the root mean square error ($RMSE_{dL}$) of the glacier length fluctuations when compared to the data set from Leclercq et al. (2014). The Table also contains information about the glacier size of the OGGM state and the RGI state in year 2003.

	s^{med}	s^{OGGM}	s^{RGI}
length (km) in 1917	9.4	-	-
length (km) in 2003	7.3	7.3	6.9
area (km^2) in 1917	10.13	-	-
area (km^2) in 2003	8.03	8.04	8.06
volume (km^3) in 1917	1.37	-	-
volume (km^3) in 2003	0.80	0.82	0.87
$RMSE_L$ (km)	0.45	-	-

4.3.3 Validation with glacier observations

The uncertainty analysis in Eis et al. (2019) showed that the uncertainty of our method reduces quickly over time. As a result, a meaningful validation of the method, which also covers the time period with the largest uncertainties, should be ideally performed with observations starting before or at the beginning of the initialization year (at the beginning of the 20th century). Remote sensing techniques are available for a relatively short time period and are consequently not sufficiently long enough for validation purposes. More suitable are direct observations of glacier

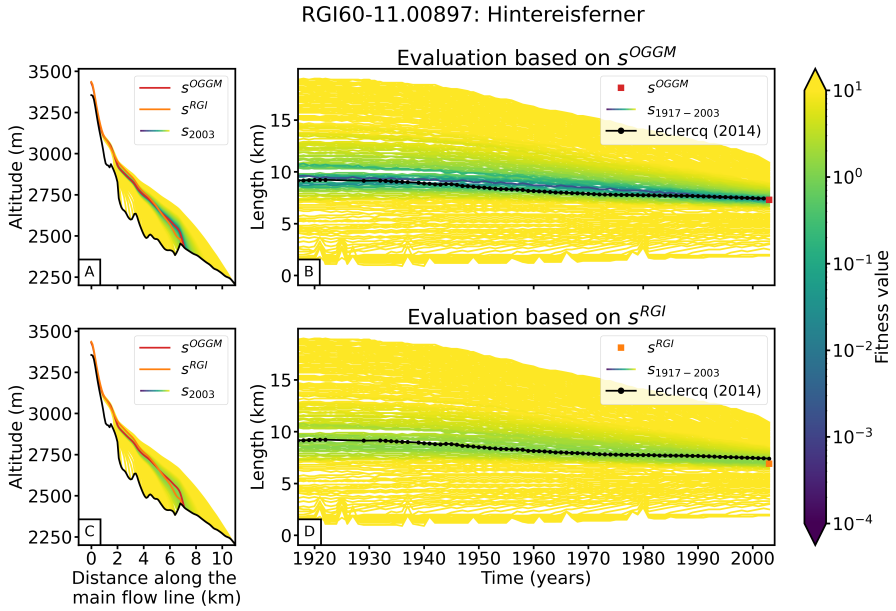

Fig. 4.3: Results for the Hintereisferner (Ötztal, Austria). Evaluation of the glacier candidates by fitness function based on geometry differences to **A,B:** the OGGM state s^{OGGM} and **C,D:** the RGI state s^{RGI}. Left: Cross sections along the main flow line in 2003. Black lines indicate the bed rock, red line the OGGM state s^{OGGM} and orange line the RGI state s^{RGI}, the remaining lines the modeled ice surfaces of all candidates, colored by their fitness value. Right: Reconstructed glacier length changes (smoothed with 5 year window) from 1917-2003. The glacier candidates are colored by their fitness values. The black line with dots shows the glacier length observations from Leclercq et al. (2014). The red square in **B** marks the length of the OGGM state in 2003, the orange square in **C** the length of the RGI state in 2003.

mass change which start to increase from 1950 onward. We here use mass-balance observations provided by the World Glacier Monitoring Service (WGMS, 2018). The Fluctuations of Glaciers (FoG) database contains annual mass-balance values for several hundreds of glaciers worldwide, but only 40 reference glaciers have a longer record than 30 years. Thus, we additionally include glacier length change observations to our validation as they date back furthest in time. They are usually obtained through annual measurements of the terminus position, but they can also be reconstructed from geomorphologic landforms (e.g. moraines), biological evidence (e.g. overridden trees, lichens) (e.g. Bushueva et al., 2016) or from historical paintings, photos and early maps (e.g. Nussbaumer and Zumbühl, 2012). The data set of Leclercq et al. (2014) includes long-term glacier length records that start not later than 1950 and cover at least 40 years. The temporal frequency and spatial accuracy of the data set increases rapidly from 1900 onward (Leclercq et al., 2014).

As the initialization method results in non-unique solutions, we use the median state s^{med} of the 5th percentile (the 5% best glacier candidates) for the validation. To this

end, we reconstruct the glacier states in the years with measurements and gain a total set of 5325 pairs of annual modeled and measured mass balances and a set of 10420 pairs of annual modeled and observed glacier length changes. The validation is performed based on five different error criteria: the model error, the mean bias error (MBE), the mean absolute error (MAE), the root mean square error (RMSE) and the correlation r. A summary of the performance can be found in Table 4.2. When referring in the following to one of the mass balance errors a subscripted mb will be added (e.g. RMSE$_{mb}$). Accordingly, we will add a subscripted L when referring to one of the glacier length errors (e.g. RMSE$_L$).

Tab. 4.2: Summary of the comparisons of modeled and measured mass balances and glacier length records. All numbers given are mean values and their standard deviation. The model error is calculated over each single measurement (M$_{mb}$=5325, M$_L$=10420), whereas the root mean square error (RMSE), the mean bias error (MBE), the mean absolute error (MAE) and the correlation r_{mb} are calculated for each individual glacier (N$_{mb}$=253, N$_L$=315). Glaciers with no modeled or observed change have to be excluded from the correlation calculation leading to different sample sizes (N$_{mb}$=250, N$_L$=302).

	mass balances	glacier lengths
Model Error	0.13 $\pm$ 0.79 (m w.e.)	-0.007 $\pm$ 0.62 (km)
MBE	0.18 $\pm$ 0.52 (m w.e.)	-0.14 $\pm$ 0.41 (km)
MAE	0.60 $\pm$ 0.34 (m w.e.)	0.35 $\pm$ 0.31 (km)
RMSE	0.71 $\pm$ 0.37 (m w.e.)	0.45 $\pm$ 0.40 (km)
Correlation	0.60 $\pm$ 0.31	0.36 $\pm$ 0.65

4.3.3.1 Mass balance validation

Before presenting the mass balance validation in detail, we show the results of three different example glaciers and the corresponding observations from WGMS (2018) in Fig. 4.4. Figure 4.4A shows an example with an almost perfect match to the observation, whereas the other two figures show two examples with a bad performance. In the example in Fig. 4.4B mass balances are well matched until 1975, but afterwards the modeled mass balances are to high compared to the observation. The glacier showed in Fig. 4.4C fits the observation on average, but the modeled amplitude is far to small . The results of each individual glacier are provided in the supplement.

Mass balance model error

The mass balance model error is calculated for each of the 5325 pairs of annual modeled and measured mass balances. For each pair, the measured mass balance is

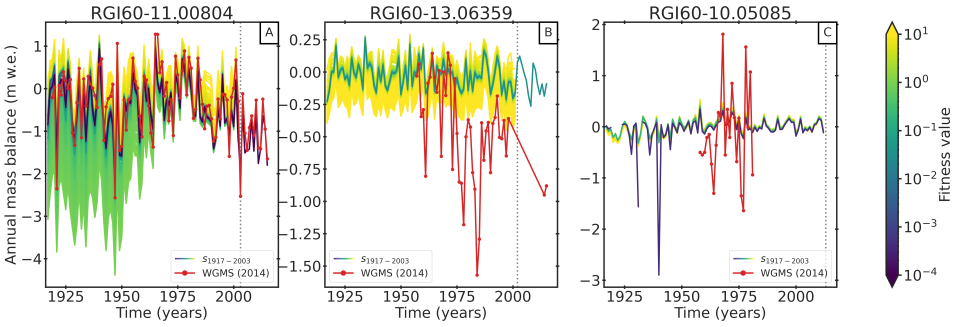

Fig. 4.4: Reconstructed annual mass balances from 1917 onward of three example glaciers. **A:** RGI60-11.00804, region 11 (Central Europe), **B:** RGI60-13.06359, region 13 (Central Asia) and **C:** RGI60-10.05085, region 10 (North Asia). The lines are colored by their fitness values. The red line with dots indicates the observed annual mass balances from WGMS (2018). The dots mark years with observations. The vertical dashed line marks t_{RGI}, from which onward only the median state is modeled forward in case observations after t_{RGI} are available.

subtracted from the modeled mass balance at the same year. Table 4.2 shows that

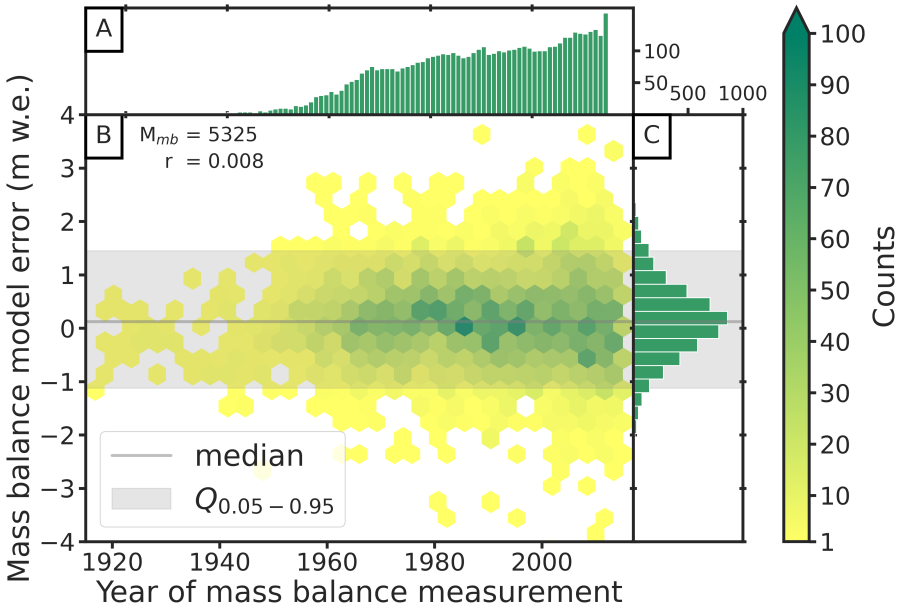

Fig. 4.5: Mass balance model error. **A:** Histogram of mass balance measurements per year. **B:** Binned scatter plot of model errors over time. The colors indicate the counts of errors in each bin. The numbers in the upper left corner indicate the total number of errors and the correlation with the time. **C:** Distribution of the modeled mass balance errors.

the mean over all mass balance model errors is with a value of -0.13 m w.e. close to zero and also the standard deviation (0.79 m w.e.) indicates a good fit between modeled and observed mass balances. Figure 4.5 shows a binned scatter plot of the mass balance model errors over time and thus provides information about their

temporal distribution. In addition the temporal distribution of the mass balance measurements (Fig. 4.5A) and the distribution of the mass balance model errors (Fig. 4.5C) are shown. With increasing number of measurements since 1960, the counts raises, especially in the middle range between -1 m w.e. and 1 m w.e. Most values are in close proximity to zero, but single errors reach values up to $\pm$ 4m w.e. The mass balance model errors are normal distributed (see Fig. 4.5). The correlation between the model error and the time is with $r = 0.008$ close to zero which indicates that there is no trend.

Mean bias error (MBE_{mb})

The mean bias error (also referred as bias, e.g. in Marzeion et al. (2012b)), is calculated for each of the 253 glaciers with mass balance measurements:

$$\mathrm{MBE_{mb}} = \frac{1}{n}\sum_{1=1}^{n}\left(B(i)_{\mathrm{modeled}} - B(i)_{\mathrm{measured}}\right), \tag{4.3}$$

where n is the total number of years with mass balance measurements for the specific glacier. Thus, the MBE_{mb} provides information about the performance of individual glaciers. Figure 4.6A shows that the MBE_{mb} is small for the majority of the glaciers. This is also reflected by the small mean (0.18 m w.e.) and median (0.14 m w.e.) values. Nevertheless, a few outliers range up to 2 m w.e. The distribution is slightly positive skewed, indicating that the mass balance is marginally overestimated by the model on average.

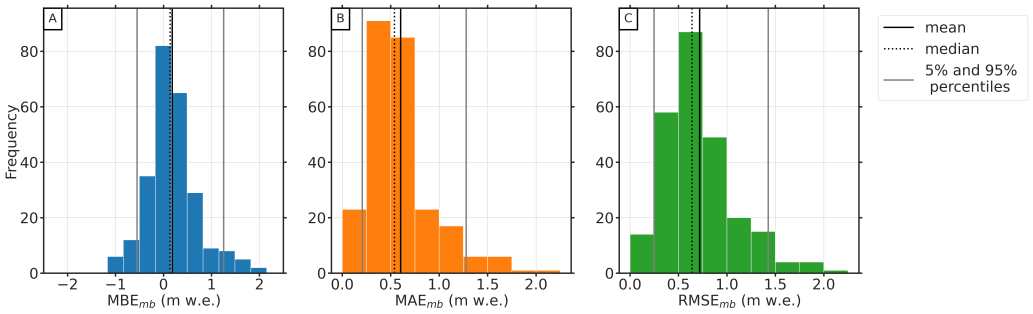

Fig. 4.6: Histogram of **A:** MBE_{mb} (mm w.e.), **B:** MAE_{mb} (mm w.e.), and **C:** $RMSE_{mb}$ (mm w.e.). Each histogram has a sample size of N_{mb}=253.

Mean absolute error (MAE_{mb}) and $RMSE_{mb}$

The root mean square error ($RMSE_{mb}$; Eq. 4.4) and the mean absolute error (MAE_{mb}; see Eq. 4.5), calculated for each glacier as well, do not consider the direction of the

error. Thus, they provide more information about the magnitude of the errors than the MBE_{mb}.

$$\text{RMSE}_{\text{mb}} = \sqrt{\frac{1}{n}\sum_{i=1}^{n}\left(B(i)_{\text{modeled}} - B(i)_{\text{measured}}\right)^2} \tag{4.4}$$

$$\text{MAE}_{\text{mb}} = \frac{1}{n}\sum_{i=1}^{n}\left|\left(B(i)_{\text{modeled}} - B(i)_{\text{measured}}\right)\right| \tag{4.5}$$

The RMSE_{mb} gives a relatively strong weight to large errors since the errors are squared before they are averaged and thus the values are larger than the ones of the MAE_{mb} (see Tab. 4.2 and Fig. 4.6B,C). Their distributions are quite similar to each other and also their mean values are in close proximity to each other (0.60 m w.e. for MAE_{mb} and 0.71 m w.e. for RMSE_{mb}.). Also their standard deviation do not differ significantly. Both measures show that the magnitude of the error is small for most glaciers. Even the few outliers fit the observation with an RMSE of about 2 m w.e. well.

Correlation r_{mb}

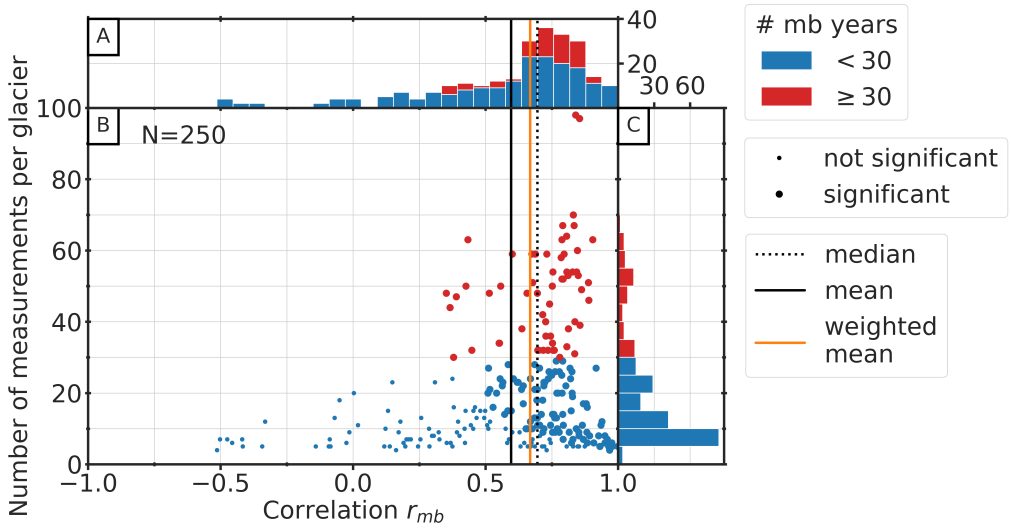

Fig. 4.7: Correlation coefficients in relation to number of mass balance measurements per glacier. Red dots or bars mark glaciers with more than 30 years of mass balance measurements and blue marks glaciers with less than 30 years. **A:** Histogram of the correlation coefficients of all glaciers. **B:** Scatter plot of the correlation against the number of mass balance measurements. A large dot indicates a correlation value that is significant at the 5% level and a small dot a not significant value. The horizontal, black line indicates the mean value over all glaciers, the orange line the average correlation weighted number of mass balance measurements per glacier and the dotted, black line the median value. **C:** Histogram of number of mass balance measurement per glacier. Note that the sample size is N=250, because the WGMS data set contains 3 glaciers with constant mass balance series and due to the zero variance it is consequently not possible to calculate the correlation.

Beside the different types of errors, we calculate the correlation between the modeled and measured mass balances over all glaciers. The negatively skewed distribution of the correlation coefficients in Figure 4.7A shows that for most glaciers the correlation is high. Nevertheless, for some single glaciers the modeled mass balances do not correlate with the measurements. Some glaciers even have a negative correlation, which distinctly influences the mean value across all glaciers. Figure 4.7B shows that there is a relation between the correlation coefficients r_{mb} and the number of mass balance measurements per glacier. All low and negative correlation coefficients result only from glaciers with less than 30 years of mass balance measurements. In addition low and negative correlation values only occur when the correlation is not significant (at the 5% level). However, Fig. 4.7A and B also shows that that the correlation is high for the majority of glaciers, even if only the ones with less than 30 years of mass balance measurements are considered. Nevertheless, it becomes clear, that the mean value (0.60) over all glaciers is largely influence by these outliers. In order to reduce this effect, we calculated an average value weighted by the number of mass balance measurements per glacier and obtain a weighted mean correlation of 0.67 across all glaciers. This shows that the modeled mass balances are in good agreement with the observations.

4.3.3.2 Glacier length validation

In addition to the validation with the mass balances time series from the WGMS data set, we will compare in this section modeled and observed glacier length changes. As before, we will use the modeled glacier length from the median state of the reconstruction. A clear advantage of glacier length fluctuations is the better temporal coverage. Some of the observations even start prior to 1850. Eis et al. (2019) showed that largest uncertainties of the reconstruction method occur at the beginning of the initialization (in this study 1917) and consequently a validation with many early observations is particularly helpful. We transform the glacier length changes from Leclercq et al. (2014) into respective glacier length values. To this end, we first determine all glacier length changes relative to the RGI inventory date t_{RGI}. When no observation is available in t_{RGI} we interpolate the length change for this year. In case the year of the last length change observation is before t_{RGI}, we use the last observation year instead. Finally, we reconstruct the observed glacier length time series with the help of the median state and add their glacier length at t_{RGI} or at the last observation year such that observed glacier length and the reconstructed glacier length are identical at this date.

In some cases t_{RGI} is long before the year of the last length change observation. In order to make use of these observations, we additionally run the median state

from t_{RGI} to the last observation year using the same past climate run as during the initialization procedure. In total we gain a set of 10420 pairs of modeled and observed glacier lengths since 1917. In Fig. 4.8 we show the results of three different example glaciers and the corresponding observed glacier length from Leclercq et al. (2014). Figure 4.8A shows an example with an almost perfect match to the observation, whereas the other two figures show two examples with a bad performance. The example in Fig. 4.8B is the glacier with largest MBE_L value. The glacier showed in Fig.4.8C has a negative correlation value of -0.77, as the best glacier candidate show a clear glacier advance over the hole time period, whereas the observation indicates a clear glacier retreat. More examples are provided in the supplement. Table 4.2 shows a summary of the performance of all tested glaciers

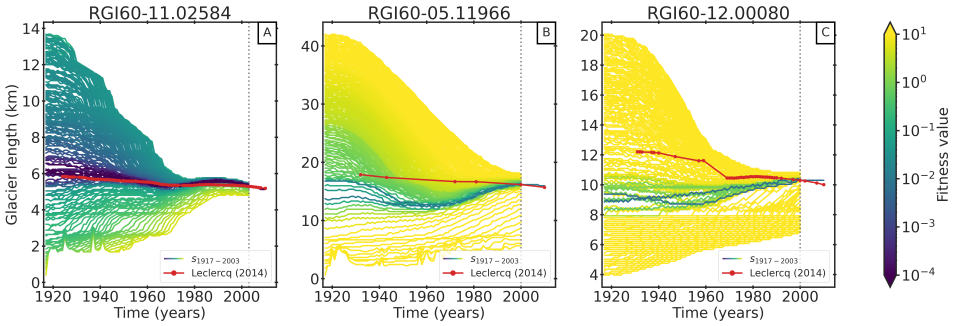

Fig. 4.8: Reconstructed glacier lengths from 1917 onward of three example glaciers. **A:** RGI60-11.02584, region 11 (Central Europe), **B:** RGI60-05.11966, region 05 (Greenland) and **C:** RGI60-11.00090, region 12 (Caucasus and Middle East). The lines are colored by their fitness values. The red line with dots indicates the observed glacier length from Leclercq et al. (2014). The dots mark years with observations. The vertical dashed line marks t_{RGI}, from which onward only the median state is modeled forward in case observations after t_{RGI} are available..

described by the length error, the mean bias error (MBE_L), the mean absolute error (MAE_L), the root mean square error (RMSE_L) and the correlation r_L.

Length error

Similar to the mass balance model error in Sect. 4.3.3.1, we calculate the length error for each of the 10420 pairs of modeled and observed glacier length. In opposition to the glacier specific errors, the number of observations for individual glaciers are of no consequence. Figure 4.9B show the distribution of the length errors over time. Most of the values range between ± 1 km (see also Fig. 4.9C) and also the small mean value over all length errors of -0.007 km indicate a good agreement with the observations. Nevertheless, a lot of outliers range up to ± 3 km and very few values have a length error about ≈ 6 km (see Fig. 4.9B). This also influences the standard deviation which has a value of 0.62 km. A correlation of the length errors with time is not identifiable (r=-0.118) and the data coverage is good over

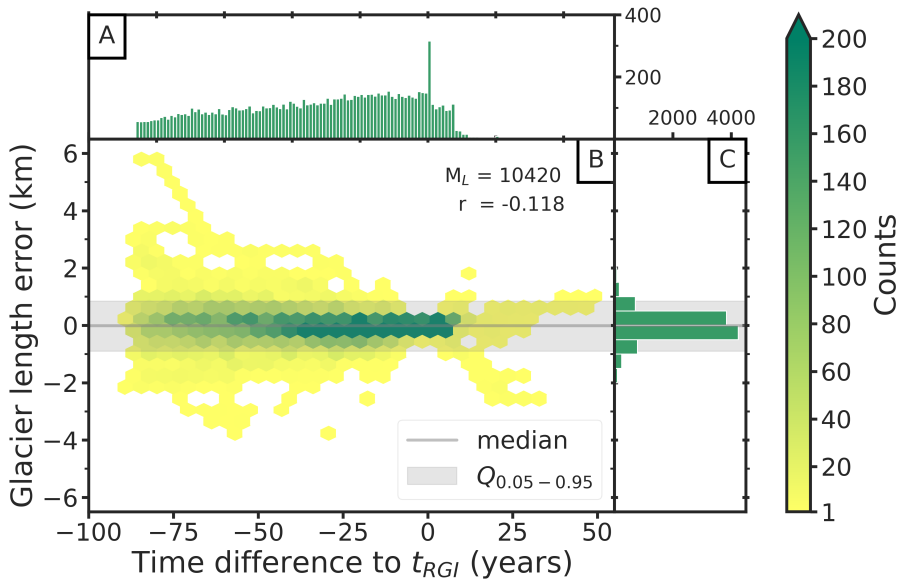

Fig. 4.9: Glacier length error. **A:** Histogram of glacier length observations per year. Note that the x-axis is displayed in time difference to t_RGI. Thus, all glacier length errors in t_{RGI} (x=0) are zero. **B:** Binned scatter plot of model errors over time. The colors indicate the counts of errors in each bin. The numbers in the upper left corner indicate the total number of model errors and the correlation with the time. **C:** Distribution of the glacier length errors.

the whole time period (see Fig. 4.9A).

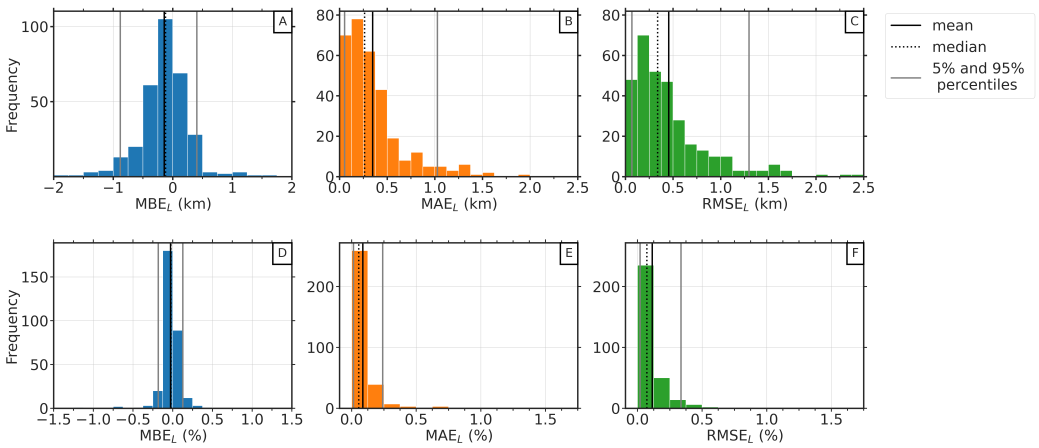

Fig. 4.10: Histograms of **A:** the mean bias errors (km), **B:** the mean absolute errors (km), and **C:** the root mean square error (km), **D:** the mean bias errors (%), **E:** the mean absolute errors (%), and **F:** the root mean square error (%). Each histogram has a sample size of N=315. The horizontal, black lines represent the mean value, the dashed lines the median and the grey line the corresponding 5th and 95th percentiles.

Mean bias error ($\mathrm{MBE_L}$)

The mean bias error ($\mathrm{M}BE_{\mathrm{L}}$) is calculated for each of the 315 glaciers with length observations. The $\mathrm{M}BE_{\mathrm{L}}$ provides information about how well the glacier length of individual glaciers are reproduced. The mean value over all $\mathrm{MBE_L}$ is with -0.14 km small, and also the standard deviation with a value of 0.41 km indicates a good fit. This can also be seen in the histogram in Fig. 4.10A which shows clearly that the majority of the values range between $\pm$ 0.5 km, but larger errors are possible as well. The 5th and 95th percentiles range from -0.89 km to 0.4 km, whereas the largest error (-1.7 km) occurs for a glacier located in south east Greenland (RGI60-05.11966). The distribution of all MBE_L values is slightly skewed left, indicating that the reconstruction method tend to underestimate the glacier lengths. As a large misfit between modeled and observed glaciers can also stem from a large glacier, we calculated additionally to the absolute error value per glacier the mean bias errors relative to the observed glacier length in 1950 (from Leclercq et al., 2014). See Fig. 4.10D for more details. The histogram of the MBE_L (in $\%$) clearly shows that a majority of values range between -0.125$\%$ and 0.125 $\%$, which is also reflect by the values of the 5th and 95th percentiles which ranges from -0.18 $\%$ to 0.13 $\%$. These very small values support the assumptions of a very good agreement between the observed and modeled glacier lengths.

Mean absolute error ($\mathrm{MAE_L}$) and $\mathrm{RMSE_L}$

The MAE_L and RMSE_L provide more insights about the magnitude of the errors than the MBE_L, as negative and positive values can not be compensated. Thus, the mean over all MAE_L and RMSE_L values are with values of 0-35 km (for MAE_L) and 0.45 km (for RMSE_L) noticeable higher than the ones from the length errors or the MBE_L (see Tab. 4.2). The standard deviations are slightly smaller (0.31 km for MAE_L and 0.4 km for RMSE_L), but this can be explained due to the reduced range of possible values (only positive). The histograms in Fig. 4.10 show that the majority of the errors is small. Considering e.g. the MAE_L than half of the errors are smaller than 0.26 km, which indicates a very good fit between the modeled and observed glacier lengths. Outliers range again up to $\approx$ 2 km for MAE_L and up to $\approx$ 2.4km for RMSE_L, but they occur very rarely. In general the RMSE_L errors are a little bit higher than the MAE_L's which is due to the relatively strong weight to large errors during the RMSE calculation. When considering the errors relative to the glacier lengths in 1950, the majority of the MAE_L (in $\%$) and RMSE_L (in $\%$) values are smaller than 0.25 $\%$. The 95th percentiles are located in both cases under 0.5$\%$ (0.24 $\%$ for the

MAE_L and 0.34% for the $RMSE_L$), which confirm the very good fit.

Correlation r_L

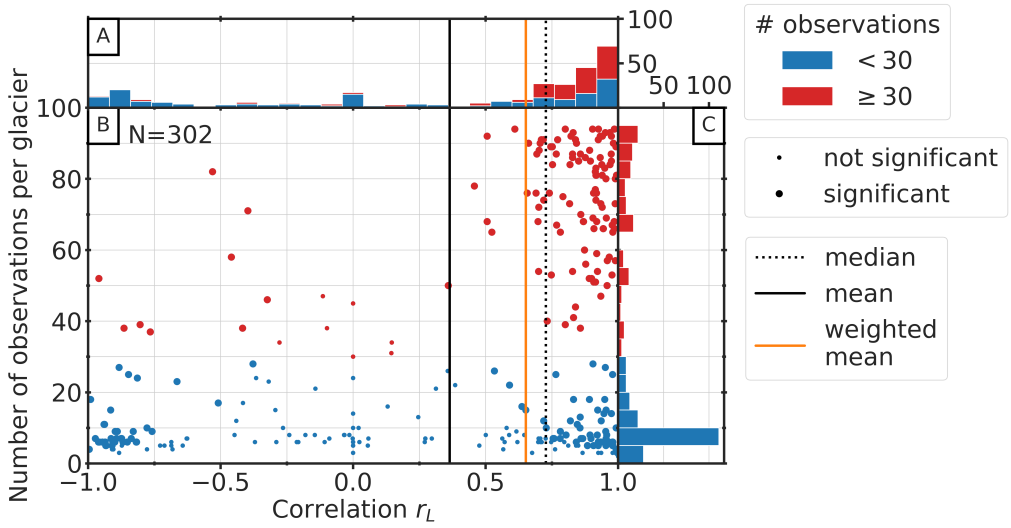

Fig. 4.11: Correlation coefficients in relation to total number of glacier length observations per glacier. Red dots or bars mark glaciers with more than 30 years of measurements and blue marks glaciers with less than 30 years. **A:** Histogram of the correlation coefficients of all glaciers. **B:** Scatter plot of the correlation against the number of glacier length observation. Horizontal, black line indicates the mean value over all glaciers, the orange line the average correlation weighted by the number of observations per glacier and the dotted, black line the median value. **C:** Histogram of number of glacier length observations per glacier. Note that the sample size is N=302, because for 13 glaciers the modeled glacier length is constant and due to the zero variance it is consequently not possible to calculate the correlation.

The results from the correlation analysis of the modeled and observed glacier lengths, calculated for each glacier individually, do not indicate a good agreement for all tested glaciers. The distribution of the individual correlation coefficients for each glacier is slightly bimodal (see Fig. 4.11A). Most correlation values range from 0.7 to 1, but 87 out of 302 glaciers have a negative correlation (some of them close to -1). In contrast to the correlation analysis from the mass balances (see Fig. 4.7B) not all negative correlation values can be explained by a low number of observations or because the correlation is not significant at the 5 % level. Fig. 4.11B shows that 12 glaciers with more than 30 length observations have a negative correlation, four of them are even in close proximity to -1. Nevertheless the histogram and the scatter plot in Fig. 4.11A and B shows that a majority of the glaciers with negative correlation values can be attributed to a low number of length observations. The negative correlation values, largely influence the mean value (0.36), for what reason the mean weighted over the number of observations per glacier is with a value of

0.65 more representative. This is also underlined by the even higher median value (0.73). (Oetztal, Austria) (Oetztal, Austria)

4.4 Hardware Requirements and Performance

For this study we used a small cluster comprising two nodes with two 14-core CPUs each, resulting in 112 parallel threads (two threads per core). As the mass balance offset calibration converges within 12 iterations, running the calibration runs is cheap. The application of the initialization method from (Eis et al., 2019) is most expensive, as hundreds of dynamical model runs need to be performed and the dynamical runs are the most expensive computations in OGGM. The size of the glacier and the required time stepping to ensure a numerical stability strongly influence the required computation time. The computation time needed to apply the initialization procedure to one glacier varies from glacier to glacier. In total, initializing the 517 glaciers in 1917 takes approximately 24 hours on our small cluster. This implies that substantial computing resources will be needed in order to apply our method to, e.g., initialize a global model run.

4.5 Conclusions

This study extends Eis et al. (2019) with the addition of mass-balance calibration runs to adapt the method to real-world use cases. During these calibration runs a glacier specific mass balance offset β_{mb} is iteratively calibrated such that the glacier state at the inventory date is in close proximity to the observation. The obtained mass balance offset β_{mb} is then applied to all (past and random climate) forward runs during the initialization procedure. We applied the initialization method for 517 glaciers for which either mass balance measurements or glacier length records are available. Water-terminating glaciers were excluded from our study. For their identification, the attribute from the RGI database was used, but this characteristic only refers to the inventory date t_{RGI}. Glaciers that were water-terminating in the past, but are not anymore at the inventory date t_{RGI}, can not be detected and thus could not be excluded from our validation - this is a potential source of large length errors.

We validate our initialization method by comparing modeled glacier changes to mass balance observations (WGMS, 2018) and to length records (Leclercq et al., 2014). For this purpose different types of errors (model error, mean bias error, mean absolute error, root mean square error and correlation) are taken into account. As the initialization can result in non-unique solutions, we use the median state of the 5th percentile for the validation. This is the best representative for the possibly large

set of acceptable glacier states (see Eis et al., 2019, for more details). Altogether the validation showed a good agreement between the modeled glacier states and the observations. Considering the mass balance observations, a mean model error (calculated over each pair of modeled and measured mass balances) of 0.13 $\pm$ 0.79 m w.e. could be achieved. And also the mean MAE$_{mb}$ of 0.60 $\pm$ 0.34 m w.e. reflects the good agreement with the observations. We found out that the correlation between the modeled and the measured time series is influenced by the number of mass balance measurements. Negative and low correlation coefficients are exclusively produced when the number of mass balance observations for this glacier is low (less than 30 years). One disadvantage of the mass balance measurements is their temporal resolution. Eis et al. (2019) showed that the uncertainties that stem from the initialization method itself are largest during the first years after the initialization. Unfortunately, most of the mass balance observations were measured after 1960. Prior mass balance measurements exist for very few individual glaciers only. For this purpose we add to our validation the comparison with glacier length records from Leclercq et al. (2014) which have a better temporal resolution at the beginning of our initialization in 1917. Considering the glacier length, the mean model error has a value of 0.14 $\pm$ 0.41 km and a mean MAE$_L$ of 0.35 $\pm$ 0.31 km. The mean correlation value is with 0.36 $\pm$ 0.65 significant smaller than the one from the mass balances, but again mainly influenced by many glaciers with a very few observations. We could show that the average correlation weighted by number of observations per glacier is with a value of 0.65 much more representative than the unweighted mean. For a better interpretation of these values, we also need to consider the uncertainties of the observations. Zemp et al. (2013) provided an error estimation for the random error from the glaciological mass balance measurements (0.34 m w.e.). To allow a comparison between the calculated model error of the initialization method and the error of the mass balance measurements, we need to calculate the mean of the absolute values of the mass balance model errors. With a value of 0.59 m w.e. it is about twice that of the random error from the glaciological mass balance measurements. Leclercq et al. (2014) provided the information about the data accuracy for each individual data point (depending on the method used for the data acquisition). 97 $\%$ of the data points used in our study can be assigned to Category 1 (direct measurements) and these measurements typically have a spatial uncertainty of less than 50 m and a time accuracy within 1 year (Leclercq et al., 2014). Compared to the obtained length errors of the initialization method, the error of the lengths observations seems to be negligibly small. Most data points of the remaining 3$\%$ are assigned either to Catergory 2 (historical sources) with a typical uncertainty range of 100-200 m or to the fifth Category for which the method of measurement is unknown and consequently the accuracy is unknown as well. Among the accuracy of the observations, other factors that could influence our validation need to be considered as well. Unfortunately, they cannot be quantified. Larger uncertainties could e.g. be produced by a wrong linking between glacier ID's

from different data sets. This especially concerns the links between the Leclercq et al. (2014) data set and the Randolph Glacier Inventory. For the linking we used the method described in Parkes and Goosse (2019) resulting in two classes of matches: positive matches and "best-effort"-matches. Especially for the second class a false linking can not be excluded. Another uncertainty could come from false outlines provided by the RGI. These occur due to uncertainties in the topography, unavailable data or because of human decisions Maussion et al. (2019). False outlines can lead to false centerlines and consequently to error in the length calculations. Furthermore, modeled and observed length changes can differ in special cases due to separation of glacier entities in the observation period. As a result, a jump in the observed glacier lengths occurs. At the same time, the model is yet not able to reproduce these jumps. This would require a merging of neighboring glaciers and is already under development. However, the merging method is not yet fully automatized.
Considering all these different uncertainty sources, we can summarize that both data sets, the mass balance observations from WGMS (2018) and the glacier length records from Leclercq et al. (2014), are well matched by the modeled glacier states and thus the initialization method from Eis et al. (2019) is verified.
Future work will include a global application, which would be the first global glacier reconstruction using a flowline model. However, a global run would consume very high computational cost. This means it will likely take multiple months on our small cluster. Computational costs could potentially be reduced by decreasing the model resolution or the number of the glacier candidates. Furthermore, the developed iterative calibration method could be expanded in order to optimize other dynamical parameters of OGGM. The sliding parameter and the creep parameter are by default not glacier specific and calibrated per default by the 253 WGMS reference glaciers. A criterion based on the glacier length in t_{RGI} could be used to determine a glacier specific sliding parameter, independently from the WGMS data set. Similarly, the creep parameter could be determined by a criteria based on the surface elevation in t_{RGI} at the head of the glacier. Such an approach could not only further improve the reconstruction, but also future projections.

Code availability

The OGGM software together with initialization method are coded in the Python language and licensed under BSD-3-Clause License. The latest version of the OGGM code is available on Github (https://github.com/OGGM/oggm), the documentation is hosted on ReadTheDocs (http://oggm.readthedocs.io), and the project webpage for communication and dissemination can be found at http://oggm.org. The OGGM version used in this study is v1.2. The code for the initialization module is available on Github (https://github.com/OGGM/initialization).

Author Contributions

JE is the main developer of the initialization module and wrote most of the paper. LL supported the development of this study and worked on methodological concepts and testing. BM and FM are the initiators of the OGGM project and helped to conceive this study. FM is the main OGGM developer.

5 Conclusion

5.1 Achievements

In Sect. 1.7 three objectives were formulated. This section highlights the objectives achieved in this work.

1. The development of an initialization method that allows the reconstruction of past glacier states by using only information about the past climate and the present day states.

This thesis introduced in Chapter 2 a framework which is very useful to simulate past and future glacier changes on a global scale: the Open Global Glacier Model (OGGM). However, in order to present realistic past changes over the course of the entire 20th century, an adequate initial state for each of the world's glaciers is required. To this end, a new initialization method was developed and presented in Chapter 3. The method only uses information about the past climate and the present day glacier state, because this is the only information given for all glaciers. A successful development was initially only possible by making use of synthetic experiments. This was necessary, because this inverse problem turns out to be ill-posed, as it leads to nonunique solutions. To narrow the range of possible initial states, we used an ensemble approach. First, a large set of physically plausible glacier states is generated using a randomized climate that represents the conditions around the initialization year. Second, a selection of glacier states is modeled forward to the present day and then the modeled states are evaluated by their difference to the observed present-day state using a fitness function. This fitness function takes e.g. differences in geometry into account and small fitness values represent small geometry differences. All initial states with a fitness value smaller than one are accepted and indicate the range of possible initial states. This range can vary from glacier to glacier and a statistical analysis showed that the reconstructability of a glacier correlates well with the response time, as well as with the surface slope.

2. The application to real-world cases.

The synthetic environment was essential for the development of the proposed initialization approach, but the main disadvantage is that the resulting initial states

do not necessarily represent the reality. This originates from the fact that the synthetic experiment state at the present day can differ from the real present day glacier state and consequently the reconstructed past evolution does not coincide with reality neither. To this end, Chapter 4 presented a further development. A glacier-specific calibration of the mass balance offset was introduced which enforces that the reconstructed state and the observed glacier state at the inventory date are as close as possible to each other. We performed the calibration of the mass balance offset, followed by the reconstruction based on the initialization approach presented in Chapter 3. With the help of an error analysis based on a comparison to glacier mass and length change observations, we were able to validate the initialization approach.

3. The identification of uncertainties of the initialization method itself and its validation by comparing the modeled glacier changes with glacier observations.

The main advantage of the synthetic environment is that the uncertainty of the initialization method itself can be identified (see Chapter 3). Uncertainties that stem e.g. from the glacier model, the calibration data or from climate observations are extracted from this first uncertainty analysis. Perfectly known boundary conditions are assumed and thus a comparison between the median state and the synthetic experiment leads to the uncertainty of the method. Important is also the evolution of the error over time. Whereas the uncertainty is largest at the beginning (here 1850), errors reduce rapidly within 60 years. The median of relative volume errors in 1850 has a value of -0.97 % and is largely influenced by a few single outliers. The skewed distribution of errors showed that the initialization method has a slight tendency to underestimate the glacier volume. After the successful application to real-world cases, the method can also be validated with a comparison against glacier observations (see Chapter 4). To this end, we use glacier mass balance observations and glacier length records which partially date back to the beginning of the 20th century and are available for a few hundred glaciers worldwide. For the validation we take the model error, the MBE, the MAE, the RMSE and the correlation into account. Each of these criteria showed that we were able to reach a good agreement with the observations, both mass balances and glacier length records. These results show that the method is usable in order to reconstruct past glaciers all over the world.

5.2 Outlook

In order to allow the application to real-world cases, a glacier individual calibration of the mass balance offset becomes necessary and was described in Chapter 4.

The parameter is determined iteratively, such that the area of the modeled glacier is as close as possible to the area of the observed glacier state at the inventory date. However, it would be possible to expand this iterative calibration method in order to optimize other dynamical parameters of OGGM. Especially parameters that are assumed to be different for individual glaciers would be convenient for such a procedure. The sliding parameter f_s, which depends on basal characteristics, and the creep parameter A, which is among other factors influenced by the ice temperature of the glacier, cannot be assumed to be globally constant. Nevertheless, these dynamical parameters are not yet considered as calibration parameters in OGGM (Maussion et al., 2019). Their inclusion in the developed iterative calibration would require a different criterion than the glacier area at the inventory date. Possible would be e.g. to optimize the sliding parameter f_s such that the glacier length at the inventory date fits the observed length of the glacier. Similarly, the creep parameter could be determined by a criterion based on the surface elevation at the head of the glacier. More improvements related to OGGM, would also help to improve the initialization method, e.g. the consideration of merging of neighboring glaciers during growing could have a large influence on the results. Large uncertainty also stem from the low reconstructability in many cases. This could be improved by using a multi-step approach. The reconstructability improves the shorter the inspected time period is (see Sect. 3.9.2). Less glacier states converge to the same state when only short time intervals are considered. It is conceivable that a splitting of the time period in multiple periods with a maximum length of e.g. 20 years could improve the nonuniqueness problem. Instead of searching one initial state, also intermediate initial states will be generated successive. In the first place, an initial state for the year 1980 could be reconstructed and in the next step the initial state for the year 1960 is searched, such that it fits the state from 1980 and so on until the original initial state is found. This kind of approach corresponds to a multiple shooting method, well known from the solution of boundary value problems (e.g. Morrison et al., 1962).

Beside the further improvement of the initialization approach, future work also includes the global application. However, this effort will be related to very high computational costs. Using the same hardware available (see Sec. 3.9.2 and 4.5), a global application will probably take at a rough estimate several months up to half a year. In order to reduce the computational costs, a reduction in model resolution could be considered. Depending on the application it could also be considered to use the results of the calibration run directly, as this is already one of the possible initial states. However, by only using the information of the calibration run, the information about the complete range of possible solutions would be lost and may increase the uncertainty strongly. Especially due to the lack of knowledge about past glacier changes on a global scale, such global reconstructions will be very helpful to determine the contribution of glaciers to global sea-level rise.

Bibliography

Adhikari, S. and S. J. Marshall (2012a). „Glacier volume-area relation for high-order mechanics and transient glacier states“. In: *Geophysical Research Letters* 39.16, pp. 1–6. DOI: 10.1029/2012GL052712 (cit. on p. 33).

– (2012b). „Parameterization of lateral drag in flowline models of glacier dynamics“. In: *Journal of Glaciology* 58.212, pp. 1119–1132. DOI: 10.3189/2012JoG12J018 (cit. on p. 32).

Allen, M. R., O.P. Dube, W. Solecki, F. Aragón-Durand, W. Cramer, S. Humphreys, M. Kainuma, J. Kala, N. Mahowald, Y. Mulugetta, R. Perez, M. Wairiu, and K. Zickfeld (2018). „Framing and Context. In: Global Warming of 1.5°C. An IPCC Special Report on the impacts of global warming of 1.5°C above pre-industrial levels and related global greenhouse gas emission pathways, in the context of strengthening the global response to the threat of climate change, sustainable development, and efforts to eradicate poverty“. In: ed. by V. Masson-Delmotte, P. Zhai, H.-O. Pörtner, D. Roberts, J. Skea, P.R. Shukla, A. Pirani, W. Moufouma-Okia, C. Péan, R. Pidcock, S. Connors, J.B.R. Matthews, Y. Chen, X. Zhou, M.I. Gomis, E. Lonnoy, T. Maycock, M. Tignor, and T. Waterfield (cit. on p. 3).

Auer, I., R. Böhm, A. Jurkovic, W. Lipa, A. Orlik, R. Potzmann, W. Schöner, M. Ungersböck, C. Matulla, K. Briffa, P. Jones, D. Efthymiadis, M. Brunetti, T. Nanni, M. Maugeri, L. Mercalli, O. Mestre, J.-M. Moisselin, M. Begert, G. Müller-Westermeier, V. Kveton, O. Bochnicek, P. Stastny, M. Lapin, S. Szalai, T. Szentimrey, T. Cegnar, M. Dolinar, M. Gajic-Capka, K. Zaninovic, Z. Majstorovic, and E. Nieplova (2007). „HISTALP—historical instrumental climatological surface time series of the Greater Alpine Region“. In: *International Journal of Climatology* 27.1, pp. 17–46. DOI: 10.1002/joc.1377 (cit. on p. 65).

Bach, E., V. Radić, and C. Schoof (2018). „How sensitive are mountain glaciers to climate change? Insights from a block model“. In: *Journal of Glaciology* 64.244, pp. 247–258. DOI: 10.1017/jog.2018.15 (cit. on p. 75).

Bahr, D. B., M. Dyurgerov, and M. F. Meier (2009). „Sea-level rise from glaciers and ice caps: A lower bound“. In: *Geophysical Research Letters* 36.3, pp. 2–5. DOI: 10.1029/2008GL036309 (cit. on p. 44).

Bahr, D. B., M. F. Meier, and S. D. Peckham (1997). „The physical basis of glacier volume-area scaling“. In: *Journal of Geophysical Research: Solid Earth* 102.B9, pp. 20355–20362. DOI: 10.1029/97JB01696 (cit. on pp. 10, 34, 43, 45).

Bahr, D. B., W. T. Pfeffer, and G. Kaser (2014). „Glacier volume estimation as an ill-posed inversion“. In: *Journal of Glaciology* 60.223, pp. 922–934. DOI: 10.3189/2014JoG14J062 (cit. on p. 24).

Bahr, D. B., W. T. Pfeffer, and G. Kaser (2015). „A review of volume-area scaling of glaciers“. In: *Reviews of Geophysics*, pp. 95–140. DOI: 10.1002/2014RG000470 (cit. on pp. 11, 34, 43, 44).

Bahr, D. B., W. T. Pfeffer, C. Sassolas, and M. F. Meier (1998). „Response time of glaciers as a function of size and mass balance: 1. Theory“. In: *Journal of Geophysical Research: Solid Earth* 103.B5, pp. 9777–9782. DOI: 10.1029/98JB00507 (cit. on pp. 5, 11).

Bamber, J., R. M. Westaway, B. Marzeion, and B. Wouters (2018). „The land ice contribution to sea level during the satellite era“. In: *Environmental Research Letters*. DOI: 10.1088/1748-9326/aac2f0 (cit. on pp. 56, 84).

Benn, D.I. and D.J.A. Evans (2010). *Glaciers and Glaciation*. Hodder Arnold Publication. Hodder Education (cit. on pp. 2, 5, 8, 9).

Blatter, H. (1995). „Velocity and stress fields in grounded glaciers: a simple algorithm for including deviatoric stress gradients“. In: *Journal of Glaciology* 41.138, pp. 333–344. DOI: 10.3189/S002214300001621X (cit. on p. 10).

Budd, W. F., P. L. Keage, and N. A. Blundy (1979). „Empirical studies of ice sliding.“ In: *Journal of Glaciology* 23.89, pp. 157–170. DOI: 10.1017/S0022143000029804 (cit. on p. 31).

Bushueva, I., O. Solomina, and N. A. Volodicheva (2016). „Fluctuations of Terskol Glacier, Northern Caucasus, Russia“. In: *Earth's Cryosphere* 20, pp. 95–104. DOI: 10.21782/KZ1560-7496-2016-3(95-104) (cit. on pp. 7, 94).

Chen, J. and A. Ohmura (1990). „Estimation of Alpine Glacier Water Resources and their Change Since the 1870s“. In: *IAHS Publ.* 193 (cit. on p. 10).

Church, J.A., P.U. Clark, A. Cazenave, J.M. Gregory, S. Jevrejeva, A. Levermann, M.A. Merrifield, G.A. Milne, R.S. Nerem, P.D. Nunn, A.J. Payne, W.T. Pfeffer, D. Stammer, and A.S. Unnikrishnan (2013). „Sea Level Change“. In: *Climate Change 2013: The Physical Science Basis. Contribution of Working Group I to the Fifth Assessment Report of the Intergovernmental Panel on Climate Change*. Ed. by T.F. Stocker, D. Qin, G.-K. Plattner, M. Tignor, S.K. Allen, J. Boschung, A. Nauels, Y. Xia, V. Bex, and P.M. Midgley. Cambridge, United Kingdom and New York, NY, USA: Cambridge University Press. Chap. 13, pp. 1137–1216. DOI: 10.1017/CBO9781107415324.026 (cit. on pp. 3, 4, 17, 56, 84).

Clarke, G. K. C., F. S. Anslow, A. H. Jarosch, V. Radić, B. Menounos, T. Bolch, and E. Berthier (2013). „Ice Volume and Subglacial Topography for Western Canadian Glaciers from Mass Balance Fields, Thinning Rates, and a Bed Stress Model“. In: *Journal of Climate* 26.12, pp. 4282–4303. DOI: 10.1175/JCLI-D-12-00513.1 (cit. on p. 11).

Clarke, G. K. C., A. H. Jarosch, F. S. Anslow, V. Radić, and B. Menounos (2015). „Projected deglaciation of western Canada in the twenty-first century“. In: *Nature Geoscience* 8.5, pp. 372–377. DOI: 10.1038/ngeo2407 (cit. on p. 40).

Cogley, J. G. (2009). „Geodetic and direct mass-balance measurements: comparison and joint analysis“. In: *Annals of Glaciology* 50.50, pp. 96–100. DOI: 10.3189/172756409787769744 (cit. on pp. 8, 17).

Cogley, J. G., R. Hock, L. A. Rasmussen, A. A. Arendt, A. Bauder, R. J. Braithwaite, P. Jansson, G. Kaser, M. Möller, L. Nicholson, and M. Zemp (2011). *Glossary of glacier mass balance and related terms*. Tech. rep. IACS Contribution No. 2. Prepared by the Working Group on Mass-balance Terminology and Methods of the International Association of Cryospheric Sciences (IACS). Paris (cit. on pp. 5, 8).

Colton, David and Rainer Kress (1992). *Inverse acoustic and electromagnetic scattering theory*. English. Vol. 93. Berlin: Springer-Verlag, pp. x + 305 (cit. on p. 62).

Cuffey, K. and W. S. B. Paterson (2010). *The Physics of Glaciers*. 4th Edition. Academic Press (cit. on pp. 4, 32, 33).

Dyurgerov, M. B. and M. F. Meier (2005). *Glaciers and the changing Earth system: a 2004 snapshot*. Vol. 58. Institute of Arctic and Alpine Research, University of Colorado Boulder (cit. on p. 8).

Dyurgerov, M. B., M. F. Meier, and D. B. Bahr (2009). „A new index of glacier area change: a tool for glacier monitoring". In: *Journal of Glaciology* 55.192, pp. 710–716. DOI: 10.3189/002214309789471030 (cit. on p. 10).

Eis, J., F. Maussion, and B. Marzeion (2019). „Initialization of a global glacier model based on present-day glacier geometry and past climate information: an ensemble approach". In: *The Cryosphere* 13.12, pp. 3317–3335. DOI: 10.5194/tc-13-3317-2019 (cit. on pp. 85–90, 92, 93, 99, 104–106).

Farinotti, D., D. J. Brinkerhoff, G. K. C. Clarke, J. J. Fürst, H. Frey, P. Gantayat, F. Gillet-Chaulet, C. Girard, M. Huss, P. W. Leclercq, A. Linsbauer, H. Machguth, C. Martin, F. Maussion, M. Morlighem, C. Mosbeux, A. Pandit, A. Portmann, A. Rabatel, R. Ramsankaran, T. J. Reerink, O. Sanchez, P. A. Stentoft, S. Singh Kumari, W. J. J. van Pelt, B. Anderson, T. Benham, D. Binder, J. A. Dowdeswell, A. Fischer, K. Helfricht, S. Kutuzov, I. Lavrentiev, R. McNabb, G. H. Gudmundsson, H. Li, and L. M. Andreassen (2017). „How accurate are estimates of glacier ice thickness? Results from ITMIX, the Ice Thickness Models Intercomparison eXperiment". In: *The Cryosphere* 11.2, pp. 949–970. DOI: 10.5194/tc-11-949-2017 (cit. on pp. 11, 31, 34, 59).

Farinotti, D., M. Huss, An. Bauder, M. Funk, and M. Truffer (2009). „A method to estimate the ice volume and ice-thickness distribution of alpine glaciers". In: *Journal of Glaciology* 55.191, pp. 422–430. DOI: 10.3189/002214309788816759 (cit. on pp. 11, 31, 32, 59, 86).

Farinotti, D., M. Huss, J. J. Fürst, J. Landmann, H. Machguth, F. Maussion, and A. Pandit (2019). „A consensus estimate for the ice thickness distribution of all glaciers on Earth". en. In: Nature Geoscience 12.3, pp. 168–173. DOI: 10.1038/s41561-019-0300-3 (cit. on pp. 12, 14, 59, 86).

Farr, T. G., P. A. Rosen, E. Caro, R. Crippen, R. Duren, S. Hensley, M. Kobrick, M. Paller, E. Rodriguez, L. Roth, D. Seal, S. Shaffer, J. Shimada, J. Umland, M. Werner, M. Oskin, D. Burbank, and D. Alsdorf (2007). „The Shuttle Radar Topography Mission". In: *Reviews of Geophysics* 45.2, RG2004. DOI: 10.1029/2005RG000183 (cit. on p. 18).

Fischer, A. and M. Kuhn (2013). „Ground-penetrating radar measurements of 64 Austrian glaciers between 1995 and 2010". In: *Annals of Glaciology* 54.64, pp. 179–188. DOI: 10.3189/2013AoG64A108 (cit. on p. 34).

Gantayat, Prateek, Anil V. Kulkarni, and J. Srinivasan (2014). „Estimation of ice thickness using surface velocities and slope: case study at Gangotri Glacier, India“. In: *Journal of Glaciology* 60.220, pp. 277–282. DOI: 10.3189/2014JoG13J078 (cit. on p. 11).

Gardner, A. S., G. Moholdt, J. G. Cogley, B. Wouters, A. A. Arendt, J. Wahr, E. Berthier, R. Hock, W. T. Pfeffer, G. Kaser, S. R. M. Ligtenberg, T. Bolch, M. J. Sharp, J. O. Hagen, M. R. van den Broeke, and F. Paul (2013). „A Reconciled Estimate of Glacier Contributions to Sea Level Rise: 2003 to 2009“. In: *Science* 340.6134, pp. 852–857. DOI: 10.1126/science.1234532 (cit. on pp. 17, 56, 84).

Giesen, R. H. and J. Oerlemans (2012). „Calibration of a surface mass balance model for global-scale applications“. In: *The Cryosphere* 6.6, pp. 1463–1481. DOI: 10.5194/tc-6-1463-2012 (cit. on pp. 17, 18, 57, 84).

– (2013). „Climate-model induced differences in the 21st century global and regional glacier contributions to sea-level rise“. In: *Climate Dynamics* 41.11, pp. 3283–3300. DOI: 10.1007/s00382-013-1743-7 (cit. on pp. 10, 11, 17, 18, 57, 84).

Gillies, Sean (2007). *Shapely: manipulation and analysis of geometric objects* (cit. on p. 50).

– (2013). *Rasterio: geospatial raster I/O for Python programmers* (cit. on p. 50).

Goelzer, H., S. Nowicki, T. Edwards, M. Beckley, A. Abe-Ouchi, A. Aschwanden, R. Calov, O. Gagliardini, F. Gillet-Chaulet, N. R. Golledge, J. Gregory, R. Greve, A. Humbert, P. Huybrechts, J. H. Kennedy, E. Larour, W. H. Lipscomb, S. Le clec'h, V. Lee, M. Morlighem, F. Pattyn, A. J. Payne, C. Rodehacke, M. Rückamp, F. Saito, N. Schlegel, H. Seroussi, A. Shepherd, S. Sun, R. van de Wal, and F. A. Ziemen (2018). „Design and results of the ice sheet model initialisation experiments initMIP-Greenland: an ISMIP6 intercomparison“. In: *The Cryosphere* 12.4, pp. 1433–1460. DOI: 10.5194/tc-12-1433-2018 (cit. on p. 57).

Goosse, H., P.-Y. Barriat, Q. Dalaiden, F. Klein, B. Marzeion, F. Maussion, P. Pelucchi, and A. Vlug (2018). „Testing the consistency between changes in simulated climate and Alpine glacier length over the past millennium“. In: *Climate of the Past* 14.8, pp. 1119–1133. DOI: 10.5194/cp-14-1119-2018 (cit. on pp. 49, 56).

Gregory, J. M., N. J. White, J. A. Church, M. F. P. Bierkens, J. E. Box, M. R. van den Broeke, J. G. Cogley, X. Fettweis, E. Hanna, P. Huybrechts, L. F. Konikow, P. W. Leclercq, B. Marzeion, J. Oerlemans, M. E. Tamisiea, Y. Wada, L. M. Wake, and R. S. W. van de Wal (2013). „Twentieth-Century Global-Mean Sea Level Rise: Is the Whole Greater than the Sum of the Parts?“ In: *Journal of Climate* 26.13, pp. 4476–4499. DOI: 10.1175/JCLI-D-12-00319.1 (cit. on pp. 17, 56, 84).

Grinsted, A. (2013). „An estimate of global glacier volume“. In: *Cryosphere* 7.1, pp. 141–151. DOI: 10.5194/tc-7-141-2013 (cit. on pp. 43–45).

Harris, I. C., P. D. Jones, T. Osborn, and D. Lister (2014). „Updated hight-resolution grids of montly climatic observations- the CRU TS3.10 Dataset“. In: *International Journal of Climatology* 34, pp. 623–642. DOI: 10.1002/joc.3771 (cit. on pp. 27, 50, 56, 87).

Harrison, W. D. (2013). „How do glaciers respond to climate? Perspectives from the simplest models“. In: *Journal of Glaciology* 59.217, pp. 949–960. DOI: 10.3189/2013JoG13J048 (cit. on pp. 5, 48).

Harrison, W. D., D. H. Elsberg, K. A. Echelmeyer, and R. M. Krimmel (2001). „On the characterization of glacier response by a single time-scale“. In: *Journal of Glaciology* 47.159, pp. 659–664. DOI: 10.3189/172756501781831837 (cit. on p. 5).

Heimbach, P. and V. Bugnion (2009). „Greenland ice-sheet volume sensitivity to basal, surface and initial conditions derived from an adjoint model“. In: *Annals of Glaciology* 50.52, pp. 67–80. DOI: 10.3189/172756409789624256 (cit. on p. 57).

Henderson, Laura S. and Kamesh Subbarao (2017). „‘Inverse Crime’ and Model Integrity in Lightcurve Inversion applied to unresolved Space Object Identification“. In: *The Journal of the Astronautical Sciences* 64.4, pp. 399–413. DOI: 10.1007/s40295-016-0105-1 (cit. on p. 62).

Hirabayashi, Y., Y. Zang, S. Watanabe, S. Koirala, and S. Kanae (2013). „Projection of glacier mass changes under a high-emission climate scenario using the global glacier model HYOGA2“. In: *Hydrological Research Letters* 7.1, pp. 6–11. DOI: 10.3178/hrl.7.6 (cit. on pp. 10, 11).

Hock, R., A. Bliss, B. Marzeion, R. H. Giesen, Y. Hirabayashi, M. Huss, V. Radić, and A. B. A. Slangen (2019). „GlacierMIP – A model intercomparison of global-scale glacier mass-balance models and projections“. In: *Journal of Glaciology* 65.251, pp. 453–467. DOI: 10.1017/jog.2019.22 (cit. on pp. 14, 56, 84).

Hoegh-Guldberg, O., D. Jacob, M. Taylor, M. Bindi, S. Brown, I. Camilloni, A. Diedhiou, R. Djalante, K. L. Ebi, F. Engelbrecht, J. Guiot, Y. Hijioka, S. Mehrotra, A. Payne, S. I. Seneviratne, A. Thomas, R. Warren, and G. Zhou (2019). „Impacts of 1.5°C Global Warming on Natural and Human Systems. In: Global Warming of 1.5°C. An IPCC Special Report on the impacts of global warming of 1.5°C above pre-industrial levels and related global greenhouse gas emission pathways, in the context of strengthening the global response to the threat of climate change, sustainable development, and efforts to eradicate poverty“. In: ed. by V. Masson-Delmotte, P. Zhai, H.-O. Pörtner, D. Roberts, J. Skea, P.R. Shukla, A. Pirani, W. Moufouma-Okia, C. Péan, R. Pidcock, S. Connors, J.B.R. Matthews, Y. Chen, X. Zhou, M.I. Gomis, E. Lonnoy, T. Maycock, M. Tignor, and T. Waterfield (cit. on pp. 4, 6).

Howat, I. M., A. Negrete, and B. E. Smith (2014). „The Greenland Ice Mapping Project (GIMP) land classification and surface elevation data sets“. In: *Cryosphere* 8.4, pp. 1509–1518. DOI: 10.5194/tc-8-1509-2014 (cit. on p. 23).

Hoyer, S. and J. J. Hamman (2017). „xarray: N-D labeled Arrays and Datasets in Python“. In: *Journal of Open Research Software* 5, pp. 1–6. DOI: 10.5334/jors.148 (cit. on p. 50).

Hunter, J. D. (2007). „Matplotlib: A 2D Graphics Environment“. In: *Computing in Science Engineering* 9.3, pp. 90–95. DOI: 10.1109/MCSE.2007.55 (cit. on p. 50).

Huss, M. (2011). „Present and future contribution of glacier storage change to runoff from macroscale drainage basins in Europe“. In: *Water Resources Research* 47.7, n/a–n/a. DOI: 10.1029/2010WR010299 (cit. on p. 17).

Huss, M. and D. Farinotti (2012). „Distributed ice thickness and volume of all glaciers around the globe“. In: *Journal of Geophysical Research: Earth Surface* 117.4, F04010. DOI: 10.1029/2012JF002523 (cit. on pp. 11, 18, 32, 44, 45, 49).

Huss, M. and R. Hock (2015). „A new model for global glacier change and sea-level rise“. In: *Frontiers in Earth Science* 3, p. 54. DOI: 10.3389/feart.2015.00054 (cit. on pp. 10, 11, 17, 18, 44, 48, 57, 84, 85).

– (2018). „Global-scale hydrological response to future glacier mass loss“. In: *Nature Climate Change* 8.2, pp. 135–140. DOI: 10.1038/s41558-017-0049-x (cit. on p. 84).

Huss, M., G. Jouvet, D. Farinotti, and A. Bauder (2010). „Future high-mountain hydrology: a new parameterization of glacier retreat“. In: *Hydrology and Earth System Sciences* 14.5, pp. 815–829. DOI: 10.5194/hess-14-815-2010 (cit. on p. 11).

Hutter, K. (1981). „The effect of longitudinal strain on the shear stress of an ice sheet: in defence of using streched coordinates“. In: *J. Glaciol.* 27.95, pp. 39–56 (cit. on p. 31).

– (1983). *Theoretical glaciology: material science of ice and the mechanics of glaciers and ice sheets*, p. 150 (cit. on p. 31).

Immerzeel, W. W., L. P. H. van Beek, M. Konz, A. B. Shrestha, and M. F. P. Bierkens (2012). „Hydrological response to climate change in a glacierized catchment in the Himalayas“. In: *Climatic Change* 110.3-4, pp. 721–736. DOI: 10.1007/s10584-011-0143-4 (cit. on pp. 17, 84).

Immerzeel, W. W., Ludovicus P. H. van Beek, and Marc F. P. Bierkens (2010). „Climate Change Will Affect the Asian Water Towers“. In: *Science* 328.5984, pp. 1382–1385. DOI: 10.1126/science.1183188. eprint: https://science.sciencemag.org/content/328/5984/1382.full.pdf (cit. on p. 3).

Jacob, T., J. Wahr, W. T. Pfeffer, and S. Swenson (2012). „Recent contributions of glaciers and ice caps to sea level rise“. In: *Nature* 482. DOI: https://doi.org/10.1038/nature10847 (cit. on pp. 56, 84).

Jarosch, A. H., C. G. Schoof, and F. S. Anslow (2013). „Restoring mass conservation to shallow ice flow models over complex terrain“. In: *Cryosphere* 7.1, pp. 229–240. DOI: 10.5194/tc-7-229-2013 (cit. on p. 35).

Jarvis, A., E. Guevara, H. I. Reuter, and A. D. Nelson (2008). *Hole-filled SRTM for the globe : version 4 : data grid*. English. Published by CGIAR-CSI on 19 August 2008. (cit. on pp. 23, 65).

Jóhannesson, T., C. F. Raymond, and E. D. Waddington (1989a). „A Simple Method for Determining the Response Time of Glaciers“. In: *Glacier Fluctuations and Climatic Change*. Ed. by Johannes Oerlemans. Dordrecht: Springer Netherlands, pp. 343–352 (cit. on pp. 3–5).

Jóhannesson, T., C. Raymond, and E. Waddington (1989b). „Time–Scale for Adjustment of Glaciers to Changes in Mass Balance“. In: *Journal of Glaciology* 35.121, pp. 355–369. DOI: 10.3189/S002214300000928X (cit. on p. 5).

Kääb, A., J. M. Reynolds, and W. Haeberli (2005). „Glacier and Permafrost Hazards in High Mountains“. In: *Global Change and Mountain Regions: An Overview of Current Knowledge*. Ed. by Uli M. Huber, Harald K. M. Bugmann, and Mel A. Reasoner. Dordrecht: Springer Netherlands, pp. 225–234. DOI: 10.1007/1-4020-3508-X_23 (cit. on pp. 3, 84).

Kaser, G., M. Grosshauser, and B. Marzeion (2010). „Contribution potential of glaciers to water availability in different climate regimes“. In: *P. Natl. Acad. Sci. Usa.* 107.47, pp. 20223–20227. DOI: 10.1073/pnas.1008162107 (cit. on pp. 17, 84).

Kienholz, C., R. Hock, and A. A. Arendt (2013). „A new semi-automatic approach for dividing glacier complexes into individual glaciers“. In: *Journal of Glaciology* 59.217, pp. 925–937. DOI: 10.3189/2013JoG12J138 (cit. on p. 40).

Kienholz, C., J. L. Rich, A. A. Arendt, and R. Hock (2014). „A new method for deriving glacier centerlines applied to glaciers in Alaska and northwest Canada“. In: *The Cryosphere* 8.2, pp. 503–519. DOI: 10.5194/tc-8-503-2014 (cit. on pp. 11, 18, 20, 24, 59, 86).

Leclercq, P. W. (2012). „Glacier fluctuations, global temperature and sea-level change“. PhD thesis. Utrecht University (cit. on p. 2).

Leclercq, P. W., J. Oerlemans, H. J. Basagic, I. Bushueva, A. J. Cook, and R. Le Bris (2014). „A data set of worldwide glacier length fluctuations“. In: *The Cryosphere* 8.2, pp. 659–672. DOI: 10.5194/tc-8-659-2014 (cit. on pp. 7, 8, 84, 86, 91, 93, 94, 99, 100, 102, 104–106).

Leclercq, P. W., J. Oerlemans, and J. G. Cogley (2011). „Estimating the Glacier Contribution to Sea-Level Rise for the Period 1800–2005“. In: *Surveys in Geophysics* 32.4, p. 519. DOI: 10.1007/s10712-011-9121-7 (cit. on pp. 8, 15, 17, 56).

Lee, V., S. L. Cornford, and A. J. Payne (2015). „Initialization of an ice-sheet model for present-day Greenland“. In: *Annals of Glaciology* 56.70, pp. 129–140. DOI: 10.3189/2015AoG70A121 (cit. on p. 57).

Linsbauer, A., F. Paul, and W. Haeberli (2012). „Modeling glacier thickness distribution and bed topography over entire mountain ranges with GlabTop: Application of a fast and robust approach“. In: *Journal of Geophysical Research: Earth Surface* 117.F3. DOI: 10.1029/2011JF002313 (cit. on p. 11).

Linsbauer, A., F. Paul, M. Hoelzle, H. Frey, and W. Haeberli (2009). „The Swiss Alps Without Glaciers - A GIS-based Modelling Approach for Reconstruction of Glacier Beds“. In: DOI: 10.5167/uzh-27834 (cit. on p. 11).

Liu, H., K. C. Jezek, B. Li, and Z. Zhao (2015). „Radarsat Antarctic Mapping Project Digital Elevation Model, Version 2“. In: *Boulder, Colorado USA. NASA National Snow and Ice Data Center Distributed Active Archive Center* (cit. on p. 23).

Lüthi, Martin P. (2009). „Transient response of idealized glaciers to climate variations“. In: *Journal of Glaciology* 55.193, pp. 918–930. DOI: 10.3189/002214309790152519 (cit. on p. 75).

Mackintosh, A. N., B. M. Anderson, and R. T. Pierrehumbert (2017). „Reconstructing Climate from Glaciers“. In: *Annual Review of Earth and Planetary Sciences* 45.1, pp. 649–680. DOI: 10.1146/annurev-earth-063016-020643 (cit. on p. 49).

Marzeion, B., N. Champollion, W. Haeberli, K. Langley, P. Leclercq, and F. Paul (2016). „Observation-Based Estimates of Global Glacier Mass Change and Its Contribution to Sea-Level Change“. In: *Surveys in Geophysics*. DOI: 10.1007/s10712-016-9394-y (cit. on p. 7).

Marzeion, B., J. G. Cogley, K. Richter, and D. Parkes (2014a). „Attribution of global glacier mass loss to anthropogenic and natural causes“. In: *Science* 345.6199, pp. 919–921. DOI: 10.1126/science.1254702 (cit. on pp. 17, 27, 56, 57, 84).

Marzeion, B., M. Hofer, A. H. Jarosch, G. Kaser, and T. Mölg (2012a). „A minimal model for reconstructing interannual mass balance variability of glaciers in the European Alps“. In: *The Cryosphere* 6.1, pp. 71–84. DOI: 10.5194/tc-6-71-2012 (cit. on p. 17).

Marzeion, B., A. H. Jarosch, and J. M. Gregory (2014b). „Feedbacks and mechanisms affecting the global sensitivity of glaciers to climate change“. In: *The Cryosphere* 8.1, pp. 59–71. DOI: 10.5194/tc-8-59-2014 (cit. on pp. 17, 18).

Marzeion, B., A. H. Jarosch, and M. Hofer (2012b). „Past and future sea-level change from the surface mass balance of glaciers“. In: *The Cryosphere* 6, pp. 1295–1322. DOI: 10.5194/tc-6-1295-2012 (cit. on pp. 10, 11, 15, 17, 18, 25, 27, 49, 51, 54, 56, 57, 84, 88, 89, 91, 97).

Marzeion, B., G. Kaser, F. Maussion, and N. Champollion (2018). „Limited influence of climate change mitigation on short-term glacier mass loss“. In: *Nature Climate Change* 8, pp. 305–308. DOI: 10.1038/s41558-018-0093-1 (cit. on pp. 6, 27, 44, 56, 84).

Marzeion, B., P. W. Leclercq, J. G. Cogley, and A. H. Jarosch (2015). „Brief Communication: Global reconstructions of glacier mass change during the 20th century are consistent“. In: *The Cryosphere* 9, pp. 2399–2404. DOI: 10.5194/tc-9-2399-2015 (cit. on pp. 8, 15, 27, 56, 84).

Maussion, F., A. Butenko, N. Champollion, M. Dusch, J. Eis, K. Fourteau, P. Gregor, A. H. Jarosch, J. Landmann, F. Oesterle, B. Recinos, T. Rothenpieler, A. Vlug, C. T. Wild, and B. Marzeion (2019). „The Open Global Glacier Model (OGGM) v1.1“. In: *Geoscientific Model Development* 12.3, pp. 909–931. DOI: 10.5194/gmd-12-909-2019 (cit. on pp. 11, 12, 57–60, 76, 84, 86, 87, 106, 110).

Maussion, F., M. Siller, and D. Rothenberg (2017). *fmaussion/salem: v0.2.1*. DOI: 10.5281/zenodo.269646 (cit. on p. 50).

McKinney, W. (2010). „Data Structures for Statistical Computing in Python“. In: *Proceedings of the 9th Python in Science Conference* 1697900.Scipy, pp. 51–56 (cit. on p. 50).

Mernild, S. H., W. H. Lipscomb, D. B. Bahr, V. Radić, and M. Zemp (2013). „Global glacier changes: A revised assessment of committed mass losses and sampling uncertainties“. In: *Cryosphere* 7.5, pp. 1565–1577. DOI: 10.5194/tc-7-1565-2013 (cit. on p. 44).

Morrison, D. D., J. D. Riley, and J. F. Zancanaro (1962). „Multiple Shooting Method for Two-Point Boundary Value Problems“. In: *Commun. ACM* 5.12, pp. 613–614. DOI: 10.1145/355580.369128 (cit. on p. 110).

Mosbeux, C., F. Gillet-Chaulet, and O. Gagliardini (2016). „Towards a better ice sheet model initialisation and basal knowledge using data assimilation“. In: *Geoscientific Model Development Discussions*, pp. 1–24. DOI: 10.5194/gmd-2016-7 (cit. on p. 57).

National Snow and Ice Data Center (comp.) (2002, updated 2019). *Glacier Photograph Collection, Version 1*. last access: 17.03.2020. Boulder, Colorado USA: NSIDC: National Snow and Ice Data Center. DOI: 10.7265/N5/NSIDC-GPC-2009-12 (cit. on p. 3).

New, M., D. Lister, M. Hulme, and I. Makin (2002). „A high-resolution data set of surface climate over global land areas“. In: *Climate Research* 21.1, pp. 1–25. DOI: 10.3354/cr021001 (cit. on pp. 50, 87).

Nussbaumer, S. U. and H. J. Zumbühl (2012). „The Little Ice Age history of the Glacier des Bossons (Mont Blanc massif, France): a new high-resolution glacier length curve based on historical documents“. In: *Climatic Change* 111.2, pp. 301–334. DOI: 10.1007/s10584-011-0130-9 (cit. on pp. 7, 94).

Nye, J. F. (1963). „On the Theory of the Advance and Retreat of Glaciers“. In: *Geophysical Journal International* 7.4, pp. 431–456. DOI: 10.1111/j.1365-246X.1963.tb07087.x (cit. on p. 5).

– (1965). „The Frequency Response of Glaciers“. In: *Journal of Glaciology* 5, pp. 567–587. DOI: 10.3189/s002214300001861x (cit. on p. 5).

Nye, J. F. and F. C. Frank (1960). „The response of glaciers and ice-sheets to seasonal and climatic changes“. In: *Proceedings of the Royal Society of London. Series A. Mathematical and Physical Sciences* 256.1287, pp. 559–584. DOI: 10.1098/rspa.1960.0127 (cit. on pp. 4, 5).

Oerlemans, J. (1994). „Quantifying Global Warming from the Retreat of Glaciers“. In: *Science* 264.5156, pp. 243–245. DOI: 10.1126/science.264.5156.243 (cit. on p. 17).

– (1997a). „A flowline model for Nigardsbreen, Norway: projection of future glacier length based on dynamic calibration with the historic record“. In: *Journal of glaciology* 24, pp. 382–389 (cit. on pp. 11, 12, 31, 34).

– (1997b). „Climate Sensitivity of Franz Josef Glacier, New Zealand, as Revealed by Numerical Modeling“. In: *Arctic and Alpine Research* 29.2, pp. 233–239 (cit. on pp. 5, 6, 74).

– (2001). *Glaciers and Climate Change*. Swets and Zeitlinger, Lisse (cit. on p. 74).

– (2005). „Extracting a Climate Signal from 169 Glacier Records“. In: *Science* 308.5722, pp. 675–677. DOI: 10.1126/science.1107046 (cit. on p. 17).

Oerlemans, J., M. Dyurgerov, and R. S. W. van de Wal (2007). „Reconstructing the glacier contribution to sea-level rise back to 1850“. In: *The Cryosphere* 1.1, pp. 59–65. DOI: 10.5194/tc-1-59-2007 (cit. on p. 8).

Oppenheimer, M., B.C. Glavovic, J. Hinkel, A.K. van de Wal R.and Magnan, A. Abd-Elgawad, R. Cai, M. Cifuentes-Jara, R.M. DeConto, Ghosh T., J. Hay, F. Isla, B. Marzeion, Meyssignac B., and Z. Sebesvari (2019). „IPCC Special Report on the Ocean and Cryosphere in a Changing Climate“. In: (cit. on p. 84).

Parkes, D. and H. Goosse (2019). „Modelling regional glacier length changes over the last millennium using the Open Global Glacier Model“. in review (cit. on pp. 91, 106).

Parkes, D. and B. Marzeion (2018). „Twentieth-century contribution to sea-level rise from uncharted glaciers“. In: *Nature* 563.7732, pp. 551–554. DOI: 10.1038/s41586-018-0687-9 (cit. on p. 2).

Pattyn, F. (2003). „A new three-dimensional higher-order thermomechanical ice sheet model: Basic sensitivity, ice stream development, and ice flow across subglacial lakes“. In: *Journal of Geophysical Research: Solid Earth* 108.B8. DOI: 10.1029/2002JB002329 (cit. on p. 10).

Pelt, W. J. J. van, J. Oerlemans, C. H. Reijmer, R. Pettersson, V. A. Pohjola, E. Isaksson, and D. Divine (2013). „An iterative inverse method to estimate basal topography and initialize ice flow models“. In: *Cryosphere* 7.3, pp. 987–1006. DOI: 10.5194/tc-7-987-2013 (cit. on p. 57).

Pelto, M. S. and C. Hedlund (2001). „Terminus behavior and response time of North Cascade glaciers, Washington, U.S.A.“ In: *Journal of Glaciology* 47.158, pp. 497–506. DOI: 10.3189/172756501781832098 (cit. on pp. 5, 6).

Pfeffer, W. T., A. A. Arendt, A. Bliss, T. Bolch, J. G. Cogley, A. S. Gardner, J. O. Hagen, R. Hock, Kaser G., C. Kienholz, E. S. Miles, G. Moholdt, N. Mölg, F. Paul, V. Radić, P. Rastner, B. H. Raup, J. Rich, M. J. Sharp, and the Randolph Consortium (2014). „The Randolph Glacier Inventory: a globally complete inventory of glaciers“. In: *Journal of Glaciology* 60, pp. 537–551. DOI: 10.3189/2014JoG13J176 (cit. on pp. 2, 18, 19, 57, 59, 65, 86, 87).

Radić, V., A. Bliss, A. C. Beedlow, R. Hock, E. Miles, and J. G. Cogley (2014). „Regional and global projections of twenty-first century glacier mass changes in response to climate scenarios from global climate models“. In: *Climate Dynamics* 42.1-2, pp. 37–58. DOI: 10.1007/s00382-013-1719-7 (cit. on pp. 10, 11).

Radić, V. and R. Hock (2011). „Regionally differentiated contribution of mountain glaciers and ice caps to future sea-level rise“. In: *Nature Geoscience* 4, pp. 91–94 (cit. on pp. 17, 18, 57, 84).

– (2014). „Glaciers in the Earth's Hydrological Cycle: Assessments of Glacier Mass and Runoff Changes on Global and Regional Scales“. In: *Surveys in Geophysics* 35.3, pp. 813–837. DOI: 10.1007/s10712-013-9262-y (cit. on pp. 17, 18, 57, 84).

Raper, S. C. B. and R. J. Braithwaite (2009). „Glacier volume response time and its links to climate and topography based on a conceptual model of glacier hypsometry“. In: *The Cryosphere* 3.2, pp. 183–194. DOI: 10.5194/tc-3-183-2009 (cit. on p. 5).

Rastner, P., T. Bolch, N. Mölg, H. Machguth, R. Le Bris, and F. Paul (2012). „The first complete inventory of the local glaciers and ice caps on Greenland“. In: *The Cryosphere* 6.6, pp. 1483–1495. DOI: 10.5194/tc-6-1483-2012 (cit. on p. 91).

Raup, B., A. Racoviteanu, S. J. S. Khalsa, C. Helm, R. Armstrong, and Y. Arnaud (2007). „The GLIMS geospatial glacier database: A new tool for studying glacier change“. In: *Global and Planetary Change* 56.1, pp. 101–110. DOI: https://doi.org/10.1016/j.gloplacha.2006.07.018 (cit. on p. 76).

Recinos, B., F. Maussion, T. Rothenpieler, and B. Marzeion (2019). „Impact of frontal ablation on the ice thickness estimation of marine-terminating glaciers in Alaska“. In: *The Cryosphere* 13.10, pp. 2657–2672. DOI: 10.5194/tc-13-2657-2019 (cit. on pp. 38, 86).

RGI Consortium (2017). *Randolph Glacier Inventory – A Dataset of Global Glacier Outlines: Version 6.0*. Tech. rep. Colorado, USA: Global Land Ice Measurements from Space. DOI: 10.7265/N5-RGI-60 (cit. on pp. 1, 19).

Rhein, M., S.R. Rintoul, S. Aoki, E. Campos, D. Chambers, R.A. Feely, S. Gulev, G.C. Johnson, S.A. Josey, A. Kostianoy, C. Mauritzen, D. Roemmich, L.D. Talley, and F. Wang (2013). „Observations: Ocean“. In: *Climate Change 2013: The Physical Science Basis. Contribution of Working Group I to the Fifth Assessment Report of the Intergovernmental Panel on Climate Change*. Ed. by T.F. Stocker, D. Qin, G.-K. Plattner, M. Tignor, S.K. Allen, J. Boschung, A. Nauels, Y. Xia, V. Bex, and P.M. Midgley. Cambridge, United Kingdom and New York, NY, USA: Cambridge University Press. Chap. 3, pp. 255–316. DOI: 10.1017/CBO9781107415324.010 (cit. on p. 4).

Richardson, S. D. and J. M. Reynolds (2000). „An overview of glacial hazards in the Himalayas“. In: *Quaternary International* 65-66, pp. 31–47. DOI: 10.1016/S1040-6182(99)00035-X (cit. on p. 17).

Roe, G. H. (2011). „What do glaciers tell us about climate variability and climate change?“ In: *Journal of Glaciology* 57.203, pp. 567–578. DOI: 10.3189/002214311796905640 (cit. on p. 17).

Roe, G. H. and M. A. O'Neal (2009). „The response of glaciers to intrinsic climate variability: Observations and models of late-holocene variations in the Pacific northwest“. In: *Journal of Glaciology* 55.193, pp. 839–854. DOI: 10.3189/002214309790152438 (cit. on p. 17).

Schiefer, E., B. Menounos, and R. Wheate (2008). „An inventory and morphometric analysis of British Columbia glaciers, Canada“. In: *Journal of Glaciology* 54.186, pp. 551–560. DOI: 10.3189/002214308785836995 (cit. on p. 11).

Schwitter, M. P. and C. F. Raymond (1993). „Changes in the longitudinal profiles of glaciers during advance and retreat“. In: *Journal of Glaciology* 39.133, pp. 582–590. DOI: 10.3189/S0022143000016476 (cit. on pp. 5, 6).

Slangen, A. B. A., F. Adloff, S. Jevrejeva, P. W. Leclercq, B. Marzeion, Y. Wada, and R. Winkelmann (2017a). „A Review of Recent Updates of Sea-Level Projections at Global and Regional Scales“. In: *Surveys in Geophysics* 38.1, pp. 385–406. DOI: 10.1007/s10712-016-9374-2 (cit. on p. 56).

Slangen, A. B. A., C. A. Katsman, R. S. W. van de Wal, L. L. A. Vermeersen, and R. E. M. Riva (2012). „Towards regional projections of twenty-first century sea-level change based on IPCC SRES scenarios“. In: *Climate Dynamics* 38.5, pp. 1191–1209. DOI: 10.1007/s00382-011-1057-6 (cit. on p. 11).

Slangen, A. B. A., B. Meyssignac, C. Agosta, N. Champollion, J. A. Church, X. Fettweis, S. R. M. Ligtenberg, B. Marzeion, A. Melet, M. D. Palmer, K. Richter, C. D. Roberts, and G. Spada (2017b). „Evaluating Model Simulations of Twentieth-Century Sea Level Rise. Part I: Global Mean Sea Level Change“. In: *Journal of Climate* 30.21, pp. 8539–8563. DOI: 10.1175/JCLI-D-17-0110.1 (cit. on pp. 4, 56, 84).

Strahler, A. N (1952). „Hypsometric (Area - Altitude) Analysis of Erosional Topography“. In: *Geological Society of America Bulletin* 63.11, pp. 1117–1142. DOI: 10.1130/0016-7606(1952)63 (cit. on p. 25).

Sugiyama, S., A. Bauder, C. Zahno, and M. Funk (2007). „Evolution of Rhonegletscher, Switzerland, over the past 125 years and in the future: application of an improved flowline model“. In: *Annals of Glaciology* 46, pp. 268–274. DOI: 10.3189/172756407782871143 (cit. on p. 11).

Sweet, W. V., R. Horton, R. E. Kopp, A. N. LeGrande, and A. Romanou (2017). „Climate Science Special Report: Fourth National Climate Assessment, Volume I“. In: Washington, DC, USA: U.S. Global Change Research Program. Chap. Sea level rise, pp. 333–363. DOI: 10.7930/J0VM49F2 (cit. on p. 4).

Vaughan, D.G., J.C. Comiso, I. Allison, J. Carrasco, G. Kaser, R. Kwok, P. Mote, T. Murray, F. Paul, J. Ren, E. Rignot, O. Solomina, K. Steffen, and T. Zhang (2013). „Observations: Cryosphere“. In: *Climate Change 2013: The Physical Science Basis. Contribution of Working Group I to the Fifth Assessment Report of the Intergovernmental Panel on Climate Change*. Ed. by T.F. Stocker, D. Qin, G.-K. Plattner, M. Tignor, S.K. Allen, J. Boschung, A. Nauels, Y. Xia, V. Bex, and P.M. Midgley. Cambridge, United Kingdom and New York, NY, USA: Cambridge University Press. Chap. 4, pp. 317–382. DOI: 10.1017/CBO9781107415324.012 (cit. on pp. 1, 6).

Wal, R. S. W. van de and J. Oerlemans (1995). „Response of valley glaciers to climate change and kinematic waves: a study with a numerical ice-flow model“. In: *Journal of Glaciology* 41.137, pp. 142–152. DOI: 10.3189/S0022143000017834 (cit. on p. 5).

Walsh, J., D. Wuebbles, K. Hayhoe, J. P. Kossin, K. Kunkel, G. L. Stephens, P. D. Thorne, R. S. Vose, B. Wehner, J. Willis, D. Anderson, S. Doney, R. Feeley, P. A. Hennon, V. Kharin, T. Knutson, F. W. Landerer, T.M. Lenton, J. J. Kennedy, and R. Somerville (2014). „Ch. 2: Our Changing Climate“. In: *Climate Change Impacts in the United States: The Third National Climate Assessment*. Ed. by J.M. Mellilo, Terese (T.C.) Richmond, and G.W. Yohe. U.S. Global Change Research Program, pp. 19–67. DOI: 10.7930/J0KW5CXT (cit. on p. 4).

Walt, S. van der, S. C. Colbert, and G. Varoquaux (2011). „The NumPy array: A structure for efficient numerical computation“. In: *Computing in Science and Engineering* 13.2, pp. 22–30. DOI: 10.1109/MCSE.2011.37 (cit. on p. 50).

Walt, S. van der, J. L. Schönberger, J. Nunez-Iglesias, F. Boulogne, J. D. Warner, N. Yager, E. Gouillart, and T. Yu (2014). „scikit-image: image processing in Python“. In: *PeerJ* 2, p. 453. DOI: 10.7717/peerj.453 (cit. on p. 50).

WCRP Global Sea Level Budget Group (2018). „Global sea-level budget 1993–present“. In: *Earth System Science Data* 10, pp. 1551–1590. DOI: 10.5194/essd-10-1551-2018 (cit. on p. 56).

WGMS (2017). *Fluctuations of Glaciers Database. World Glacier Monitoring Service, Zurich, Switzerland*. DOI: 10.5904/wgms-fog-2017-10 (cit. on pp. 51, 91).

– (2018). „Fluctuations of Glaciers Database“. In: *World Glacier Monitoring Service, Zurich, Switzerland*. DOI: 10.5904/wgms-fog-2018-11 (cit. on pp. 7, 9, 56, 86, 87, 94–96, 104, 106).

Winkelmann, R., M. A. Martin, M. Haseloff, T. Albrecht, E. Bueler, C. Khroulev, and A. Levermann (2011). „The Potsdam Parallel Ice Sheet Model (PISM-PIK) - Part 1: Model description“. In: *Cryosphere* 5.3, pp. 715–726. DOI: 10.5194/tc-5-715-2011 (cit. on p. 18).

Wouters, B., A. S. Gardner, and G. Moholdt (2019). „Global Glacier Mass Loss During the GRACE Satellite Mission (2002-2016)“. In: *Frontiers in Earth Science* 7, p. 96. DOI: 10.3389/feart.2019.00096 (cit. on pp. 56, 84).

Zekollari, H., J. J. Fürst, and P. Huybrechts (2014). „Modelling the evolution of Vadret da Morteratsch, Switzerland, since the Little Ice Age and into the future“. In: *Journal of Glaciology* 60.224, pp. 1208–1220. DOI: 10.3189/2014JoG14J053 (cit. on p. 5).

Zekollari, H., M. Huss, and D. Farinotti (2019). „Modelling the future evolution of glaciers in the European Alps under the EURO-CORDEX RCM ensemble“. In: *The Cryosphere* 13.4, pp. 1125–1146. DOI: 10.5194/tc-13-1125-2019 (cit. on pp. 12, 57, 78, 85).

Zekollari, H. and P. Huybrechts (2015). „On the climate–geometry imbalance, response time and volume–area scaling of an alpine glacier: insights from a 3-D flow model applied to Vadret da Morteratsch, Switzerland“. In: *Annals of Glaciology* 56.70, pp. 51–62. DOI: 10.3189/2015AoG70A921 (cit. on pp. 5, 75).

Zemp, M., R. J. Armstrong, I. Gärtner-Roer, W. Haeberli, M. Hoelzle, A. Kääb, J. S. Kargel, S. J. S. Khalsa, G. J. Leonard, F. Paul, and B. H. Raup (2014). „CHAPTER 1 Introduction : Global glacier monitoring — a long-term task integrating in situ observations and remote sensing“. In: (cit. on p. 6).

Zemp, M., H. Frey, I. Gärtner-Roer, S. U. Nussbaumer, M. Hoelzle, F. Paul, W. Haeberli, F. Denzinger, A. P. Ahlstrøm, B. Anderson, and et al. (2015). „Historically unprecedented global glacier decline in the early 21st century“. In: *Journal of Glaciology* 61.228, pp. 745–762. DOI: 10.3189/2015JoG15J017 (cit. on pp. 7, 8, 51, 56, 84).

Zemp, M., W. Haeberli, M. Hoelzle, and F. Paul (2006). „Alpine glaciers to disappear within decades?“ In: *Geophysical Research Letters* 33.13. DOI: 10.1029/2006GL026319 (cit. on pp. 62, 79).

Zemp, M., M. Hoelzle, and W. Haeberli (2009). „Six decades of glacier mass-balance observations: a review of the worldwide monitoring network“. In: *Ann. Glaciol.* 50.50, pp. 101–111. DOI: 10.3189/172756409787769591 (cit. on p. 17).

Zemp, M., M. Huss, E. Thibert, N. Eckert, R. McNabb, J. Huber, M. Barandun, H. Machguth, S. U. Nussbaumer, I. Gärtner-Roer, L. Thomson, F. Paul, F. Maussion, S. Kutuzov, and J. G. Cogley (2019). „Global glacier mass changes and their contributions to sea-level rise from 1961 to 2016“. In: *Nature* 568.7752, pp. 382–386. DOI: 10.1038/s41586-019-1071-0 (cit. on pp. 9, 56, 84).

Zemp, M., E. Thibert, M. Huss, D. Stumm, C. Rolstad Denby, C. Nuth, S. U. Nussbaumer, G. Moholdt, A. Mercer, C. Mayer, P. C. Joerg, P. Jansson, B. Hynek, A. Fischer, H. Escher-Vetter, H. Elvehøy, and L. M. Andreassen (2013). „Reanalysing glacier mass balance measurement series“. In: *The Cryosphere* 7.4, pp. 1227–1245. DOI: 10.5194/tc-7-1227-2013 (cit. on p. 105).

List of Figures

List of Tables

Affirmation in Lieu of an Oath

Versicherung an Eides Statt / Affirmation in lieu of an oath
gem. § 6 Abs. 5 der Promotionsordnung Dr. rer. nat. im Fachbereich 8 vom 22.06.2011 /
according to § 6 (5) of the Doctoral Degree Rules and Regulations of 22 June, 2011

Ich / I, Julia Eis
(Vorname / First Name, Name / Name, Anschrift / Address, ggf. Matr.-Nr. / student ID no., if applicable)

versichere an Eides Statt durch meine Unterschrift, dass ich die vorliegende Dissertation selbständig und ohne fremde Hilfe angefertigt und alle Stellen, die ich wörtlich dem Sinne nach aus Veröffentlichungen entnommen habe, als solche kenntlich gemacht habe, mich auch keiner anderen als der angegebenen Literatur oder sonstiger Hilfsmittel bedient habe und die zu Prüfungszwecken beigelegte elektronische Version (PDF) der Dissertation mit der abgegebenen gedruckten Version identisch ist. / *With my signature I affirm in lieu of an oath that I prepared the submitted dissertation independently and without illicit assistance from third parties, that I appropriately referenced any text or content from other sources, that I used only literature and resources listed in the dissertation, and that the electronic (PDF) and printed versions of the dissertation are identical.*

Ich versichere an Eides Statt, dass ich die vorgenannten Angaben nach bestem Wissen und Gewissen gemacht habe und dass die Angaben der Wahrheit entsprechen und ich nichts verschwiegen habe. / *I affirm in lieu of an oath that the information provided herein to the best of my knowledge is true and complete.*

Die Strafbarkeit einer falschen eidesstattlichen Versicherung ist mir bekannt, namentlich die Strafandrohung gemäß § 156 StGB bis zu drei Jahren Freiheitsstrafe oder Geldstrafe bei vorsätzlicher Begehung der Tat bzw. gemäß § 161 Abs. 1 StGB bis zu einem Jahr Freiheitsstrafe oder Geldstrafe bei fahrlässiger Begehung. / *I am aware that a false affidavit is a criminal offence which is punishable by law in accordance with § 156 of the German Criminal Code (StGB) with up to three years imprisonment or a fine in case of intention, or in accordance with § 161 (1) of the German Criminal Code with up to one year imprisonment or a fine in case of negligence.*

Ort / Place, Datum / Date

Unterschrift / Signature